Answers to Question of Referee 1:

Questions asked by referee is in straight font, *answers by the authors are given in ITALICS after the corresponding Question*. Modified text is given in small straight font in RED. In order to facilitate the location of text and/or Figures and table additions the reader will find a "Marked Copy" in "Track mode" where added text, Figures and Tables may be found suitably marked.

Questions/*Answers*/Modified or Added Text:

2- Page 7, line 185, silicon has a cutoff of 1500 cm^{-1} in the FTIR so how can the range extend from 4000-700 cm-1?

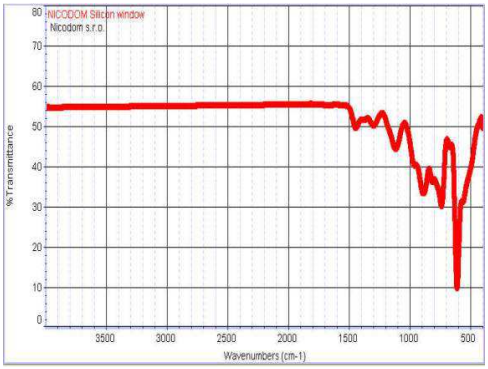

Fig. 1a: Absorption spectrum of Si window (commercially available material from Nicodom sro)

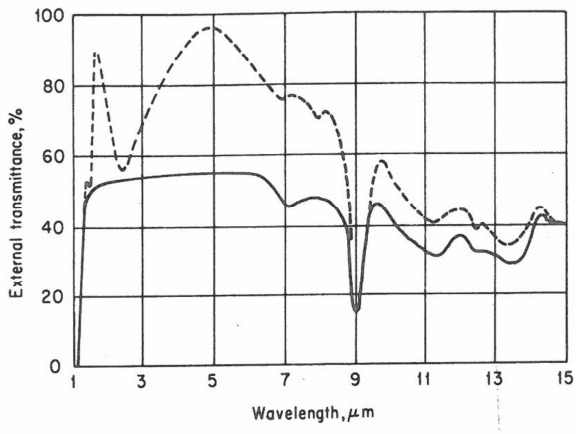

Fig. 125 Transmission of silicon, thickness 2.5 mm. Dashed curve is for a sample coated to reduce reflection loss. [*From Texas Instruments (no date)*.]

Fig. 1b: Taken from the Handbook of Optics (Optical Society of America, McGraw-Hill book Co. 1978)

Figures 1a and 1b present transmission curves of Si windows that always have a very thin coating (on the order of 50-100 nm) SiO_2 that protects the bulk of Si from oxidation. Although transmission is reduced in the 1500 to 600 nm range it is sufficiently transmitting to enable high-quality absorption spectra to be recorded. In our case the DIGILAB FTS 575 provides high throughput thanks to its 3" collection optics. The centerburst signal reduces from 9V to 3V after passage across 2a pair of 5mm thick KCl and a 2.0 mm thick Si window with external location of the HgCdTe detector cooled at 77 K.

3- Page 8, lines 219-220, the authors discuss that the transition in phases was observed via FTIR yet no FTIR or MS spectra were shown in the entire 52 pages of the manuscript. It would be interesting to the readers to show sample spectra and also to mention in a table the m/z and the wavenumbers where hydrates, HNO_3, HCl and water were observed.

We agree with the referee regarding the presentation of raw FTIR/MS data of the discussed ternary $HNO_3/HCl/H_2O$ chemical systems. To this effect we have added two new Figures (6 and 7) displaying combined FTIR/MS sample data as well as corresponding Table 3. However, for the binary system HNO_3/H_2O we have presented the corresponding combined sample FTIR absorption/MS data already in the Iannarelli and Rossi (2015) publication (J. Geophys. Res. 120, 11707-11727, 2015) such that renewed presentation in the present context would appear not to be appropriate. We therefore point out this reference when discussing the thermodynamic and kinetic data of the simple binary HNO_3/H_2O system.

We refrain at this point from showing raw data (FTIR absorption spectra and MS data as a function of time) because representative samples have been shown by Iannarelli and Rossi (2015) for α- and β-NAT. We will defer the presentation of raw data on the interaction of HCl on α- and β-NAT to Section 3.3 below.

The following text is introduced into chapter 3.3 which introduces the ternary $HCl/HNO_3/H_2O$ system.

Figure 6 displays raw data from repetitive pulsed dosing of HCl onto an α-NAT/ice substrate as a function of elapsed time. The individual pulses, of which there were twelve and identifiable by sharp peaks on top of the red columns in the lower panel displaying the MS signals of HCl (red, m/e 36), H_2O (blue, m/e 18) and HNO_3 (black, m/e 46) corresponded to (4-5) x 10^{16} molecule per pulse resulting in a total HCl dose of approximately 3 x 10^{17} molecules. This is the dose effectively administered to the α-NAT when the fraction of HCl going to the vessel walls and escaping the SFR has been subtracted. This dose approximately corresponds to 1000 molecular monolayers of HCl adsorbed onto the substrate. The temperature of the cryostat is displayed as the green trace in the lower panel, and with every T-increase the MS steady-state levels of HCl, H_2O and HNO_3 increase concomitantly. (During the pulsed admission of HCl the MS levels of HNO_3 and H_2O are subject to artifacts owing to rapid switching). Turning to the upper panel of Figure 6 we display a series of FTIR transmission spectra from 700 to 4000 cm^{-1} at specific times during the repetitive pulsing experiment which are indicated in the lower panel by a series of color-coded "sp1" and continuing going from red to purple. The principal peak positions have been collected in Table 3 and will be discussed below in terms of changes in the "pure" α-NAT/ice absorption spectra owing to the presence of increasing adsorbed HCl. The enlarged IR-spectral range in the upper panel of Figure 6 displays the effect of the HCl adsorption particularly well by showing a non-monotonic sequence of IR absorption peaks not present in the "pure" reference spectra from Iannarelli and Rossi (2015). The raw MS data from the lower panel of Figure 6 have been used to calculate the kinetic and thermodynamic data displayed in Figure 8.

Figure 7 displays raw data from repetitive pulsed dosing of HCl onto a β-NAT/ice substrate in analogy to Figure 6. The eleven individual pulses corresponded to (6-7) x 10^{16} molecule per pulse resulting in a total HCl dose of approximately 4 x 10^{17} molecules which amounts to 1300 molecular monolayers or so. Like in Figure 6 the upper panel displays a series of color-coded FTIR absorption spectra in transmission with the principal peak positions collected in Table 3. As for Figure 6 the MS steady-state levels at the different temperatures will be used to derive the kinetic and thermodynamic data of Figure 9 as a function of temperature. In addition, Figure S6 presents an enlarged graph for the non-exponential decay of a HCl pulse interacting with both α- and β-NAT on a 30 s time scale consisting of a fast and a slowly-decaying portion. The evaluation of such pulsed admission MS signals has been presented in the past (Iannarelli and Rossi, 2014, Supplemental Information (SI)) and the present analysis and fitting of the HCl MS signals follows the same scheme.

A look at Table 3 should provide an answer as to whether or not there is an identifiable spectral fingerprint of HCl adsorbed on α-or β-NAT in the FTIR absorption spectrum of the combined α- or β-NAT/HCl system displayed in Figures 6 and 7. The first column of Table 3 reveals the spectral fingerprint of HCl for α-NAT/HCl in terms of additional peaks (*in italics*) that are not present in the reference spectrum (pure α-NAT) recorded using the identical instrument and presented in the third column. There seem to be two spectral regions where the presence of HCl may be apparent, namely in the 1618-1644 cm^{-1} region corresponding to the broad bending vibration of the proton-ordered waters of hydration (Ritzhaupt and Devlin, 1991; Martin-Llorente et al., 2006), and more importantly, the band at 1328 cm^{-1} that overlaps with the 1339 cm^{-1} vibration, the latter of which is not changing with increasing HCl dose. The series of FTIR absorption spectra displayed in Figure 6 shows the non-monotonous change of intensity at this transition (1328 cm^{-1}): sp1 (red), sp2 (yellow) and sp3 (green) display the growth of a shoulder to the red of the 1375 cm^{-1} peak, sp4 (turquoise), sp5 (blue) and sp6 (purple) show the separate peak in its decline (1328 cm^{-1}) owing to evaporation of HCl together with NAT. For β-NAT the analogous situation is displayed in the second and fourth column of Table 3 and Figure 7. Here the presence of HCl is more discrete within the FTIR absorption spectrum of β-NAT as Table 3 suggests the well-separated peak to the blue of the 3227 cm^{-1} ice peak at 3360 cm^{-1} to be a HCl tracer as it looks very similar to the HCl/H_2O system (Iannarelli and Rossi, 2014; Chiesa and Rossi, 2013). The peaks identified to appear in the FTIR spectrum upon HCl adsorption may be found in the fifth column of Table 3 which displays the principal IR peaks in the reference HCl/H_2O system, except the 1200 cm^{-1} vibration found in column 1 and 2 whose origin remains unclear.

4- Page 13, lines 369-372, the authors discussed the difference between Alpha-NAT and HCl; yet no HCl results were shown in Figure 2.

The purpose of that statement regarding the difference between $R_{ev}(H_2O)$ in the HCl vs. the HNO_3 hydrate was to alert the reader to a significant difference between the two hydrates. We have inserted the two references that deal with the HCl hydrates (amorphous HCl hydrate and HCl Hexahydrate).

This result is very different compared to the previously studied case of HCl amorphous and crystalline hexahydrate using the same apparatus (Iannarelli and Rossi, 2013), where the evaporation of H_2O takes place at a rate characteristic of pure ice despite the presence of adsorbed HCl on the ice and is in agreement with the findings of Delval and Rossi (2005).

5- Page 14, line 421, can the authors comment how the relative errors were calculated and why same error in PV (30%) and TO (60%) experiments were observed on both the NAT and NAD films?

Although preferred from the point of view of avoiding sample saturation, we attribute twice the uncertainty to the TO compared to the PV technique. TO involves taking a difference of two large numbers in the denominator of Equations (7) and (8), which is the reason to attribute a larger experimental uncertainty to this method.

The largest uncertainty in our experiment is that of the flow rate introduced into the reactor, which is assigned a relative error of 25%. The flow rate measurement affects the calibration of the MS and therefore the measurement of all the concentrations in the reactor (Eq. 4). Therefore, we estimate a global relative error of 30% for PV experiments and double this uncertainty for TO experiments because Equations (7) and (8) imply a difference of two large numbers in many cases, as discussed above. We therefore assign a global 60% relative error to results obtained in TO experiments.

6- Page 15, lines 448-453, again the authors talk about comparisons to HCl experiments however no HCl data are present in Figure 4b. Which figure the authors want the reader to check to compare HCl case to figure 4a, please mention the figure since HCl experiments are introduced in the next Section.

As discussed above for alpha-NAT we are referring to a previous study on the BINARY HCl/H_2O phase (Iannarelli and Rossi, 2013) whereas chapter 3.3 below deals with the TERNARY $HCl/HNO_3/H_2O$ system.

As in the case of α-NAT, this result is very different compared to the case of HCl hydrates studied before using the same apparatus (Iannarelli and Rossi, 2013) where the evaporation of H_2O is not influenced by the presence of adsorbed HCl on the ice and takes place at a rate characteristic of pure ice for all HCl concentrations used.

7- Page 17, lines 484-488, why are the authors making assumptions regarding the substrates can't they get information on changes due to HCl from FTIR?

In response to your discussion point 3 above we have introduced Figures 6 and 7 displaying FTIR absorption spectra in the presence of HCl whose principal peak positions have been collected in the new Table 3 (not reproduced here but included in the new manuscript version). Regarding the ternary $HCl/HNO_3/H_2O$ system treated here we had to make some verified assumptions in order to keep the experimental parameter space to an acceptable level. All three simplifying assumptions have been verified in the current laboratory experiments.

In order to restrain the number of independent measurements on this ternary system to a practical level we had to make some assumptions and/or simplifications in order to measure the unknown parameters of Eq. (2) for each gas used. Specifically, we made the following reasonable assumptions, both for α-NAT and β-NAT substrates which have been experimentally verified in laboratory experiments:

8- Page 18, lines 534-535, the authors mentioned a decrease in ïA¸a¸-ïA¸c´-NAT as a function of increasing temperature but looking at figure 7a it looks like there was no change in the signal within experimental error.

Figure 9a in fact shows a slight decrease of the HCl accommodation coefficient on β-NAT similar to α-NAT (Figure 8a) where the decrease is a little larger over a similar T-range. However, as the referee suggests it may or may not be significant for β-NAT.

…decreases as a function of temperature in the range 177-201 K, varying from 0.025 at 177 K to 0.016 at 201 K which may or may not be significant.

9- Page 19, lines 563-574 are the two distinct temperature regimes in Figure 2a due to surface disorder on ice?

We certainly suggest this to be due to contamination-induced surface disorder that is discussed in the next few paragraphs and that has been highlighted in the studies of McNeill et al. However, at this point this remains a suggestion because we do not have structural proof of this hypothesis because in the present case the term "multidiagnostic" does not extend the investigation to structural studies.

10- Page 24, lines 704-709 why only TO experiments were possible for HNO3? This point is not so clear.

The answer to this question has been given in Section 2.2, line 275-279.

11- Page 25, lines 753-758 can the authors comment why their results for HCl experiments were different from those by Haynes (2002)?

We have the suspicion that the difference has to do with the fact that Hynes et al. (2002) performed their experiments at significantly higher temperatures which possible enables reversibility. This is mentioned on pg. 28, lines 834-837.

12- Figures 2-7 although the C2 authors mentioned the symbols in the text but it was so confusing to keep going back and forth between the text and the figure given the extra length of this manuscript and the different systems studied. I recommend that the authors explain the symbols in the caption for every figure.

The captions have been written according to the guidelines of ACP. Owing to the complexity of the Figures we have added explanation of the symbols inside the Figures.

Answers to Question of Referee 2:

Questions asked by referee is in straight font, *answers by the authors are given in ITALICS after the corresponding Question*. Modified text is given in small straight font in RED. In order to facilitate the location of text and/or Figures and table additions the reader will find a "Marked Copy" in "Track mode" where added text, Figures and Tables may be found suitably marked.

General Comments:

However, the organization and motivation needs to be made clearer, both in the introduction and in the atmospheric implications. Both sections read like a "data dump" with little explanation to identify the key discrepancies or limitations in the literature. Why are the authors conducting this study, 20+ years after some of the initial studies were conducted?

Referee 2 raises an important point: Why unfold the glory of heterogeneous chemistry once more (or once and for all?) after 20 years of (waning) interest? It may have escaped the attention of Referee 2 that we report unique kinetic data secured by a consistency check (called thermochemical kinetics by the late S.W. Benson). There are NO available data in the literature on absolute rates of evaporation, not only for ice, but also for ices contaminated to various degrees by atmospheric trace gases. These data determine the evaporative lifetimes of various ice particles thought to be important in the UT/LS, and we have introduced a synoptic Table (Table 5 in the Discussion Section) in order to demonstrate the usefulness and the atmospheric importance of the kinetic data. Needless to say that we have made the point that in most cases the evaporative lifetimes enable heterogeneous processing to occur in a realistic time frame.

Why have 20 years gone by before coming forth with such seemingly important and useful data? The answer to this is multifactorial. It also has to do with the multidiagnostic capabilities of the present instrument that we have built up since 2003 in order to correct for the shortcomings of other experiments (Hanson and Ravishankara – single diagnostics flow tubes; Tolbert and coworkers – spectroscopy in chamber experiments, essentially w/o kinetics capabilities, Aerodyne group Chuck Kolb and Doug Worsnop performing single diagnostic equilibrium experiments for constructing phase diagrams, etc.). We have built an instrument with a decisive improvement in that it provides a unique spot of lowest temperature in a Stirred Flow Reactor w/o extraneous and uncontrolled cold spots that would perturb the reaction kinetics (through condensation of molecule of interest on an unidentified cold spot rather than on an optical support (FTIR, FTRAS, Quartz Crystal MicroBalance (QCMB), optical (HeNe) interferometry, etc.). We believe that the present measurements reveal hitherto unknown kinetic data at an unprecedented level of detail that are checked for mutual consistency by comparing the calculated equilibrium vapor pressure with known literature values.

The Introduction has been curtailed a bit in order to concentrate on the issues at hand. On the other hand, the paper has to be useful also for the non-specialist by providing at least the rudiments of a suitable atmospheric context. The impression of a "data dump" is not wrong, except that it is sometimes unavoidable. We have made every effort to "lighten up" the text accordingly. Suffice it to say that we are proud and lucky to be able to present a manifold of hopefully useful data to the scientific community. More often than not papers seem to contain less than meets the eye, we think that we are in the contrary position of "more than meets the eye"!

Instead, the intro leads with a nice (but unnecessary) review of general PSC chemistry, something that is now several decades old and the overview of which is not necessary.

See above paragraph in relation to presenting a self-contained account of atmospheric context.

The atmospheric implications section goes on a tangent (incorrectly, at that) on water vapor measurement instruments that really aren't related to the current study results. Both of these

aspects distract the reader from the high-quality, laboratory study and their results. While this paper will be eventually publishable, it requires some significant revisions in its current form.

We are heeding the advice of Referee 2 and have cut 90% of the material covering the Cryogenic Mirror Hygrometer. The only thing left is a brief description of the experiments of Gao et al. (2016) and the ramifications of the kinetic results of the present study.

Detailed (key) Points:

Lines 56-129: a review of PSC chemistry has been common knowledge for decades; this section reads like a review article and is not necessary for the manuscript; indeed, it distracts from the critical questions that this study is trying to examine.

In the interest of presenting a self-contained story we decided to keep this part in the Introduction.

Lines 130-157: While this is a thorough review of the literature, it reads to some extent like a "data dump". The experiments were done under different conditions to some extent. Are there real discrepancies between these results? Perhaps a table of past literature and your results would be more clear/helpful. At the very least, one should summarize the point of this section: e.g. there are discrepancies, there may or may not, too hard to say given the different experimental conditions, etc. and whatever it is, this is the motivation for our study! As written, the reader is left to search through a lot of data with no clear idea on whether there is true disagreement or not. And then explicitly tell what aspect of the study will your work address in this regard.

We have summarized the planned experiments in lines 152-169 by emphasizing at the end the thermochemical as well as the mass balance aspect which are the two novel aspects that make our measurements unique. On the other hand, we have refrained from evaluating the disparate kinetic results in the literature mentioned briefly on lines 116-149 that collect all relevant literature results to date. It is incumbent on reviews such as JPL and IUPAC rather than on original research papers to evaluate kinetic results of atmospheric importance.

In addition, all experiments have been performed under strict mass balance control by considering how many molecules of HNO_3, HCl and H_2O were present in the gas vs. the condensed phase (including the vessel walls) at any given time. These experiments have been described by Iannarelli and Rossi (2015). Most importantly, the consistency of the accommodation and evaporation kinetics has been checked using the method of thermochemical kinetics (Benson, 1976) by calculating the equilibrium vapor pressure and comparing it with values of published phase diagrams. In addition, the present work is the first to present absolute rates of evaporation of all involved constituents (H_2O, HNO_3, HCl) thus enabling predictions on evaporative lifetimes of ice particles under atmospheric conditions.

Paragraph 158-163: Now suddenly the authors switch their literature review to HNO3 on pure ice. Only the last two sentences of this paragraph seem relevant to the work, at least for the introduction. And even then, there should be a transitional statement such as "The complications/discrepancies of HNO3 and H2O update on NAT surfaces is also evident when examining HCl uptake on NAT." or similar.

As you guess the single component uptake kinetics of HCl and HNO_3 on pure ice are also important when discussing uptake on binary chemical systems such as HNO_3/H_2O (this work) or HCl/H_2O (Iannarelli and Rossi, 2013).

In the investigation of the properties of binary chemical systems the behavior of the simple single-component systems is an important stepping stone.

Line 192+: The authors mention that the inlet system was modified but then failed to even provide a brief sentence or two on the actual modification. If it is important to mention at the start, please briefly summarize the modification.

Done

We therefore minimized the volume of the admission system and only retained the absolutely necessary total pressure gauge for measuring the absolute inlet flow rate (molecule s^{-1}).

Line 222-224: Not entirely an apples-to-apples comparison. The RAIR study was most sensitive to very thin films (< 10s-100 nm) and the very near surface properties. At thicker films and higher dose rates, they observed similar results as past studies and even the current study in the manuscript. The technique in the manuscript most likely was not sensitive to the presence of very thin films that were observed in the RAIR study.

We intended from the outset to avoid thick films owing to kinetic complications. Very often thin films occur as islands on the substrate or on the ice film such that the kinetics are ill-defined. Therefore, we chose to study the binary systems as thick films using the absorption cross sections that we have measured on thick films.

Line 236-239: This is one of my main concerns experimentally about the study. The excess ice, even if it stabilizes NAT, will impact the vapor pressures of water inside the chamber. Is one always on the ice-NAT phase line? If not, to what extent does each phase determine the partial pressure of water observed in the chamber? This has implications for the later results for the accuracy of H2O partial/vapor pressures and H2O kinetics. Why not just make a pure NAT film like to past thin film studies? NAT is a pretty stable film to make. The excess ice phase present needs to be discussed in more detail and a logical, reasoned argument why it doesn't complicate the interpretation of the results (or to what extent it does).

Figure 2 (introduced as supplemental Figure S5 into the SI section) presents a phase diagram of the binary system HNO_3/H_2O. According to Gibb's Phase Rule we have two components and three phases leading to a single degree of freedom. The dashed lines are isotherms, and as long you keep T constant you see that the equilibrium vapor pressure P_{vap} of H_2O or HNO_3 change within one and 3.5 orders of magnitude, respectively, depending on the composition (mass) of both solid phases, either H_2O or HNO_3 rich. The symbols (red for α-, black for β-NAT) represent experiments characterized by a given value of P_{HNO3} and P_{H2O} depending on the evaporation history of the ice sample. You also see the parameter space for the polar lower stratosphere and the number of points falling into the corresponding phase space of NAT. Riding the coexistence line is only interesting for the construction of the phase diagram in case it is not known. From Figure 2 you can read off both H_2O and HNO_3 vapor pressures and conclude that the present experiments are indeed relevant for the UT/LS as far as the vapor pressures are concerned (see your question below).

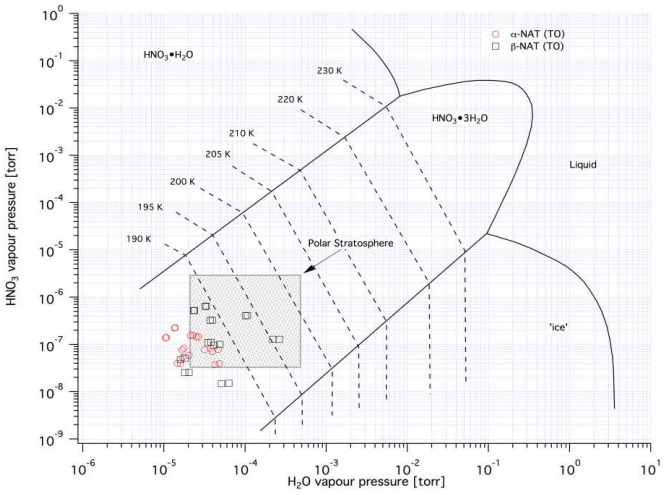

Figure 2: Phase diagram for the HNO_3/H_2O system in the range of atmospheric interest. The phase diagram is taken from Chapter 2 "The Probable Role of Stratospheric "Ice" Clouds: Heterogeneous Chemistry of the "Ozone Hole" by M.J. Molina, "The Chemistry of the Atmosphere: Its Impact on Global Change", J. Calvert (ed.), IUPAC Chemrawn 21 Series, Blackwell Scientific Publications.

Lines 624-633: Report the entropies of evaporation as well – do they make sense with physical principles? If not, why? And elsewhere in the manuscript.

Taking $\exp(\Delta S^0_{ev}/2.303R) = 10^{13.8}$ after conversion from Torr into an atmosphere we obtain $\Delta S^0_{ev} = 264.6\ JK^{-1}mol^{-1}$ or 63.25 cal K^{-1} mol^{-1}. If we make the assumption that all H_2O comes from NAT we have to divide by three owing to the fact that the decomposition of the trihydrate liberates three moles of H_2O. We therefore have a value of 0.333x63.25 cal K^{-1} mol^{-1} or 21.1 cal K^{-1} mol^{-1} which exactly corresponds to Trouton's rule. However, this may just be fortuitous, also because we have a multicomponent system with several phases, each with its own thermodynamic parameters as we have to contend with the T-dependence of the combined system. The reason we are not discussing entropies of vaporization in this context is that the temperature range over which the measurements were taken is too small to obtain a reliable intercept, or in other words, the extrapolation of 1/T ➔ 0.0 is too uncertain given the measurement range. This uncertainty owing to extrapolation is much larger than any potential effects of hydrogen bonding of H_2O, HNO_3 or HCl which is known to affect Trouton's rule (towards an increase of Trouton's constant).

Line 660-661: Could a similar explanation be used to invoke discrepancies between your results and those in the literature (JPL recommendations)?

We are not sure about your question. Which discrepancies and which JPL recommendations?

Line 681: Can the absolute value of 12 kJ/mole be explained physically in terms of hydrogen bonds? Why or why not?

From the point of view of the numerical value 12 kJ/mole is approximately1/3 to ¼ of a "normal" hydrogen bond. However, this single value is difficult to interpret in the absence of other supporting values. However, we feel that it is related to the fact that α-NAT is not the

most stable form of NAT. This primarily concerns the arrangement of H_2O in the lattice which becomes tighter in β-NAT and therefore stabilizes the solid hydrate.

Line 686-7: Warshawsky et al. GRL 1999 also quantified this process of a sealing NAT layer slowing ice evaporation, and these were done a much lower HNO3 partial pressures than in the Biermann et al. study. Related to this, what are the partial pressures of HNO3 used in these experiments? Are they relevant to the atmosphere at all? They seem like they were much higher than what is expected in the atmosphere based upon the discussion and comparison to other laboratory studies. Please cite the HNO3 partial pressures used in these experiments.

Please see above in conjunction with the binary phase diagram displayed in Figure 2 and/or Figure S5.We would like to affirm that the present conditions indeed are relevant to the UT/LS atmosphere as indicated in Figure 2 above by the symbols. Thank you for the Warshawsky citation that I routinely take from Maggie Tolbert's review article in Annual Rev. Phys. Chem.

$R_{ev}(H_2O)$ on both α-NAT and β-NAT is smaller compared to $R_{ev}(H_2O)$ on pure ice. This is in agreement with the results of Tolbert and Middlebrook (1990), Middlebrook et al. (1996), Warshawsky et al. (1999) and Delval and Rossi (2005) who showed that ice coated with a number of molecular layers of NAT evaporates H_2O at a slower rate than pure ice. On the other hand, our results are in contrast with the findings of Biermann et al. (1998) who report that no significant decrease of the H_2O evaporation rate was observed in HNO_3-doped ice films. The discrepancy may possibly be caused by the high total pressure of 0.85 mbar in their reactor compared to all other competitive studies cited above that use high-vacuum chambers with total pressures lower by typically a factor of 500 or more. It is very likely that the experiments performed by Biermann et al. (1998) were not sensitive to changes in evaporation rates despite the fact that both the HNO_3 and H_2O concentrations used as well as the thickness of the accumulated NAT layers in their no. 5 experiment were of the same magnitude as in the competing studies. A hint to that effect is the unexpected time dependence of the ice evaporation rate in Biermann et al. (1998) that shows an induction time of 30 minutes as opposed to the expected linear decrease from the beginning of evaporation (see below). We are unable to attribute the source of the measured H_2O vapor in the presence of two H_2O-containing solid phases in our chemical system, namely pure H_2O ice and NAT. We restate that the partial pressures at constant temperature are controlled by the (relative) composition of the system in agreement with the single degree of freedom resulting from Gibb's Phase Rule and the data displayed in the binary HNO_3/H_2O phase diagrams displayed in Figures 3, 5 and S5.

Atmospheric implications: There is a data dump of numbers here once again, many of which were already described in detail in the discussion section. What are the key points, circling back to the motivation in the introduction and past literature experiments? e.g. Does the JPL kinetic data need to be revised (as suggested in the discussion in several places)? What are the implications of these much different values? How has this study broadened the range of past studies or explained potential discrepancies or unanswered questions in the past literature? What future research is needed? etc.

Many of the questions raised by Referee 2 for the "Conclusions and Atmospheric Implications" Section (5) are out of scope for a publication providing fundamental kinetics and thermodynamic data. We are unable to tackle all the suggested questions and do not see it as our task to provide evaluations of rate data on behalf of the JPL or IUPAC panels because this activity is built on consensus. We are happy to provide the best available answers surrounding the HNO_3 hydrates to date. However, we have added Table 5 that is a vivid example and illustration of the usefulness of the obtained data in an atmospheric context, namely absolute rates of evaporation.

A look at Table 5 reveals evaporative lifetimes of various ice particles with respect to H_2O evaporation. Equation (26) and (27) present the rudiments of a very simple layer-by-layer molecular model used to estimate evaporation lifetimes (θ_{tot}) at atmospheric conditions (Alcala et al., 2002; Chiesa and Rossi, 2013):

$$\theta_{tot} = (r/a)N_{ML}/J_{ev}^{rh} \quad (26)$$

$$J_{ev}^{rh} = J_{ev}^{max}(1-rh/100) \quad (27)$$

with r, a, rh and N_{ML} being the radius of the ice particle, shell thickness, relative humidity in % and the number of molecules cm^{-2} corresponding to one monolayer. J_{ev}^{rh} and J_{ev}^{max} are the evaporation fluxes of H_2O at rh and rh = 0, the latter corresponding to the maximum value of J_{ev}.which we calculate following Equation (2) or (8). The salient feature of this simple evaporation model is the linear rate of change of the radius or diameter of the particle, a well- and widely known fact in aerosol physics in which the shrinking or growing size (diameter)

of an aerosol particle is linear with time if the rate of evaporation is zero order, that is independent of a concentration term. Table 5 lists the evaporation life times which are not defined in terms of an e-folding time when dealing with first-order processes. In this example the lifetime is the time span between the cradle and death of the particle, this means from a given diameter 2r and "death" at 2r = 0. The chosen atmospheric conditions correspond to 190 K, rh = 80%, a = 2.5 Å for H_2O and 3.35 Å for all other systems, r = 10 µm and estimated values 6 x 10^{14}, 3 x 10^{14} and 1 x 10^{15} molec cm^{-2} for N_{ML} of HNO_3, HCl and H_2O. It is immediately apparent that there is a large variation of θ_{tot} values for atmospherically relevant conditions which goes into the direction of increasing opportunities for heterogeneous interaction with atmospheric trace gases, even for pure ice (PSC type II). Table 5 is concerned with the most volatile component, namely H_2O. If we now turn our attention to the least volatile component such as HNO_3 in β-NAT we obtain θ_{tot} = 5.1 d and 33.9 d for 0 and 85% HNO_3 atmospheric saturation, the former being the maximum possible evaporation rate for 0% HNO_3 saturation. The other boundary conditions are 190 K, polar upper tropospheric conditions at 11 km altitude (226.3 mb at 210 K), 1 ppb HNO_3, 10 ppm H_2O corresponding to 85% HNO_3 saturation. This goes to show that laboratory experiments on gas-condensed phase exchange of lower volatility components in atmospheric hydrates are fraught with complications. It follows as a corollary that both HCl, but especially HNO_3 contamination of H_2O ice is bound to persist for all practical atmospheric conditions.

Also, the discussion on NAT-coated ice impacting field measurements is speculative, unsupported, and shows several large gaps of awareness in UTLS water vapor measurements. First, the authors cite the problems of "reliable and reproducible measurements" of water vapor in the field UTLS measurements. However, as noted above, I have serious questions on how one can reliably interpret the accuracy of the water vapor measurements in their laboratory setup given that two phases exist at conditions well off the ice/NAT equilibrium line (and higher HNO3 partial pressures than usually exist in the UTLS) – so it isn't clear to me how these laboratory results are that representative of the UTLS itself. Second, the CU/NOAA chilled mirror hygrometer has a long measurement history and is best described most recently by the Vömel et al. JGR, 2007 and/or Vömel et al., AMTD, 2016. More importantly, it compared extremely well in recent intercomparison campaigns to the reference standard (see Fahey et al. AMT 2014), an instrument/technique that probably is (in this reviewers' opinion) the most accurate/uncertainty-documented H2O measurement in the community. Third, HNO3 has not been shown in the NOAA tests to impact the frost layer (ice vapor pressure) at relevant HNO3 concentrations (Thornberry et al., AMT 2011). Fourth, there are numerous diode laser-based hygrometers by many leading groups in the world; in fact, I would argue the NOAA TDL is one of the most recent and, though promising and a quality measurement, has some of the least amount of field data to characterize its strengths and weaknesses. More recent AquaVIT2 UT/LS water vapor intercomparisons showed some improved agreement in general from most of the UTLS hygrometers, whether diode laser-based at any wavelength (1.3, 1.4, 2.6 microns), laser-induced fluorescence, chilled mirrors, or other techniques. Therefore, I'm not sure the authors' results are applicable to explaining whether or not an instrument may work with the limited knowledge of the measurement instruments themselves and better agreement now being observed. This is especially true since the manuscript's lab results appear to be at HNO3 concentrations/thicknesses well above what is possible in the UTLS. The Gao et al. 2016 JPC-A dealt with very small amounts of residual HNO3 within ice and not related to thick NAT coatings here. For all of these reasons, I suggest removing these paragraphs on H2O measurements and expanding on the kinetics and the implications thereof/discrepancies.

First we agree with Referee 2 that we are in no way specialists in the question of H_2O vapor measurements under UT/LS conditions. We therefore take out this section entirely and only mention the Gao et al. (2016) measurements at the very end as they directly relate to the present kinetic results inasmuch as the persistence of the lower volatility components in ice, namely HNO_3, is concerned. We are a bit surprised at the explicit reaction of Referee 2 concerning the atmospheric relevance of the present study. We resolutely take exception to his statements to be "well off the ice/NAT equilibrium line (and higher HNO_3 partial pressures than usually exist in the UTLS)". Figure 2 (S5 in the SI Section) clearly points out that (1) the UT/LS conditions are in the middle, not the limits of the NAT existence area within the

relevant phase diagram, and that (2) the HNO_3 partial pressure are not higher than usually exist in the UT/LS region. If anything, they are a bit lower because we have emphasized lower temperatures. In addition, we assert in contrast to Referee 2 that the NAT layers, typically 300 nm or less thick in the present study, are well representative of "what is possible in the UTLS"! In the end we consider it wise to continue to question measurement concepts for field applications using fundamental research instruments and methods. It is incumbent on us active in the laboratory to alert field scientists to possible shortcomings and artifacts of routinely applied methods and techniques used in the field.

Heterogeneous Kinetics of H_2O, HNO_3 and HCl on HNO_3 hydrates (α-NAT, β-NAT, NAD) in the range 175-200 K

R. Iannarelli[1,2] and M. J. Rossi[1]

[1]Laboratory of Atmospheric Chemistry (LAC), Paul Scherrer Institute (PSI), CH-5232 PSI Villigen, Switzerland; [2]New address: Safety, Prevention and Health Domain, RI DSPS-SCC , Station 6, Ecole Polytechnique Fédérale de Lausanne (EPFL), CH-1015 Ecublens, Switzerland.

Correspondence to: M. J. Rossi (michel.rossi@psi.ch)

Abstract

Experiments on the title compounds have been performed using a multidiagnostic stirred-flow reactor (SFR) in which the gas- as well as the condensed phase has been simultaneously investigated under stratospheric temperature~~ conditions~~ in the range 175-200 K. Wall interactions of the title compounds have been taken into account using Langmuir adsorption isotherms in order to close the mass balance between deposited and desorbed (recovered) compounds. Thin solid films at 1 µm typical thickness have been used as a proxy for atmospheric ice particles and have been deposited on a Si window of the cryostat whith~~ere~~ the optical element being~~was~~ the only cold point in the deposition chamber~~system~~. FTIR absorption spectroscopy~~metry~~ in transmission as well as partial and total pressure measurement using residual gas MS and sensitive pressure gauges have been employed in order to monitor growth and evaporation processes as a function of temperature using both pulsed and continuous gas admission and ~~continuous~~ monitoring under SFR conditions. Thin solid H_2O ice films were used as the starting point throughout, with the initial spontaneous formation of α-NAT followed by the gradual transformation of α-➔ β-NAT ~~starting~~ at T > 185 K. NAD was spontaneously formed ~~at once~~ at somewhat larger partial pressures of HNO_3 deposited on pure H_2O ice. In contrast to published reports the formation of α-NAT proceeded without prior formation of an amorphous HNO_3/H_2O layer and always resulted in β-NAT. For α- and β-NAT the temperature dependent accommodation coefficient $\alpha(H_2O)$ and $\alpha(HNO_3)$, the evaporation flux $J_{ev}(H_2O)$ and $J_{ev}(HNO_3)$ and the resulting saturation vapor pressure $P_{eq}(H_2O)$ and $P_{eq}(HNO_3)$ were measured and compared to binary phase diagrams of HNO_3/H_2O in order to afford thermochemical check~~control~~ of the kinetic parameters. The

resulting kinetic and thermodynamic parameters of activation energies for evaporation (E_{ev}) and standard heats of evaporation ΔH_{ev}^0 of H_2O and HNO_3 for α- and β-NAT, respectively, led to an estimate for the relative standard enthalpy difference between α- and β-NAT of -6.0 ± 20 kJ/mol in favor of β-NAT, as expected, despite a significantly larger value of E_{ev} for HNO_3 in α-NAT. This in turn implies a substantial activation energy for HNO_3 accommodation in α- compared to β-NAT where $E_{acc}(HNO_3)$ is essentially zero. The kinetic (α(HCl), J_{ev}(HCl)) and thermodynamic (P_{eq}(HCl)) parameters of HCl-doped α- and β-NAT have been determined under the assumption that HCl adsorption did not significantly affect α(H_2O) and α(HNO_3) as well as the evaporation flux $J_{ev}(H_2O)$. J_{ev}(HCl) and P_{eq}(HCl) on both α- and β-NAT are larger than the corresponding values for HNO_3 across the investigated temperature range but significantly smaller than the values for pure H_2O ice at T < 200 K. ~~This means that once contaminated with HCl the "impurity" HCl will persist along with HNO_3 upon complete evaporation of the atmospheric ice particle..~~

1 Introduction

Heterogeneous processes taking place on ice clouds in the Upper Troposphere (UT) or on Polar Stratospheric Clouds (PSC's) in the Lower Stratosphere (LS) have, since a long time, been recognized as one of the major ozone depleting mechanism (Solomon et al., 1986). PSC's consist of either particles of crystalline nitric acid trihydrate (NAT) (type Ia), ternary $H_2SO_4/HNO_3/H_2O$ supercooled solutions (type Ib) or pure H_2O ice (type II) (Zondlo et al. 2000) and are formed during the polar winter season when temperatures are sufficiently low in order to allow H_2O supersaturation that ultimately leads to cloud formation in the dry stratosphere subsequent to ice nucleation (Peter, 1997).

Ozone is depleted during the Arctic and Antarctic spring season after unreactive chlorine reservoir compounds, $ClONO_2$ and HCl, are converted into molecular chlorine and rapidly photolyze into active atomic chlorine during the spring season (Solomon, 1990). The presence of PSC's enables heterogeneous chemical reactions such as Reaction (R1), which represents one of the most efficient stratospheric heterogeneous reactions (Friedl et al, 1986; Molina et al., 1985, 1987):

$$ClONO_2(g) + HCl(s) \rightarrow Cl_2(g) + HNO_3(s) \qquad (R1)$$

Reaction (R1) is orders of magnitude faster than the corresponding homogeneous gas phase process (Molina et al., 1985) and the most important chlorine-activating reactions in the polar stratosphere~~. The contribution to ozone destruction from Reaction (R1) is twofold: first, the released molecular Cl_2 rapidly photolyzes into atomic Cl establishing a cycle of O_3 destruction and, second, the overall removal of nitrogen oxides from the gas phase by entrapment of HNO_3 in the ice, facilitates O_3 destruction through a gas phase catalytic cycle similar to the one~~ are reported in Reactions (R2)-(R4):

$$X + O_3 \rightarrow XO + O_2 \qquad \text{(R2)}$$

$$XO + O \rightarrow X + O_2 \qquad \text{(R3)}$$

$$\text{net: } O_3 + O \rightarrow O_2 + O_2 \qquad \text{(R4)}$$

where X is H, OH, NO, Cl or Br leading to HO_x, NO_x, ClO_x and BrO_x catalytic cycles, respectively.

Reaction (R1) increases the concentration of HNO_3 in the condensed phase and when PSC particles become sufficiently large they~~and~~ fall out of the stratosphere~~, active nitrogen is permanently removed through denitrification which has been observed in the field~~ (Fahey et al., 2001~~). Lower concentrations of nitrate owing to the absence of HNO_3~~ which inhibits ~~reactions such as~~ Reaction (R5):

$$ClO + NO_2 + M \rightarrow ClONO_2 + M \qquad \text{(R5)}$$

and prevents formation of ~~which form~~ reservoir species with longer atmospheric residence times.

The study of HNO_3 interaction with ice in the temperature and pressure ranges typical of the UT/LS is crucial in order to understand the de-nitrification process initiated by reaction (R1) and its effectiveness in the overall ozone destruction mechanism. To this purpose, many research groups (Voigt et al., 2000, 2005; Fahey et al., 2001; Schreiner et al., 2003; Gao et al., 2004; Höpfner et al., 2006) have studied the composition of PSC's using both *in situ* and remote sensing techniques both in the Arctic as well as above Antarctica. A balloon borne experiment at first detected non-crystalline HNO_3 hydrates (Schreiner et al., 1999), later both balloon borne (Voigt et al., 2000; Schreiner et al., 2003) and aircraft campaigns (Voigt et al., 2005) obtained unambiguous proof of the presence of crystalline HNO_3 hydrates (NAT) at altitudes between 18 and 24 km in the Arctic. The presence of β-NAT, through the

identification of type Ia PSC's, has been unambiguously confirmed by Höpfner et al. (2006) using the MIPAS instrument on a satellite platform by comparison of measured limb-emission spectra of polar stratospheric clouds with measured optical constants in the region of the symmetric NO_3 peak at ν_2 = 820 cm^{-1}.

The existence of several crystalline hydrates of nitric acid has been confirmed for several years. Hanson and Mauersberger (1988) have identified two stable hydrates, namely, nitric acid monohydrate (NAM, HNO_3•H_2O) and nitric acid trihydrate (NAT, HNO_3•$3H_2O$) the latter of which is thought to be ~~by measuring the vapour pressure of mixtures of ice and HNO_3. The observed vapour pressures of HNO_3 and H_2O in the polar atmosphere indicate that only NAT may be~~ of atmospheric importance. Several distinct crystalline hydrates of HNO_3 have been found by Ritzhaupt and Devlin (1991) in their work examining the infrared absorption spectrum of thin film samples. By depositing the equilibrium vapours of aqueous HNO_3 solutions of different concentrations at 293 K they observed nitric acid dihydrate (NAD, HNO_3•$2H_2O$), NAM and NAT. Ji and Petit have performed an extensive ~~in-depth and ground-breaking~~ investigation on the thermochemical properties of NAD (Ji and Petit, 1993).

Tolbert and coworkers have also reported infrared absorption spectra of NAM, NAD and NAT in a series of studies. Tolbert and Middlebrook (1990) have co-condensed calibrated mixtures of H_2O/HNO_3 vapours onto a cryostat ~~cold support~~ and assigned the absorption spectra of the growing thin films to nitric acid hydrates (NAM, NAD or NAT) according to the ratio of the dosing gases. Koehler et al. (1992) have observed the Fourier transform infrared (FTIR) absorption spectra in transmission of nitric acid hydrate thin films and measured their composition using temperature-programmed desorption (TPD). They confirmed the previously assigned spectra of NAD and NAM. They were also the first to observe two distinct structures of NAT: a low-temperature and metastable structure ~~they~~ called α-NAT whose structure has recently been elucidated (Weiss et al., 2016) and a thermodynamically stable high-temperature structure named β-NAT. Middlebrook et al. (1992) observed that NAD consistently converts to β-NAT when exposed to H_2O partial pressures typical of the stratosphere and therefore proposed that NAD is also metastable under stratospheric conditions.

Several other groups have investigated the structure of nitric acid hydrates and published absorption spectra of both α-NAT and β-NAT in the mid-IR range, using grazing incidence Reflection Absorption IR spectroscopy (RAIRS) (Zondlo et al., 1998; Zondlo et al., 2000;

Ortega et al., 2003; Ortega et al., 2006; Herrero et al., 2006; Escribano et al., 2007) and FTIR in transmission (Tso and Leu, 1996; Martin-Llorente et al., 2006; Ortega et al., 2006).

~~The study of the phase diagram of the system H_2O/HNO_3 showed evidence that NAD may as well occur in at least two different structures (Beyer and Hansen, 2002). The two structures are both metastable and convert into NAM and NAT depending on experimental conditions. Grothe et al. (2004) also reported polymorphism of NAD where the formation of α NAD or β NAD strongly depended on the temperature of crystallization.~~

Compared to the molecular properties of the nitric acid hydrates knowledge of the kinetic parameters of trace gases interacting with HNO_3 hydrates is scarce. Middlebrook et al. (1992) have used time-dependent FTIR monitoring of the optical density of growing NAT films during deposition to measure the uptake of H_2O and HNO_3 on NAT. They reported a value of $\gamma_{NAT}(HNO_3) > 0.4$ for HNO_3 net uptake (γ) on NAT at T = 197 K whereas ~~the range~~ $2.0\times10^{-3} \leq \gamma_{NAT}(H_2O) \leq 1.0\times10^{-2}$ is reported for H_2O~~, respectively~~. The range measured for $\gamma_{NAT}(H_2O)$ corresponds to the HNO_3 pressure used during the deposition. Using evaporation experiments in a slow-flow reactor Biermann et al. (1998) measured the accommodation coefficient of H_2O on β-NAT substrates, $\alpha_{\beta-NAT}(H_2O)$, from the thickness of the substrate measured using FTIR absorption. They found no temperature dependence, reporting lower limiting values of $\alpha_{\beta-NAT}(H_2O) = (2.2 – 6.0)\times10^{-2}$ in the ~~temperature~~ range 192-202 K.

Delval and Rossi (2005) have used a multidiagnostic flow reactor, similar to the one used in this work, coupled with a quartz crystal microbalance (QCMB) for the measurement of the evaporation rate of H_2O from α-NAT and β-NAT thin films. They reported a positive temperature dependence of $\alpha_{\alpha-NAT}(H_2O)$ and a negative temperature dependence of $\alpha_{\beta-NAT}(H_2O)$ in the ~~temperature~~ range 179-208 K.

Hanson (1992) also measured the uptake coefficient of HNO_3 on NAT using a cold coated-wall flow tube with HNO_3 deposited on ice condensed on the cold flow tube walls and reported $\gamma_{NAT}(HNO_3) > 0.3$. A rapid uptake was observed which decreased as the surface coverage or dose of HNO_3 increased. Furthermore, the observed steady state partial pressure of HNO_3 over the ice substrate is about a factor of 5 higher than the HNO_3 vapor pressure over NAT and thus indicates that no hydrate was actually formed during the experiments. Therefore, the observed uptake has most likely to be attributed to uptake on other cold surfaces in the flow reactor.

Reinhardt et al. (2003) reported $\gamma_{NAT}(HNO_3) = 0.165$ in the temperature range 160 to 170 K. They used a slow flow reaction cell coupled with DRIFTS (Diffuse Reflectance Infrared Fourier Transform Spectroscopy) for the detection of adsorbed species and downstream FTIR for the detection of gas phase HNO_3.

In the investigation of the properties of binary chemical systems the behavior of the simple single-component systems is an important stepping stone. Hynes et al. (2002) observed continuous uptake of HNO_3 on water-ice films below 215 K and time dependent uptake above 215 K, with the maximum uptake $\gamma_{ice}(HNO_3)$ decreasing from 0.03 at 215 K down to 0.006 at 235 K. They also observed that the uptake of HCl at 218 K on ice surfaces previously dosed with HNO_3 is reversible. Furthermore, the adsorption of HNO_3 on ice surfaces which contained previously adsorbed HCl indicates that HCl is displaced from surface sites by HNO_3.

In this work, the results for the kinetics of H_2O and HNO_3 gas interacting with spectroscopically characterized~~solid~~ HNO_3 hydrates will be presented. The independent measurement of the rate of evaporation R_{ev} [molec s^{-1} cm^{-3}] and the accommodation coefficient α of H_2O and HNO_3 on α- and β-NAT substrates is performed using a combination of steady state and real-~~-~~time pulsed valve experiments. Results on the kinetics of the ternary system HCl on HNO_3 hydrates will also be presented. All experiments reported in this work have been performed using a multidiagnostic stirred flow reactor (SFR) in the molecular flow regime, which has been described in detail before (Chiesa and Rossi, 2013; Iannarelli and Rossi, 2014). In addition, all experiments have been performed under strict mass balance control by considering ~~with a knowledge on~~ how many molecules of HNO_3, HCl and H_2O were present in the gas vs. the condensed phase (including the vessel walls) at any given time. These experiments have been described by Iannarelli and Rossi (2015)~~.~~. Most importantly, the consistency of the accommodation and evaporation kinetics has been checked using the method of thermochemical kinetics (Benson, 1976) by calculating the equilibrium vapor pressure and comparing it with values of published phase diagrams. In addition, the present work is the first to present absolute rates of evaporation of all involved constituents (H_2O, HNO_3, HCl) thus enabling predictions on evaporative lifetimes of ice particles under atmospheric conditions.

Formatiert: Tiefgestellt

Formatiert: Tiefgestellt

2 Experimental Apparatus and Methodology

2.1 Experimental Apparatus and Growth Protocols

Figure 1 shows a diagram~~schematic~~ of the reactor used in this work with the experimental diagnostic tools and Table 1 reports its characteristic parameters. Briefly, it consists of a low-pressure stainless steel reactor, which may be used under static (all valves closed) or stirred flow (gate valve closed, leak valves open) conditions. We use absolute total pressure measurement and calibrated residual gas mass spectrometry (MS) to monitor the gas phase and FTIR spectroscopy in transmission for the condensed phase. Thin solid films of up to 2 µm thickness are grown on a temperature controlled Si substrate and an average of 8 scans are recorded at 4 cm^{-1} resolution in the spectral range 700-4000 cm^{-1} at typical total scan time of 45-60 s.

The 1" Si window is the only cold spot in the reactor exposed to admitted gases and therefore the only place where gas condensation occurs. This allows the establishment of a 1:1 correspondence between the thin film composition and the changes in the gas partial pressures in the reactor. Experimental proof of mass balance has previously been reported for this setup (Delval et al., 2003; Chiesa and Rossi, 2013; Iannarelli and Rossi, 2014; 2015).

The introduction of HNO_3 in the system forced us to slightly modify the inlet system used previously (Iannarelli and Rossi, 2014) in order to take into account the fact that HNO_3 is an extremely "sticky" molecule that interacts with the internal surfaces of the reservoir vessel of the inlet system as well as with the reactor walls of the SFR (Iannarelli and Rossi, 2015). We therefore minimized the volume of the admission system and only retained the absolutely necessary total pressure gauge for measuring the absolute inlet flow rate (molecule s^{-1}).

Formatiert: Hochgestellt

Similarly to the case of HCl and H_2O (Iannarelli and Rossi, 2014) we have described the HNO_3 interaction with the reactor walls using a Langmuir adsorption isotherm and determined the concentration of HNO_3 in the ice sample after calibration of HNO_3 following the methodology described in Iannarelli and Rossi (2015). Table 2 reports the values of the fit parameters of the Langmuir adsorption isotherms for all the gases interacting with the stainless steel (SS304) internal surfaces of the SFR. Binary combinations of HNO_3/H_2O and HCl/H_2O have been used to describe the interaction of the acidic probe gas with the vessel walls in the presence of H_2O vapor.

The protocol for the growth of α-NAT, β-NAT and NAD thin films has also been described in Iannarelli and Rossi (2015). Briefly, the protocol for either hydrate always starts with the growth of pure ice: the chamber is backfilled under SFR conditions with water vapor at flow rates between 5×10^{15} and 10^{16} molec s^{-1}, corresponding to a partial pressure of H_2O, $p(H_2O)$ between 4.7 and 9.4×10^{-4} Torr (both apertures open), with the Si substrate held at temperature in the range 167 to 175 K. The pure ice film grows on both sides of the Si substrate to a thickness of typically 1 μm until~~and~~ the H_2O flow is halted (Iannarelli and Rossi, 2014). The temperature of the support is then set to the value used for the growth of the desired HNO_3 hydrate at a typical rate of ±0.3 K min^{-1}.

The growth protocols for α-NAT and NAD are similar and start after the deposition of a pure ice film: the temperature of the Si substrate is held in the range 180 to 185 K for α-NAT and at 168 K for NAD. The sample is exposed for approximately 10 min at SFR conditions to HNO_3 vapor at flow rates in the range 3 to 7×10^{14} molecule s^{-1} for α-NAT and 9×10^{14} molecule s^{-1} for NAD. The typical total dose of HNO_3 admitted into the reactor is 2 to 3×10^{17} molecules and 4×10^{17} molecules for α-NAT and NAD, respectively, with almost all of it adsorbed onto the ice film. In both cases, we observe the formation of a new phase after approximately 5 min of exposure as shown in the change of the FTIR absorption spectrum. The present experimental conditions seem to show that no nucleation barrier is present for α-NAT and NAD growth, in agreement with previous works (Hanson, 1992; Middlebrook et al., 1992; Biermann et al., 1998). In contrast, Zondlo et al. (2000) have shown that crystalline growth occurs via an intermediate stage of supercooled H_2O/HNO_3 liquid forming over ice. After exposure the temperature of the substrate is set to the desired value for the kinetic experiments on α-NAT or NAD as a substrate.

The protocol for the growth of β-NAT is different compared to NAD and α-NAT hydrates as it only starts after the growth of an α-NAT film. After the HNO_3 flow has been halted, the α-NAT/ice system is set to static conditions and the temperature increased to 195 K. During the temperature increase the α-NAT film converts to β-NAT as shown by means of FTIR spectroscopy (Koehler et al., 1992; Iannarelli and Rossi, 2015), and once the conversion is completed the temperature is set to the desired value to start the kinetic experiments using β-NAT as substrate. Typical growth protocols under mass balance control showing both the FTIR transmission as well as the corresponding MS signals of HNO_3 as a function of deposition time have been published previously (Iannarelli and Rossi, 2015).

In all samples used for this work, we never have a pure HNO_3 hydrate because we always operate under conditions of excess or comparable amounts of pure ice. Excess ice has been shown to have a stabilizing effect on both α-NAT and β-NAT (Weiss et al., 2016) and in all our experiments the presence of excess ice has been confirmed by~~from~~ FTIR spectra (Iannarelli and Rossi, 2015).

2.2 Experimental Methodology

The experimental methodology used in this work is an extension of the methodology reported in Iannarelli and Rossi (2014) where the combination of real-time pulsed valve and steady state experiments allowed the independent measurement of the rate of evaporation R_{ev} [molec s^{-1} cm^{-3}] and the accommodation coefficient α of HCl and H_2O on crystalline and amorphous HCl hydrates.

For each gas X (X = H_2O, HNO_3, HCl) admitted into the reactor in the presence of ice, the following flow balance equation holds at steady state:

$$F_{in}(X) + F_{des}(X) + F_{ev}(X) = F_{SS}(X) + F_{ads,w}(X) + F_{ads,ice}(X) \qquad (1)$$

All terms in Equation (1) are flow rates in molec s^{-1} with the terms from left to right corresponding to ~~: F_{in} is the flow rate of~~ molecules admitted into the reactor (F_{in}), ~~F_{des} the flow rate of~~ molecules desorbing from the reactor walls (F_{des}), ~~F_{ev} the flow rate of~~ molecules evaporating from the ice surface (F_{ev}), ~~F_{SS} the flow rate of~~ molecules effusing through the leak valve into the MS chamber (F_{SS}), ~~$F_{ads,w}$ the flow rate of~~ molecules adsorbing onto the reactor walls ($F_{ads,w}$) and ~~$F_{ads,ice}$ the flow rate of~~ molecules adsorbing onto the ice film ($F_{ads,ice}$).

Formatiert: Tiefgestellt

Under the assumption that the adsorption onto the walls may be described as a Langmuir-type adsorption, Eq. (1) may be expressed as follows for a gas X:

$$V \cdot R_{in}(X) + N_{TOT} \cdot k_{des,w}(X) \cdot \theta + V \cdot R_{ev}(X) =$$
$$= V \cdot R_{SS}(X) + S_w \cdot \frac{\alpha_w(X) \cdot \bar{c}}{4}(1-\theta)\,[X]_{SS} + S_{film} \cdot \frac{\alpha_{film}(X) \cdot \bar{c}}{4}[X]_{SS} \qquad (2)$$

where V is the reactor volume in cm^3, $R_{in}(X)$ the rate of molecules X admitted into the chamber in molec·s^{-1}·cm^{-3}, N_{TOT} the total number of molecules X adsorbed on~~to~~ the reactor walls, $k_{des,w}(X)$ the desorption rate constant from the reactor walls in s^{-1}, θ the fractional surface coverage in terms of a molecular monolayer, $R_{ev}(X)$ the rate of evaporation of X from the ice in molec·s^{-1}·cm^{-3}, $R_{SS}(X)$ the rate of effusion through the leak valve in molec·s^{-1}·cm^{-3},

S_w and S_{film} the surfaces of the reactor walls and the thin film in cm^2, $\alpha_w(X)$ and $\alpha_{film}(X)$ the accommodation coefficients of X on the walls and on the thin film, $[X]_{SS}$ the concentration at steady state in molec cm^{-3} and $\bar{c}$ the mean thermal velocity of a molecule in $cm \cdot s^{-1}$, respectively. The mathematical derivation of Eq. (2) may be found in Supplement B of Iannarelli and Rossi (2014).

Pulsed valve (PV) experiments and Langmuir adsorption isotherms have been used in order to measure $k_{des,w}(X)$ and $\alpha_w(X)$ (Iannarelli and Rossi, 2014), leaving only two unknown parameters in Eq. (2): $R_{ev}(X)$ and $\alpha_{film}(X)$. The Langmuir adsorption isotherms are shown in Figure S1 of Supplement A whereas the parameters for the best fit are reported in Table 2.

In the case of H_2O, once the selected substrate has been grown according to the protocol briefly described above, the film is set to a chosen temperature. After steady state conditions are established, a series of H_2O pulses are admitted into the reactor. The exponential decay of the MS signal at m/z 18 (k_d) is given by the sum of the measured k_{esc}, the adsorption rate constant on the walls (k_w) and the adsorption rate constant (k_c) onto the ice, namely $k_d = k_{esc} + k_w + k_c$, in the aftermath of a pulse. The accommodation coefficient $\alpha_{film}(H_2O)$ may ~~be~~ then be calculated according to Eq. (3):

$$\alpha_{film}(H_2O) = \frac{k_c(H_2O)}{\omega(H_2O)} \quad (3)$$

where $\omega(H_2O)$ is the calculated gas-surface collision frequency in s^{-1} and is reported in Table 1.

The steady state MS signal established before the pulse series represents the calibrated flow rate of molecules effusing through the leak valve, $F_{SS}(H_2O)$, in Eq. (1) and ~~it~~ may be used to calculate the concentration at steady state $[X]_{SS}$ according to Eq. (4):

$$[X]_{SS} = \frac{F_{SS}(X)}{k_{esc}(X)V} \quad (4)$$

where $k_{esc}(X)$ is the effusion rate constant of gas X out of the reactor in s^{-1} (see Table 1). Finally, $[X]_{SS}$ is used to calculate $R_{ev}(X)$ using Eq. (2).

Subsequently, the film is set to a higher temperature, $F_{SS}(H_2O)$ is recorded and a series of H_2O pulses applied to the same ice sample. This experimental protocol has been repeated for each measured point in the temperature interval of interest.

Under the present experimental conditions, PV experiments of HNO_3 leading to transient supersaturation of HNO_3 are hampered by excessive pulse broadening, most probably owing to the strong adsorption of HNO_3 on ice and the stainless steel vessel walls that makes the observation and interpretation of a HNO_3 pulse difficult for low doses in the presence of ice. In this case the advantage of the PV technique as a real-time method of observation is lost.

Therefore, in order to measure the kinetics of HNO_3 gas in the presence of α-NAT, β-NAT and NAD ice films we have used the two-orifice method first described by Pratte et al. (2006). It has been modified to take into account the interaction of HNO_3 with the internal walls of the SFR. The two-orifice method has also been used to measure the kinetics of H_2O on HNO_3 hydrates in order to compare these results with the results of PV experiments for H_2O.

The two-orifice (TO) method allows the separation of the rate of evaporation $R_{ev}(X)$ and the condensation rate constant $k_c(X)$ of a gas X by choosing two different escape orifices and measuring the corresponding value of concentration $[X]_{SS}$ at steady state of gas X inside the reactor. By alternatively opening the small orifice (S) and both orifices (M) (see Figure 1), two steady state equations hold for a probe gas X which are reported in Eqs. (5) and (6) taking into account the interaction with the reactor walls:

$$R_{ev}(X) + \frac{N_{TOT}}{V} \cdot k_{des,w}(X) \cdot \theta = (k_c(X) + k_{esc}^{S}(X)) \cdot [X]_{SS}^{S} + \frac{k_w(X)}{V} \cdot (1-\theta) \cdot [X]_{SS}^{S} \quad (5)$$

$$R_{ev}(X) + \frac{N_{TOT}}{V} \cdot k_{des,w}(X) \cdot \theta = (k_c(X) + k_{esc}^{M}(X)) \cdot [X]_{SS}^{M} + \frac{k_w(X)}{V} \cdot (1-\theta) \cdot [X]_{SS}^{M} \quad (6)$$

where the superscripts~~ indexes~~ indicate small orifice only (S) or both orifices (M) open, respectively.

The kinetic parameters $R_{ev}(X)$ and $k_c(X)$ are calculated from Eqs. (7) and (8) as follows:

$$k_c(X) = \frac{k_{esc}^{M}(X) \cdot [X]_{SS}^{M} - k_{esc}^{S}(X) \cdot [X]_{SS}^{S}}{[X]_{SS}^{S} - [X]_{SS}^{M}} - k_w(X) \cdot (1-\theta) \quad (7)$$

$$R_{ev}(X) = \frac{(k_{esc}^{M}(X) - k_{esc}^{S}(X)) \cdot [X]_{SS}^{S} \cdot [X]_{SS}^{M}}{[X]_{SS}^{S} - [X]_{SS}^{M}} - \frac{N_{TOT}}{V} \cdot k_{des,w}(X) \cdot \theta \quad (8)$$

This method leads to larger uncertainties for both $R_{ev}(X)$ and $k_c(X)$ compared to the combined PV and steady state method used before. The reason lies in the fact that two similarly large numbers, namely $[X]_{SS}^{S}$ and $[X]_{SS}^{M}$, are subtracted in the denominators of equations Eqs. (7) and (8) leading to a small and therefore~~n~~ uncertain value of $k_c(X)$ and $R_{ev}(X)$. In other words,

the noise in the signal from the MS is such that the two data sets for the small orifice and both orifices open are sometimes insufficiently linearly independent of each other within experimental uncertainty.

We also used the combination of real-time PV and steady state experiments using HCl as a probe gas and applied the experimental method described previously in order to measure the kinetics of HCl, R_{ev}(HCl) and α(HCl), in the presence of α-NAT and β-NAT ice films.

Once the kinetics $R_{ev}(X)$ and $k_c(X)$ have been measured using the combination of PV and steady state experiments (H_2O, HCl) or the two-orifice method (HNO_3, H_2O), we may calculate the equilibrium vapo~~u~~r pressure $P_{eq}(X)$ for each gas according to Eq. (9):

$$P_{eq}(X) = \frac{R_{ev}(X)}{k_c(X)} \cdot \frac{RT}{N_A} \qquad (9)$$

where R is the molar gas constant in cm^3 Torr K^{-1} mol^{-1}, T the temperature of the thin film in K and N_A Avogadro's constant in molec mol^{-1}.

3 Results

3.1 Crystalline α-NAT Thin Films

The kinetic results for the heterogeneous interaction of H_2O and HNO_3 with α-NAT and NAD thin films obtained in PV and TO experiments are displayed in Figure 2. Full symbols represent PV experiments: full red circles correspond to experiments on α-NAT substrates, and full green squares to experiments on NAD substrates. Empty symbols represent TO experiments with red circles representing H_2O and black triangles HNO_3 results. Pure ice experiments are displayed as inverse blue triangles for comparison purposes. The calculated relative error for PV experiments is 30% whereas for TO experiments we estimate a relative error of 60%. We refrain at this point from showing raw data (FTIR absorption spectra and MS data as a function of time) because representative samples have been shown by Iannarelli and Rossi (2015) for α- and β-NAT. We will defer the presentation of raw data on the interaction of HCl on α- and β-NAT to Section 3.3 below.

Figure 2a shows the measured accommodation coefficients $\alpha_{\alpha-NAT}(X)$, (X = H_2O, HNO_3), as a function of temperature. $\alpha_{\alpha-NAT}(H_2O)$ in PV experiments (full red circles) decreases as a function of temperature in the range 167-188.5 K, varying from 0.08 at 167 K to 3.1×10^{-3} at 188.5 K, which is a factor of 30 lower than $\alpha_{ice}(H_2O)$ on pure ice at the same temperature. The scatter in the data is not an artifact and is due to the sample-to-sample variability of the

Formatiert: Schriftart: Symbol

Formatiert: Schriftart: Symbol

Formatiert: Schriftart: Symbol

Formatiert: Schriftart: Symbol

crystalline samples we use and the randomness of the crystalline nucleation process. The variability may be in surface composition, morphology and smoothness as shown in previous studies (McNeill et al., 2007; Iannarelli and Rossi, 2014).

$\alpha_{\alpha-\mathrm{NAT}}(H_2O)$ in TO experiments (empty red circles) yields different results. For temperatures lower than 185 K it is equal to $\alpha_{\alpha-\mathrm{NAT}}(H_2O)$ on α-NAT in PV experiments within experimental error. For temperatures higher than 185 K $\alpha_{\alpha-\mathrm{NAT}}(H_2O)$ increases as a function of temperature in contrast to results of PV experiments (full red circles) varying from 8×10^{-3} at 183 K to 0.08 at 193.5 K, being equal to $\alpha_{ice}(H_2O)$ on pure ice within experimental error at the highest temperature. This result compares favorably with the results of Delval and Rossi (2005) which showed a positive temperature dependence of $\alpha_{\alpha-\mathrm{NAT}}(H_2O)$ in the temperature range 182-207 K. $\alpha_{\mathrm{NAD}}(H_2O)$ in PV experiments (~~green~~ full green squares) is equal within experimental error to $\alpha_{\alpha-\mathrm{NAT}}(H_2O)$.

$\alpha_{\alpha-\mathrm{NAT}}(HNO_3)$ (black empty triangles) increases as a function of temperature in the measured temperature range from a value of approximately 0.005 at 181 K to a value of 0.13 at 188 K. The narrow temperature range follows from the high uncertainties of the two-orifice method at low temperatures and the increasingly rapid conversion of α-NAT to β-NAT at high temperatures. These values are lower by a factor of 2 to 40 compared to the preferred values indicated by the IUPAC Subcommittee on Gas Kinetic Data Evaluation (Crowley et al., 2010).

Figure 2b shows results for the rate of evaporation $R_{ev}(X)$ in molec s^{-1} cm^{-3} as a function of temperature. The same symbols as for panel (a) are used. $R_{ev}(H_2O)$ on α-NAT in PV experiments is lower by a factor of 2 compared to $R_{ev}(H_2O)$ on pure ice at temperatures lower than 175 K. For temperatures higher than 175 K, $R_{ev}(H_2O)$ on α-NAT is lower on average by up to a factor of 50 compared to $R_{ev}(H_2O)$ on pure ice. This result is very different compared to the previously studied case of HCl amorphous and crystalline hexahydrate using the same apparatus (Iannarelli and Rossi, 2013), where the evaporation of H_2O takes place at a rate characteristic of pure ice despite the presence of adsorbed HCl on the ice and is in agreement with the findings of Delval and Rossi (2005).

$R_{ev}(H_2O)$ on α-NAT measured using the TO method is equal within experimental error to $R_{ev}(H_2O)$ obtained in PV experiments. $R_{ev}(H_2O)$ on NAD is equal to within experimental error to $R_{ev}(H_2O)$ on α-NAT. The full black line shows the rate of evaporation of pure water for the system in use, calculated from literature results of the equilibrium vapor pressure

(Marti and Mauersberger, 1993) using α = 1, whereas the dashed black line represents extrapolated values of $R_{ev}(H_2O)$ for temperatures lower than 173 K using the expression provided by Mauersberger and coworkers (Marti and Mauersberger, 1993; Mauersberger and Krankowsky, 2003).

Figure 2c shows the results for $P_{eq}(X)$ in Torr calculated according to Eq. (9) for both H_2O and HNO_3 as a function of temperature. The same symbols as in panels (a) and (b) are used. $P_{eq}(H_2O)$ of α-NAT calculated from the kinetic parameters measured in PV experiments is lower by a factor of approximately 3 compared to $P_{eq}(H_2O)$ on pure ice at temperatures higher than 180 K. For temperatures lower than 180 K $P_{eq}(H_2O)$ of α-NAT is close to $P_{eq}(H_2O)$ of pure ice because the present samples are water-rich (Molina, 1994) with a HNO_3 mole fraction of less than 10%.

$P_{eq}(H_2O)$ of α-NAT calculated from the results of TO experiments is lower by up to a factor of 10 compared to $P_{eq}(H_2O)$ of pure ice in the temperature range 180-193.5 K. At temperatures lower than 180 K, $P_{eq}(H_2O)$ of α-NAT from TO experiments is equal within experimental error to $P_{eq}(H_2O)$ of α-NAT in PV experiments. $P_{eq}(HNO_3)$ of α-NAT is lower by a factor of 1000 in the temperature range 181-188 K compared to $P_{eq}(H_2O)$ on pure ice.

The values obtained for the equilibrium vapor pressure have been compared with the HNO_3/H_2O phase diagram constructed by McElroy et al. (1986); Hamill et al. (1988); Molina (1994). Figure 3 shows the results for α-NAT and metastable NAD films, PV and TO experiments. The solid lines represent the coexistence conditions for two phases and the dashed lines represent vapor pressures of liquids with composition given as % (w/w) of HNO_3. The shaded rectangular area represents typical polar stratospheric conditions. The slope m of the coexistence lines depends on the difference of the enthalpies of sublimation of the two acid hydrate species, namely NAM and NAT, according to Eq. (10) (Wooldridge et al., 1995):

$$m = \frac{\Delta H^1_{subl} - \Delta H^2_{subl}}{(n_1 - n_2)\,R} \qquad (10)$$

where ΔH^1_{subl} and ΔH^2_{subl} are the enthalpies of sublimation of the acid hydrates in kJ/mol, n_1 and n_2 the number of water molecules of the respective hydrate and R is the gas constant in J mol^{-1} K^{-1}. The slope of the ice/NAT coexistence line is calculated from Wooldridge et al.

(1995) as $m_{ice/NAT}$ = (50.9 kJ/mol)/R and for ~~the slope of the~~ NAT/NAM ~~coexistence line is calculated as~~ $m_{NAT/NAM}$ = (55.9 kJ/mol)/R.

All α-NAT experiments lie in the existence area of nitric acid trihydrate, as expected. On the other hand, α-NAT under polar stratospheric conditions (shaded rectangular area) is unstable and starts to convert into the stable β-NAT phase (Koehler et al., 1992). The small number of α-NAT samples we reported in the shaded gray area is further confirmation of results reported in the literature because lower temperatures are needed to slow down the conversion of α to β-NAT. NAD samples are expected to lie closer to the monohydrate region, given their composition close to the H_2O:HNO_3 = 2:1 stoichiometry (Iannarelli and Rossi, 2015). Nevertheless, the pure ice phase is still dominant in the present~~our~~ samples and all ~~our~~ samples are water-rich (Molina, 1994) with a HNO_3 mole fraction ~~, even in NAD films,~~ of less than 10%. even in NAD films.

Formatiert: Schriftart: Symbol

Formatiert: Schriftart: Symbol

3.2 Crystalline β-NAT Thin Films

The results for β-NAT thin films obtained in PV and TO experiments are displayed in Figure 4. Full and empty red squares represent PV and TO experiments, respectively, with red squares representing H_2O and black triangles HNO_3 results. Pure ice experiments are displayed as inverse blue triangles for comparison. ~~The calculated relative error for PV experiments is 30% whereas for TO experiments we estimate a relative error of 60%.~~

The largest uncertainty in our experiment~~s~~ is that of the flow rate introduced into the reactor, which is assigned ~~corresponds to~~ a relative error of 25%. The flow rate measurement affects the calibration of the MS and therefore the measurement of all the concentrations in the reactor (Eq. 4). Therefore, we estimate a global relative error of 30% for PV experiments and double this uncertainty for TO experiments because Equations (7) and (8) imply a difference of two large numbers in many cases, as discussed above. We therefore assign a global 60% relative error to results obtained in TO experiments.

Formatiert: Schriftart: 12 Pt.

Figure 4a shows the measured $\alpha_{\beta-NAT}(X)$ as a function of temperature: ~~.~~ $\alpha_{\beta-NAT}(H_2O)$ resulting from~~in~~ PV experiments (full red squares) is~~shows~~ scattered similar to ~~the case of~~ $\alpha_{HH}(HCl)$ on crystalline HCl hexahydrate (Iannarelli and Rossi, 2014) ~~. Also in this case, a variation of~~ up to a factor of 10 for results at the same temperature ~~is observed~~. We may interpret this result akin to ~~like in~~ the HCl hexahydrate case where the scatter may be caused by the variability of the surface composition, the morphology or the smoothness of the ice

surface (McNeill et al., 2007). Similar results have recently been presented by Moussa et al. (2013) regarding the nitric acid-induced surface disorder on ice. In any case, all results show that $\alpha_{\beta-NAT}(H_2O)$ is at least a factor of 10 lower than $\alpha_{ice}(H_2O)$ on pure ice in the temperature range 182-200 K.

$\alpha_{\beta-NAT}(H_2O)$ in TO experiments (empty red squares) on the other hand, increases as a function of temperature in the temperature range 182-198 K varying from 0.013 at 182 K to approximately 0.1 at 198 K, being equal at the highest temperature to $\alpha_{ice}(H_2O)$ on pure ice within experimental error. This result is in contrast to Delval and Rossi (2005) who report a negative temperature dependence of $\alpha_{\beta-NAT}(H_2O)$ in the temperature range 182-207 K. A possible reason~~s~~ for the different behavior of PV and TO experiments may be intrinsic in the nature of PV experiments: the ice surface is exposed to a series of pulses of H_2O and the free sites may be saturated before the introduction of each consecutive pulse. We suspect this to~~may~~ be the reason for the discrepancy between PV and TO experiments and we will consider the results of TO experiments as the preferred values of this work despite the larger experimental scatter.

Like $\alpha_{\beta-NAT}(H_2O)$, the values of $\alpha_{\beta-NAT}(HNO_3)$ (black empty triangles) increase as a function of temperature in the measured temperature range from a value of approximately 0.015 at 182 K to a value of 0.08 at 195.5 K. However, the values have a large estimated uncertainty. These values are lower by a factor of 2 to 10 compared to the preferred values indicated by the IUPAC Subcommittee on Gas Kinetic Data Evaluation (Crowley et al., 2010) in the temperature range 190 to 200 K.

Figure 4b shows results for $R_{ev}(X)$ in molec s^{-1} cm^{-3} as a function of temperature. The same symbols as in panel (a) are used. $R_{ev}(H_2O)$ on β-NAT in PV experiments is lower by a factor of 50 compared to $R_{ev}(H_2O)$ on pure ice in the temperature range 182-200 K. As in the case of α-NAT, this result is very different compared to the case of HCl hydrates studied before using the same apparatus (Iannarelli and Rossi, 2013) where the evaporation of H_2O is not influenced by the presence of adsorbed HCl on the ice and takes place at a rate characteristic of pure ice for all HCl concentrations used.

$R_{ev}(H_2O)$ on β-NAT measured using the TO method is close to $R_{ev}(H_2O)$ obtained in PV experiments, the former being approximately a factor of 2 higher. $R_{ev}(HNO_3)$ on β-NAT increases in the temperature range 182-195.5 K with a steeper slope compared to $R_{ev}(H_2O)$,

the former being smaller by approximately a factor of 1000 at 182 K~~low~~ and 50 at 196 K ~~higher temperature~~ compared to $R_{ev}(H_2O)$ of β-NAT. It varies from 2×10^8 at 182 K to 8.5×10^9 molec s^{-1} cm^{-3} at 195.5 K.

Figure 4c shows the results for $P_{eq}(X)$ in Torr calculated according to Eq. (9) for both H_2O and HNO_3 as a function of temperature. The same symbols as in panels (a) and (b) are used. $P_{eq}(H_2O)$ of β-NAT calculated from the results of TO experiments is lower by up to a factor of 10 in the middle of the covered T-range compared to $P_{eq}(H_2O)$ of pure ice in the temperature range 182-195.5 K. $P_{eq}(H_2O)$ of β-NAT calculated from the kinetic parameters measured in PV agrees with TO experiments within experimental uncertainty. Saturation effects in PV experiments will affect both the accommodation (α) and evaporation (J_{ev}) process to the same extent such that P_{eq} should be invariant to the chosen experimental procedure (PV or TO). However, there is a noticeable scatter in $P_{eq}(H_2O)$ for β-NAT on display in Figure 4c which presumably reflects the range of different compositions of the binary HNO_3/H_2O system. According to Gibb's Phase Rule we have three phases and two components which leads to a single degree of freedom for the system. At constant temperature different HNO_3/H_2O mixing ratios will lead to different values of $P_{eq}(H_2O)$ if we stay on an isotherm. This corresponds to a vertical cut in the binary phase diagram for β-NAT in Figure 5. It shows that we expect $P_{eq}(H_2O)$ values between a factor of ten or so for the experimental points that "fill" the NAT phase diagram more or less homogeneously within the used T range.

~~The scatter of $P_{eq}(H_2O)$ is of the same magnitude as the scatter of $\alpha_{\beta-NAT}(H_2O)$ and may likewise be explained by an increase in the substrate roughness or inhomogeneous nature of the β-NAT surface owing to exposure to repetitive transient saturation of H_2O in the aftermath of each pulse.~~ In addition,

Figure 5 shows ~~the HNO_3/H_2O phase diagram with the results obtained for β-NAT films: all β-NAT experiments lie in the existence area of nitric acid trihydrate and~~ that the majority of points are in the rectangular shaded area representing polar stratospheric conditions:~~.~~ ~~As already mentioned,~~ β-NAT is the stable phase under these conditions and our results agree well with the literature (McElroy et al., 1986; Hamill et al., 1988; Molina, 1994; Koehler et al., 1992). A more complete manner to display the binary phase diagram is presented in Figure S5 (Supplementary Information). It shows both the HNO_3 and H_2O partial pressures in one single plot close to selected isotherms marked by straight intersecting dashed lines. It is

Formatiert: Tiefgestellt
Formatiert: Tiefgestellt
Formatiert: Tiefgestellt
Formatiert: Tiefgestellt
Formatiert: Tiefgestellt
Formatiert: Tiefgestellt
Formatiert: Schriftart: Symbol
Formatiert: Tiefgestellt
Formatiert: Tiefgestellt
Formatiert: Tiefgestellt
Formatiert: Tiefgestellt

immediately apparent that both HNO_3 and H_2O partial pressures are comparable to upper tropospheric/lower stratospheric values.

3.3 HCl kinetics on α-NAT and β-NAT Thin Films

As already mentioned, we used a combination of real-time PV and steady state experiments using HCl as probing gas in order to measure the kinetics of HCl interacting with α-NAT and β-NAT ice films. Figure 6 displays raw data from repetitive pulsed dosing of HCl onto an α-NAT/ice substrate as a function of elapsed time. The individual pulses, of which there were twelve and identifiable by sharp peaks on top of the red columns in the lower panel displaying the MS signals of HCl (red, m/e 36), H_2O (blue, m/e 18) and HNO_3 (black, m/e 46) corresponded to (4-5) x 10^{16} molecule per pulse resulting in a total HCl dose of approximately 3 x 10^{17} molecules. This is the dose effectively administered to the α-NAT when the fraction of HCl going to the vessel walls and escaping the SFR has been subtracted. This dose approximately corresponds to 1000 molecular monolayers of HCl adsorbed onto the substrate. The temperature of the cryostat is displayed as the green trace in the lower panel, and with every T-increase the MS steady-state levels of HCl, H_2O and HNO_3 increase concomitantly. (During the pulsed admission of HCl the MS levels of HNO_3 and H_2O are subject to artifacts owing to rapid switching). Turning to the upper panel of Figure 6 we display a series of FTIR transmission spectra from 700 to 4000 cm^{-1} at specific times during the repetitive pulsing experiment which are indicated in the lower panel by a series of color-coded "sp1" and continuing going from red to purple. The principal peak positions have been collected in Table 3 and will be discussed below in terms of changes in the "pure" α-NAT/ice absorption spectra owing to the presence of increasing adsorbed HCl. The enlarged IR-spectral range in the upper panel of Figure 6 displays the effect of the HCl adsorption particularly well by showing a non-monotonic sequence of IR absorption peaks not present in the "pure" reference spectra from Iannarelli and Rossi (2015). The raw MS data from the lower panel of Figure 6 have been used to calculate the kinetic and thermodynamic data displayed in Figure 8.

Figure 7 displays raw data from repetitive pulsed dosing of HCl onto a β-NAT/ice substrate in analogy to Figure 6. The eleven individual pulses corresponded to (6-7) x 10^{16} molecule per pulse resulting in a total HCl dose of approximately 4 x 10^{17} molecules which amounts to 1300 molecular monolayers or so. Like in Figure 6 the upper panel displays a series of color-coded FTIR absorption spectra in transmission with the principal peak positions collected in Table 3. As for Figure 6 the MS steady-state levels at the different temperatures will be used

Formatiert: Tiefgestellt
Formatiert: Tiefgestellt
Formatiert: Schriftart: Symbol
Formatiert: Tiefgestellt
Formatiert: Tiefgestellt
Formatiert: Hochgestellt
Formatiert: Hochgestellt
Formatiert: Schriftart: Symbol
Formatiert: Tiefgestellt
Formatiert: Tiefgestellt
Formatiert: Tiefgestellt
Formatiert: Tiefgestellt
Formatiert: Hochgestellt
Formatiert: Schriftart: Symbol

to derive the kinetic and thermodynamic data of Figure 9 as a function of temperature. In addition, Figure S6 presents an enlarged graph for the non-exponential decay of a HCl pulse interacting with both α- and β-NAT on a 30 s time scale consisting of a fast and a slowly-decaying portion. The evaluation of such pulsed admission MS signals has been presented in the past (Iannarelli and Rossi, 2014, Supplemental Information (SI)) and the present analysis and fitting of the HCl MS signals follows the same scheme.

A look at Table 3 should provide an answer as to whether or not there is an identifiable spectral fingerprint of HCl adsorbed on α-or β-NAT in the FTIR absorption spectrum of the combined α- or β-NAT/HCl system displayed in Figures 6 and 7. The first column of Table 3 reveals the spectral fingerprint of HCl for α-NAT/HCl in terms of additional peaks (*in italics*) that are not present in the reference spectrum (pure α-NAT) recorded using the identical instrument and presented in the third column. There seem to be two spectral regions where the presence of HCl may be apparent, namely in the 1618-1644 cm^{-1} region corresponding to the broad bending vibration of the proton-ordered waters of hydration (Ritzhaupt and Devlin, 1991; Martin-Llorente et al., 2006), and more importantly, the band at 1328 cm^{-1} that overlaps with the 1339 cm^{-1} vibration, the latter of which is not changing with increasing HCl dose. The series of FTIR absorption spectra displayed in Figure 6 shows the non-monotonous change of intensity at this transition (1328 cm^{-1}): sp1 (red), sp2 (yellow) and sp3 (green) display the growth of a shoulder to the red of the 1375 cm^{-1} peak, sp4 (turquoise), sp5 (blue) and sp6 (purple) show the separate peak in its decline (1328 cm^{-1}) owing to evaporation of HCl together with NAT. For β-NAT the analogous situation is displayed in the second and fourth column of Table 3 and Figure 7. Here the presence of HCl is more discrete within the FTIR absorption spectrum of β-NAT as Table 3 suggests the well-separated peak to the blue of the 3227 cm^{-1} ice peak at 3360 cm^{-1} to be a HCl tracer as it looks very similar to the HCl/H_2O system (Iannarelli and Rossi, 2014; Chiesa and Rossi, 2013). The peaks identified to appear in the FTIR spectrum upon HCl adsorption may be found in the fifth column of Table 3 which displays the principal IR peaks in the reference HCl/H_2O system, except the 1200 cm^{-1} vibration found in column 1 and 2 whose origin remains unclear.

~~The current experimental setup does not allow the measurement of the kinetics of 3 gases at the same time. We therefore~~ In order to restrain the number of independent measurements on this ternary system to a practical level we had to make some assumptions and/or simplifications in order to measure the unknown parameters of Eq. (2) for each gas used.

Formatiert: Schriftart: Symbol
Formatiert: Schriftart: Symbol
Formatiert: Schriftart: Symbol
Formatiert: Schriftart: Symbol
Formatiert: Schriftart: Symbol
Formatiert: Schriftart: Symbol
Formatiert: Schriftart: Kursiv
Formatiert: Schriftart: Symbol
Formatiert: Hochgestellt
Formatiert: Hochgestellt
Formatiert: Hochgestellt
Formatiert: Hochgestellt
Formatiert: Hochgestellt
Formatiert: Hochgestellt
Formatiert: Schriftart: Symbol
Formatiert: Schriftart: Symbol
Formatiert: Hochgestellt
Formatiert: Hochgestellt
Formatiert: Tiefgestellt
Formatiert: Tiefgestellt
Formatiert: Hochgestellt

Specifically, we made the following reasonable assumptions, both for α-NAT and β-NAT substrates which have been experimentally verified in laboratory experiments:

- $R_{ev}(H_2O)$ on NAT remains unchanged in the presence of HCl
- $\alpha_{NAT}(H_2O)$ remains unchanged in the presence of HCl
- $\alpha_{NAT}(HNO_3)$ remains unchanged in the presence of HCl

Under these assumptions, no additional measurements of the heterogeneous kinetics of H_2O in the presence of HCl have been performed. We have measured the steady-state flow $F_{SS}(HNO_3)$ before each HCl pulse series and used previously measured $\alpha_{\alpha-NAT}(HNO_3)$ and $\alpha_{\beta-NAT}(HNO_3)$ from TO experiments on α-NAT and β-NAT phases in order to calculate $R_{ev}(HNO_3)$ and $P_{eq}(HNO_3)$ according to Eqs. (8) and (9) in HCl-PV experiments as well. As a net result we measure or calculate the following kinetic parameters for α-NAT and β-NAT substrates: $R_{ev}(HCl)$, $\alpha_{NAT}(HCl)$ and $R_{ev}(HNO_3)$ in the presence of HCl.

~~Figure 6~~8 displays the results of HCl-PV experiments on α-NAT substrates. Full red diamonds represent the results for HCl whereas full black circles represent HNO_3 results using $\alpha_{\alpha-NAT}(HNO_3)$ from TO experiments and $F_{SS}(HNO_3)$ from HCl-PV experiments. Empty black triangles represent results for HNO_3 in TO experiments reported from Figure 2 for comparison.

~~Figure 6~~8a displays the measured $\alpha_{\alpha-NAT}(X)$ as a function of temperature. $\alpha_{\alpha-NAT}(HCl)$ (full red diamonds) slightly decreases as a function of temperature in the range 177.5-199.5 K, being equal to $\alpha_{ice}(H_2O)$ on pure ice at low temperatures and lower by a factor of 4 at T = 199.5 K. The decrease seems to be significant. Values of $\alpha_{\alpha-NAT}(HNO_3)$ measured in TO experiments in the absence of HCl are reported as empty black triangles in agreement with the third above-listed assumptions. We used these values in order to calculate $R_{ev}(HNO_3)$ and $P_{eq}(HNO_3)$ in the presence of HCl.

~~Figure 6~~8b shows results for $R_{ev}(X)$ in molec s^{-1} cm^{-3} as a function of temperature. The same symbols as in panel (a) are used. $R_{ev}(HCl)$ on α-NAT slightly increases as a function of temperature, but ~~and~~ is lower by a factor of 1000 in the measured temperature range 177.5-199.5 K compared to $R_{ev}(H_2O)$ on pure ice. $R_{ev}(HNO_3)$ increases as a function of temperature, varying from 1×10^8 at 181 K to 9×10^9 molec s^{-1} cm^{-3} at 189 K. The presence of HCl does not have any effect on the rate of evaporation of HNO_3 from α-NAT films: we observe no increase of $F_{ss}(HNO_3)$ following HCl pulses and $R_{ev}(HNO_3)$ in the presence of adsorbed HCl

molecules (full black circles) is identical within experimental error to $R_{ev}(HNO_3)$ of α-NAT films free of adsorbed HCl (empty black triangles). However, this result is contingent upon the assumptions listed before, namely $\alpha_{\alpha-NAT}(HNO_3)$ being independent of the presence or absence of HCl.

~~Figure 6~~8c shows the results for $P_{eq}(X)$ in Torr calculated according to Eq. (9) for both HCl and HNO_3 as a function of temperature. The same symbols as in panel (a) and (b) are used. $P_{eq}(HCl)$ for HCl-doped~~of~~ α-NAT is lower by a factor of approximately 100 compared to $P_{eq}(H_2O)$ on pure ice in the measured temperature range. A comparison with the results of $P_{eq}(HCl)$ of crystalline HCl hexahydrate and amorphous HCl/H_2O mixtures calculated using the same experimental methodology (Iannarelli and Rossi, 2014) shows that $P_{eq}(HCl)$ of HCl-doped α-NAT is lower by a factor of approximately 10 compared to $P_{eq}(HCl)$ of crystalline hexahydrate in the overlapping temperature range (177.5-193.5 K).

$P_{eq}(HCl)$ of amorphous HCl/H_2O mixtures is higher by a factor of 20 compared to $P_{eq}(HCl)$ of HCl-doped α-NAT at low temperatures (177.5 K) with the difference being constant or slightly decreasing at high temperatures (199.5 K) where $P_{eq}(HCl)$ of the amorphous mixture is only a factor of 4 higher than $P_{eq}(HCl)$ of α-NAT.

$P_{eq}(HNO_3)$ on HCl-doped α-NAT films is equal within experimental error to $P_{eq}(HNO_3)$ of α-NAT films free of adsorbed HCl. It is lower by a factor of 1000 compared to $P_{eq}(H_2O)$ on pure ice in the measured temperature range 177.5-199.5 K.

~~Figure 7~~9a (symbols have the same meaning as in ~~Figure 6~~8) shows the measured values of $\alpha_{\beta-NAT}(X)$ as a function of temperature. $\alpha_{\beta-NAT}(HCl)$ slightly decreases as a function of temperature in the range 177-201 K, varying from 0.025 at 177 K to 0.016 at 201 K which may or may not be significant. As for the case of α-NAT, we assume that $\alpha_{\beta-NAT}(HNO_3)$ (empty black triangles) equals the measured values of $\alpha_{\beta-NAT}(HNO_3)$ on HCl-free β-NAT in two-orifice experiments whose results are displayed in Figure 4a.

~~Figure 7~~9b shows results for the $R_{ev}(X)$ in molec s^{-1} cm^{-3} as a function of temperature. The same symbols as in Panel (a) are used. $R_{ev}(HCl)$ on β-NAT is equal at higher temperature within experimental uncertainty to $R_{ev}(HCl)$ on α-NAT and is lower by a factor of 1000 in the temperature range 177- 201 K compared to $R_{ev}(H_2O)$ on pure ice. $R_{ev}(HNO_3)$ on HCl-doped β-NAT films, being equal within experimental error to $R_{ev}(HNO_3)$ of undoped β-NAT films,

indicates that adsorbed HCl molecules seem to have no effect on the rate of evaporation of HNO_3 from β-NAT films in the presence of HCl as well, at least in the given T range.

~~Figure 7~~9c shows the results for $P_{eq}(X)$ in Torr calculated according to Eq. (9) for both HCl and HNO_3 as a function of temperature. The same symbols as in panel (a) and (b) are used. $P_{eq}(HCl)$ of HCl-doped β-NAT is lower by a factor of approximately 100 compared to $P_{eq}(H_2O)$ on pure ice. $P_{eq}(HCl)$ of HCl-doped β-NAT is identical within experimental uncertainty to $P_{eq}(HCl)$ of HCl-doped α-NAT in the measured temperature range 177-201 K and the same observations are valid when comparing $P_{eq}(HCl)$ of crystalline HCl hexahydrate with amorphous HCl/H_2O mixtures (Iannarelli and Rossi, 2014).

4 Discussion

In this work we have been able to grow HNO_3 hydrates at temperatures relevant to the stratosphere with tight control on the deposition conditions whose details have been published by Iannarelli and Rossi (2015) as far as the mass balance is concerned. Spontaneous~~Direct~~ crystallization of α-NAT film on pure ice has been observed upon HNO_3 deposition. Under the present~~ system~~ conditions β-NAT was never observed to crystallize directly upon HNO_3 deposition but was always obtained as the stable form after conversion of α-NAT films. Temperatures higher than 185 K are necessary for the conversion to occur on the time scale of the experiments we have performed.

$\alpha_{\alpha-NAT}(H_2O)$ shows two distinct temperature dependent regimes. At temperatures lower than 180-185 K it decreases as a function of temperature reaching a minimum of approximately 0.003 at 185 K as displayed in Figure 2a. For temperatures higher than 185 K, $\alpha_{\alpha-NAT}(H_2O)$ increases as a function of temperature, being equal to $\alpha_{ice}(H_2O)$ on pure ice and $\alpha_{\beta-NAT}(H_2O)$ at 193.5 K. An Arrhenius representation of the evaporative flux $J_{ev}(H_2O)$ (see Table 1) on α-NAT shows two distinct regimes of temperature dependence, as well. ~~Figure 8~~10 reports the results for PV and TO experiments as full and empty red circles, respectively. We keep the two data sets separated for clarity, but the results of PV and TO experiments are indistinguishable within experimental uncertainty in the measured temperature range.

Eqs. (11) and (12) present the two-parameter representations of the Arrhenius lines for $J_{ev}(H_2O)$ displayed in ~~Figure 8~~10. Equations (11) and (12) represent the solid and dashed red lines, respectively, with R = 8.314 J K^{-1} mol^{-1} used throughout:

$$181\ \mathrm{K} \leq \mathrm{T} \leq 193.5\ \mathrm{K}:\ \log \mathrm{J_{ev}}(\mathrm{H_2O})[\mathrm{molec} \cdot \mathrm{cm}^{-2} \cdot \mathrm{s}^{-1}] = (35.9 \pm 2.8) - \frac{(75.3 \pm 9.9) \times 10^3}{2.303\ \mathrm{RT}} \quad (11)$$

$$167\ \mathrm{K} \leq \mathrm{T} \leq 181\ \mathrm{K}:\ \log \mathrm{J_{ev}}(\mathrm{H_2O})[\mathrm{molec} \cdot \mathrm{cm}^{-2} \cdot \mathrm{s}^{-1}] = (15.1 \pm 1.2) - \frac{(3.5 \pm 4.2) \times 10^3}{2.303\ \mathrm{RT}} \quad (12)$$

Table 4 reports a synopsis of the kinetic (J_{ev}) as well as the thermodynamic (P_{eq}) parameters calculated for all experiments of the present work.

The considerable scatter in the kinetic data, reflected in the significant uncertainties of Eqs. (11) and (12), may be explained by the variability of the surface composition of the film as well as the surface roughness and surface disorder of the ice substrates, in analogy to the HCl case (Iannarelli and Rossi, 2014). For HCl the scatter in the kinetic data was thought to be due to the stochastic nature of crystal growth of hexahydrate films compared to amorphous mixtures of HCl/H_2O of similar composition and does not represent a lack of reproducibility.

Moussa et al. (2013) have observed variations of up to a factor of 10 of the HNO_3 vapor pressure of "smooth" ice samples exposed to HNO_3 as a result of induced surface disorder. The exposure of the present samples to repeated high H_2O supersaturation during PV experiments may lead to surface increased disorder due to liquefaction and/or reconstruction. In the high temperature regime we calculate an activation energy for H_2O evaporation $E_{ev}(H_2O)$ = (75.3 ± 9.9) kJ mol^{-1}, and in the low temperature regimes almost no temperature dependence is observed with an activation energy for H_2O evaporation of $E_{ev}(H_2O)$ = (3.5 ± 4.2) kJ mol^{-1}.

The discontinuity in the Arrhenius representation of kinetic parameters has already been observed in pure ice as reported by Chaix et al. (1998); Delval et al. (2003); Delval and Rossi (2004); Pratte et al. (2006). The temperatures at which the discontinuity occurs are higher in previous work: Delval et al. (2003) reported a discontinuity at approximately 208 K in their work on H_2O evaporation from HCl and HBr doped ice substrates. In a quartz crystal microbalance study of H_2O evaporation from pure ice the change in slope is reported at 193 ± 2 K (Delval and Rossi, 2004) comparable with the temperature of 188 ± 2 K reported by Pratte et al. (2006) in their work on the kinetics of H_2O evaporation and condensation on different types of ice.

No clear explanation for this break has yet been advanced. The discontinuity may be an indication of the formation of a new disordered structure similar to the quasi-liquid layer induced by HCl as proposed by McNeill et al. (2006). The observation of the break in pure ice

samples as well, however, strongly suggests that the onset of a quasi-liquid layer may be independent of the presence of HCl and that the history and evolution of the sample play a role in the arrangement of the structure, similarly to the case of the presence of cubic ice at high temperature in common hexagonal ice that finally turned out to be a perturbed hexagonal ice structure (Kuhs et al., 2012).

In the case of β-NAT we have good agreement between PV (dotted line) and TO (solid line) experiments of $P_{eq}(H_2O)$ as shown in the van 't Hoff representation displayed in Figure ~~-~~11

As already mentioned, the ice surface is exposed to a series of pulses of H_2O during PV experiments. The free sites may be saturated before the introduction of each consecutive pulse resulting in the discrepancy between PV and TO experiments. We therefore believe that the results from PV experiments are more precise but less accurate owing to partial surface saturation whereas the TO experiments are less precise but more accurate. We chose the latter as the preferred values of this work despite the larger scatter in the data compared to the PV experiments.

Eqs. (13) and (14) reports the best linear fit for TO and PV experiments on β-NAT displayed in Figure 11, respectively:

Formatiert: Schriftart: Symbol

$$\log P_{eq}(H_2O)[\mathrm{Torr}] = (16.7 \pm 4.9) - \frac{(76.7 \pm 17.7)\times 10^3}{2.303\ \mathrm{RT}} \qquad \text{TO – Preferred} \qquad (13)$$

$$\log P_{eq}(H_2O)[\mathrm{Torr}] = (16.7 \pm 3.0) - \frac{(75.5 \pm 11.1)\times 10^3}{2.303\ \mathrm{RT}} \qquad \text{PV} \qquad (14)$$

The enthalpies of evaporation of H_2O on β-NAT films calculated for the two measurement techniques are $\Delta H^0_{ev,TO}(H_2O)$ = (76.7 ± 17.7) kJ mol^{-1} for TO and $\Delta H^0_{ev,PV}(H_2O)$ = (75.5 ± 11.1) kJ mol^{-1} for PV experiments, respectively. The results show good agreement between the two experimental techniques despite the experimental scatter. The average value of $\Delta H^0_{ev}(H_2O)$ = (76.1 ± 14.4) kJ mol^{-1} is slightly higher, as expected, but not significantly different compared to α-NAT films. Figure S2 of Supplement C displays a van't Hoff plot for α-NAT with $\Delta H^0_{ev}(H_2O)$ = (70.3 ± 14.1) and (56.5 ± 5.1) kJ mol^{-1} for TO and PV experiments, respectively. Both values are identical within experimental uncertainty whose average yields $\Delta H^0_{ev}(H_2O)$ = (63.~~4~~4 ± 9.6) kJ mol^{-1} and which leads to a standard enthalpy of formation slightly larger than that for β-NAT, as expected.

However, we do not have good agreement between TO and PV experiments for the kinetic parameters of β-NAT: a discrepancy is observed in the results of the two measurement

techniques regarding $R_{ev}(H_2O)$ and $\alpha(H_2O)$ for β-NAT. Figure 4 already shows a discrepancy in $\alpha(H_2O)$ (full and empty red squares in panel a) with the results of TO experiments being larger by a factor of approximately 5 at 185 K increasing to a factor of 100 at 200 K compared to PV experimental results across the whole temperature range. The same qualitative trend, albeit to a smaller extent, is observed for $R_{ev}(H_2O)$ (Figure 4b) and the Arrhenius representation of $J_{ev}(H_2O)$ on β-NAT clearly shows the discrepancy between the different measurement techniques.

The two-parameter representations of the Arrhenius lines displayed in Figure 12 for β-NAT are reported in Eqs. (15) and (16) for TO (solid line) and PV (dotted line) experiments, respectively:

Formatiert: Schriftart: Symbol

$$\log J_{ev}(H_2O)[\mathrm{molec \cdot cm^{-2} \cdot s^{-1}}] = (36.0 \pm 1.3) - \frac{(77.0 \pm 4.9)\times 10^3}{2.303\ \mathrm{RT}}\ \mathrm{TO-Preferred} \qquad (15)$$

$$\log J_{ev}(H_2O)[\mathrm{molec \cdot cm^{-2} \cdot s^{-1}}] = (28.7 \pm 0.7) - \frac{(52.1 \pm 2.4)\times 10^3}{2.303\ \mathrm{RT}}\ \mathrm{PV} \qquad (16)$$

Contrary to the case of α-NAT, no discontinuity in $J_{ev}(H_2O)$ has been observed in the Arrhenius plot of β-NAT displayed in Figure 12. We attribute the discrepancy between PV and TO experiments to the fact that the former may be subject to partial saturation of uptake and evaporation in the aftermath of transient supersaturation (PV). A look at the results of $\alpha_{\alpha-\mathrm{NAT}}(H_2O)$ in Figure 2a reveals that the results of the TO measurement technique agrees well with the PV technique in the overlapping temperature range. However, this plot displays a "hole" of a factor of 20 centered in the neighborhood of~~around~~ T = 180 ± 3 K with respect to the values at the fringes of the temperature interval. There are indications that PV experiments on α-NAT substrates may yield lower values of $\alpha_{\alpha-\mathrm{NAT}}(H_2O)$ at high temperatures in excess of approximately 182 K (Figure 2a), similarly to the results for $\alpha_{\beta-\mathrm{NAT}}(H_2O)$ for a β-NAT film (Figure 4a). This might be an indication that PV experiments are very sensitive to the interfacial nature of the sample. In other words, transient supersaturation (PV) and "passive" steady-state (TO) experiments may address different properties of the gas-condensed surface interface. This is the first time such a large discrepancy between two kinetic measurements techniques has been observed. As expected, thermodynamic results are not affected for reasons of microscopic reversibility because both forward ($\alpha(H_2O)$) and reverse reactions ($J_{ev}(H_2O)$) are affected to the same extent which cancels out for the calculation of the values of thermodynamic parameters.

Figure S3 of Supplement C shows the results of PV experiments using H_2O as a probe gas on α-NAT and β-NAT substrates. Red and black circles represent the decay of series of two pulses on α- and β-NAT, respectively, with the first and second pulse labeled accordingly. In the case of α-NAT films (red circles), the decay of the second pulses is equal to within 20-30% of the decay of the initial pulses, and only in a few cases at temperatures higher than 180 K is the decay of the second pulse significantly slower than the initial pulse. In the case of β-NAT films, the decay of second pulses is consistently slower than the decay of first pulses in most cases. This indicates that the surface of β-NAT films exposed to a transient supersaturation of H_2O vapor is more prone to saturation compared to α-NAT.

As mentioned before, we consider the results of TO experiments ~~as~~ preferred for β-NAT this work despite its~~the~~ larger uncertainty. The enthalpies of evaporation $\Delta H^0_{ev,TO}(H_2O)$ = (76.7 ± 17.7) kJ mol^{-1} and the activation energy for evaporation $E_{ev}(H_2O)$ = (77.0 ± 4.9) kJ mol^{-1} are equal to within experimental uncertainties. We calculate an activation energy of accommodation for H_2O on β-NAT of $E_{acc}(H_2O) = E_{ev}(H_2O) - \Delta H^0_{ev,TO}(H_2O) = 0$. Therefore, no activation energy is required for the accommodation process of H_2O on β-NAT which is an expected experimental outcome. In contrast, the activation energy for H_2O accommodation on α-NAT is computed as $E_{acc}(H_2O) = E_{ev}(H_2O) - \Delta H^0_{ev,average}(H_2O)$ = 75.3 – 63.4~~4~~ = 11.9~~1.9~~ kJ/mol when using a value averaged over the PV and TO experiment of 63.4~~4~~ kJ/mol for $\Delta H^0_{ev,average}(H_2O)$. This small, but possibly significant positive activation energy is consistent with the positive temperature dependence of $\alpha_{\alpha-NAT}(H_2O)$ ~~$\alpha_{\beta-NAT}(H_2O)$~~ displayed in Figure 2~~4~~a for the TO experiment at T > 182 K, that is in the high T-range.

$R_{ev}(H_2O)$ on both α-NAT and β-NAT is smaller compared to $R_{ev}(H_2O)$ on pure ice. This is in agreement with the results of Tolbert and Middlebrook (1990), Middlebrook et al. (1996), Warshawsky et al. (1999) and Delval and Rossi (2005) who showed that ice coated with a number of molecular layers of NAT evaporates H_2O at a slower rate than pure ice. On the other hand, our results are in contrast with the findings of Biermann et al. (1998) who report that no significant decrease of the H_2O evaporation rate was observed in HNO_3-doped ice films. The discrepancy may possibly be ~~due~~ caused~~to~~ by the high total pressure of 0.85 mbar in their reactor compared to all other competitive studies cited above that use high-vacuum chambers with total pressures lower by typically a factor of 500 or more. It is very likely that the experiments performed by ~~low HNO_3 concentration used by~~ Biermann et al. (1998) were not sensitive to changes in evaporation rates despite the fact that both the HNO_3 and H_2O

Formatiert: Schriftart: Symbol

Formatiert: Tiefgestellt

Formatiert: Tiefgestellt

Formatiert: Tiefgestellt

concentrations used as well as the thickness of the accumulated NAT layers in their no. 5 experiment were of the same magnitude as in the competing studies.~~compared to our experimental conditions as well as probable wall losses due to HNO_3-wall interaction which was not taken into account in contrast to the present approach~~. A hint to that effect is the unexpected time dependence of the ice evaporation rate in Biermann et al. (1998) that shows an induction time of 30 minutes as opposed to the expected linear decrease from the beginning of evaporation (see below). We are unable to attribute the source of the measured H_2O vapor in the presence of two H_2O-containing solid phases in our chemical system, namely pure H_2O ice and NAT. We restate that the partial pressures at constant temperature are controlled by the (relative) composition of the system in agreement with the single degree of freedom resulting from Gibb's Phase Rule and the data displayed in the binary HNO_3/H_2O phase diagrams displayed in Figures 3, 5 and S5.

Delval and Rossi (2005) report that the initial evaporation of H_2O in their experiments was always that of pure ice and that $R_{ev}(H_2O)$ gradually decreases with the evaporation of excess H_2O and the increase in the average HNO_3 mole fraction. They refer to this difference as "high and low evaporation rate" regime of H_2O.

Our observation is somewhat different compared to Delval and Rossi (2005): $R_{ev}(H_2O)$ on α-NAT and β-NAT is smaller compared to $R_{ev}(H_2O)$ on pure ice over the whole temperature range and for all samples. The reason lies in the fact that the average mole fraction of HNO_3 of the present samples is higher by at least a factor of 10 compared to the one used by Delval and Rossi (2005). Therefore all our samples are in the "low evaporation rate" regime of H_2O and our results compare well with the results of Delval and Rossi (2005) once they evaporate excess H_2O and reach the "low evaporation rate" regime.

Figure 13 displays both the Arrhenius plots of $J_{ev}(HNO_3)$ (A) and the van 't Hoff plots of $P_{eq}(HNO_3)$ (B) for the interaction of HNO_3 with α- and β-NAT films. We would like to briefly remind the reader that only TO experiments were possible for HNO_3 experiments because no sharp pulses could be generated with pure HNO_3, presumably owing to the tendency of nitric acid to stick to the inner surfaces, mainly on stainless (austenitic) steel. This has been verified by measuring the Langmuir adsorption on that same surface (Figure S1, Table 2). The following equations define the corresponding straight lines based on the present measurements. For α-NAT (Eqs. (17) and (18)) and β-NAT ~~films~~ (Eqs. (19) and (20)) films we find the following results:

Formatiert: Tiefgestellt

Formatiert: Tiefgestellt

Formatiert: Tiefgestellt

Formatiert: Tiefgestellt

Formatiert: Tiefgestellt

Formatiert: Tiefgestellt

α-NAT: $$\log J_{ev}(HNO_3)[\mathrm{molec \cdot cm^{-2} \cdot s^{-1}}] = (62.3 \pm 7.8) - \frac{(178.0 \pm 27.4)\times 10^3}{2.303\ \mathrm{RT}} \quad (17)$$

$$\log P_{eq}(HNO_3)[\mathrm{Torr}] = (29.3 \pm 12.0) - \frac{(128.6 \pm 42.4)\times 10^3}{2.303\ \mathrm{RT}} \quad (18)$$

β-NAT: $$\log J_{ev}(HNO_3)[\mathrm{molec \cdot cm^{-2} \cdot s^{-1}}] = (40.6 \pm 2.4) - \frac{(102.0 \pm 8.6)\times 10^3}{2.303\ \mathrm{RT}} \quad (19)$$

$$\log P_{eq}(HNO_3)[\mathrm{Torr}] = (19.8 \pm 3.3) - \frac{(96.5 \pm 12.0)\times 10^3}{2.303\ \mathrm{RT}} \quad (20)$$

We calculate an activation energy for HNO_3 evaporation on α-NAT and β-NAT of $E_{ev}(HNO_3)$ = (178.0 ± 27.4) kJ mol^{-1} and $E_{ev}(HNO_3)$ = (102.0 ± 8.6) kJ mol^{-1}, respectively. These values are higher compared to $E_{ev}(HCl)$ = (87.0 ± 17) kJ mol^{-1}, the activation energy for HCl evaporation on hexahydrate. This result is within expectation given the higher hydrogen bond energy of HNO_3 compared to HCl with H_2O.

Similar to the case of H_2O, no activation energy for accommodation of HNO_3 on β-NAT is required since the evaporation activation energy $E_{ev}(HNO_3)$ = (102.0 ± 8.6) kJ mol^{-1} and the enthalpy of evaporation $\Delta H^0_{ev}(HNO_3)$ = (96.5 ± 12.0) kJ mol^{-1} are equal within experimental uncertainty~~ies~~. In contrast, a substantial activation energy of H~~2~~NO~3~ mass accommodation of 49.4 kJ/mol is calculated from $E_{acc}(H_2NO_3) = E_{ev}(H_2NO_3) - \Delta H^0_{ev,TO}(H_2NO3)$ = 178.0 – 128.6 = 49.9 kJ/mol which may have to do with the fact that α-NAT is metastable owing to its unstable H_2O crystal structure (Weiss et al., 2016).

The thermodynamic parameters obtained above, namely $\Delta H^0_{ev}(H_2O)$ and $\Delta H^0_{ev}(HNO_3)$ for both α- and β-NAT may now be used to estimate the relative stability of α- vs. β-NAT as follows. The evaporation/condensation equilibrium for both forms of NAT may be represented in equation (21) where $\Sigma\Delta H_{ev}{}^0 = 3\,\Delta H^0_{ev}(H_2O) + \Delta H^0_{ev}(HNO_3)$ in agreement with the relevant stoichiometry:

$$HNO_3 \bullet 3H_2O(s) \leftrightarrows 3H_2O(g) + HNO_3(g) \qquad (\Sigma\Delta H_{ev}{}^0) \quad (21)$$

For α- and β-NAT we obtain $\Sigma\Delta H_{ev}{}^{0,\alpha}$ and $\Sigma\Delta H_{ev}{}^{0,\beta}$ equal to 318.8~~8~~ and 324.8 kJ/mol, respectively, when we use the average of the TO and PV experiment for H_2O and the TO value listed above for HNO_3 evaporation. Specifically, we have used (63.4~~4~~ ± 9.6) and (128.6 ± 42.2) for H_2O- and (76.1 ± 14.4) and (96.5 ± 12.0) for HNO_3-evaporation for α- and β-NAT, respectively, as displayed above. Finally, we arrive at the difference $\Sigma\Delta H_{ev}{}^{0,\alpha}$ - $\Sigma\Delta H_{ev}{}^{0,\beta}$ = -6.0~~0~~ ± 20.0 kJ/mol which shows that β-NAT is marginally more stable than α-

Formatiert: Nicht Hochgestellt/ Tiefgestellt

Formatiert: Tiefgestellt

Formatiert: Nicht Hochgestellt/ Tiefgestellt

Formatiert: Tiefgestellt

Formatiert: Nicht Hochgestellt/ Tiefgestellt

Formatiert: Tiefgestellt

NAT. This is true despite the fact that the standard heat of evaporation for HNO_3 in α-NAT ($\Delta H_{ev}^{0}(HNO_3)$) is significantly larger than for β-NAT by 32.1 kJ/mol which may be expressed by the fact that the calculated "affinity" of HNO_3 towards ice in the α-NAT is larger than for β-NAT as claimed by Weiss et al. (2016). However, this fact only addresses the behavior of HNO_3 without taking into consideration the partial stability of the H_2O network in the total crystal structure. In view of the large uncertainty, mainly brought about by the TO experiment, we regard this result as an estimate to the true standard enthalpy difference between α- and β-NAT.

The results of HCl kinetic measurements displayed in Figure 8 and Figure 9 show that $R_{ev}(HCl)$ is always higher than $R_{ev}(HNO_3)$, with the latter being equal regardless of the presence of absorbed HCl molecules in the condensed phase. Hynes et al. (2002)~~ also~~ observed that HCl uptake on HNO_3 dosed ice was always nearly reversible in their experiments, in contrast to HCl uptake on clean ice. Although the same HNO_3 dosed ice surface has been dosed repeatedly at different HCl concentrations by Hynes et al. (2002), the degree of reversibility was found to be unaffected by previous experiments. In contrast, we never observed such reversibility. In our experiments, HCl always remained on the surface, evaporating at a rate only slightly faster than HNO_3 both for α-NAT and β-NAT and similarly to $R_{ev}(HCl)$ of crystalline hexahydrate (Iannarelli and Rossi, 2014). However, a possible influence of the temperature cannot be excluded at this time, as the experiments performed by Hynes et al. (2002) have been performed at distinctly higher temperatures, namely in the range 210-235 K, compared to the experiments discussed here.

Similar behavior has been observed by Kuhs et al. (2012) with respect to the presence of cubic ice or "ice I_c" in common hexagonal ice I_h. I_h is expected to be the prevalent ice phase at temperatures relevant to atmospheric processing on thermodynamic grounds. Apparent formation of I_c has been observed over a wide temperature range and evidence pointed towards the fact that the resulting phase is not pure cubic ice but instead composed of disordered cubic and hexagonal stacking sequences. Kuhs et al. (2012) studied the extent and relevance of the stacking disorder using both neutron as well as X-ray diffraction as indicators of the "cubicity" of vapor deposited ice at temperatures from 175 to 240 K and could simply not find proof for the formation of cubic ice I_c under atmospheric conditions.

Kuhs et al. (2012) discovered that even at temperatures as high as 210 K, the fraction of cubic sequences in vapor deposited ice is still approximately 40%. The rate of decrease in cubicity

depends on the temperature, being very slow at temperatures lower than 180 K and increasingly rapid at temperatures higher than 185 K. Furthermore, even at high temperatures the complete transformation into pure ice I_h was never observed, with a few percent of cubic stacking sequences still remaining in the ice, even after several hours at 210 K and disappeared only upon heating to 240 K. In addition, the combination of neutron and X-ray diffraction experiments of Kuhs et al. (2012) cannot distinguish the difference between the bulk and the interface whereas our measurement techniques, in particular PV experiments, are very sensitive to the nature and properties of the sample interface.

In light of these results we speculate that the presence of two hydrates of HNO_3, namely α-NAT and β-NAT, may depend on the cubicity or stack-disorder of the ice upon which the NAT grows. HNO_3 adsorbed on cubic ice I_c tends to form α-NAT crystalline structures which upon heating converts to β-NAT while the ice loses part of its cubicity. The temperature at which the conversion from α-NAT to β-NAT is accelerated, T = 185 K, is the same temperature Kuhs et al. (2012) report as the temperature at which the rate of decrease in cubicity increases. Our hypothesis is that the formation of α-NAT or β-NAT may highly depend on the environment in which the NAT phase grows and on the presence of high or low fractions of "I_c".

Figure1414 displays both the Arrhenius plots of J_{ev}(HCl) (A) and the van 't Hoff plots of P_{eq}(HCl) (B) for the interaction of HCl with α-NAT and β-NAT films. As for the case of HNO_3, only TO experiments were performed with HCl as a probe gas. Full red circles and black triangles represent the interaction of HCl with α- and β-NAT films, respectively.

The following equations define the corresponding straight lines resulting from the present measurements. For α-NAT (Eqs. (22) and (23)) and β-NAT films (Eqs. (24) and (25)) we find the following results:

α-NAT: $$\log J_{ev}(\mathrm{HCl})[\mathrm{molec}\cdot\mathrm{cm}^{-2}\cdot\mathrm{s}^{-1}] = (34.8 \pm 5.3) - \frac{(78.3 \pm 19.2)\times 10^3}{2.303\ \mathrm{RT}} \quad (22)$$

$$\log P_{eq}(\mathrm{HCl})[\mathrm{Torr}] = (15.7 \pm 3.2) - \frac{(78.4 \pm 11.4)\times 10^3}{2.303\ \mathrm{RT}} \quad (23)$$

β-NAT: $$\log J_{ev}(\mathrm{HCl})[\mathrm{molec}\cdot\mathrm{cm}^{-2}\cdot\mathrm{s}^{-1}] = (28.6 \pm 1.3) - \frac{(56.7 \pm 4.6)\times 10^3}{2.303\ \mathrm{RT}} \quad (24)$$

$$\log P_{eq}(\mathrm{HCl})[\mathrm{Torr}] = (13.3 \pm 1.6) - \frac{(69.6 \pm 5.8)\times 10^3}{2.303\ \mathrm{RT}} \quad (25)$$

Despite the considerable scatter of the data displayed in Figure1414 it may be pointed out that the enthalpy of HCl evaporation is identical for α- and β-NAT within the stated experimental uncertainty: We compare ΔH^0_{ev}(HCl) of 78.4 ± 11.4 and 69.6 ± 5.8 kJ/mol for α- and β-NAT (equations (23) and (25)). On the other hand, we have equality, perhaps fortuitously, between E_{ev}(HCl) and ΔH^0_{ev}(HCl) for α-NAT following equations (22) and (23) which leads to the conclusion that HCl accommodation on α-NAT is not an activated process with essentially zero activation energy similar to the situation for HNO_3 interacting with β-NAT. On the other hand, this type of argument would lead to a negative activation energy for HCl accommodation on β-NAT because the enthalpy of evaporation of HCl from β-NAT is smaller than E_{ev}(HCl) from β-NAT. ~~However, the kinetic data on J_{ev}(HCl) from both α- and β-NAT are very scattered which may make a quantitative comparison a futile exercize~~However, the kinetic data of J_{ev}(HCl) for β-NAT may be affected by saturation of HCl uptake because experiments have been performed using the PV admission. This situation may be similar to the kinetic results of $J_{ev}(H_2O)$ for β-NAT displayed in Figure 12 that shows a significantly smaller value for $E_{ev}(H_2O)$ in PV vs. TO experiments (52.1 vs. 75.5 kJ/mol, see also Table 4) whereas the saturation effect seems not to affect the kinetic data for α-NAT. The anomalously large experimental uncertainty for HNO_3 TO experiments on α-NAT displayed in Table 4 certainly has to do with the restricted temperature interval over which we were able to monitor α-NAT before it converted to β-NAT. This may be seen in the synoptic overview of the van't Hoff plots for HNO_3 interacting with NAT displayed in Figure S4 of Supplement D. This restricted T range is also visible in Figure 13A for $J_{ev}(HNO_3)$ from α-NAT..

5 Atmospheric implications and conclusion

In this study we have confirmed that exposure of ice films to HNO_3 vapor pressures at temperatures ~~akin to the ones~~ found in the stratosphere leads to formation of NAT hydrates.

Of the two known forms of NAT, namely α-NAT and β-NAT, the latter is the thermodynamically stable one whereas metastable α-NAT is likely to be of lesser importance in the heterogeneous processes at UT/LS atmospherically relevant conditions.

$R_{ev}(H_2O)$ on α-NAT and β-NAT films are very different compared to the case of HCl/ice where the evaporation of H_2O is not influenced by the presence of adsorbed HCl on the ice and takes place at a rate characteristic of pure ice. This has important implications on the

lifetime of atmospheric ice particles. Ice particles with adsorbed HNO_3 forming NAT have longer lifetimes compared to ice particles with adsorbed HCl, being amorphous or crystalline $HCl \bullet 6H_2O$. In light of our results we raise the question if HCl-containing ice particles are of significant atmospheric relevance as substrates for heterogeneous reactions due to their reduced lifetimes and concurrent reduced opportunities to enable heterogeneous atmospheric reactions such as Reaction (1).

$J_{ev}(H_2O)$ on α-NAT presents a discontinuity at 185 K akin to that observed in pure ice by Delval and Rossi (2004); Pratte et al. (2006). The resulting Arrhenius representation at high temperatures larger than 181 ± 2 K is:

$$\log J_{ev}(H_2O)[\mathrm{molec \cdot cm^{-2} \cdot s^{-1}}] = (35.9 \pm 2.8) - \frac{(75.3 \pm 9.9)\times 10^3}{2.303\ \mathrm{RT}} \quad (11)$$

$J_{ev}(H_2O)$ on β-NAT shows two values depending on the measurement techniques as a result of the propensity of the PV experiment to saturate the gas-condensate interface. TO experiments are less precise but more accurate owing to the fact that they are less prone to saturation compared to PV experiments. Therefore, we report results of TO experiments as preferred values, whereas we rule out kinetic PV results owing to possible saturation problems and note in passing that β-NAT is apparently more prone to saturation than α-NAT. The Arrhenius representation~~s~~ for the preferred TO results is:

$$\text{TO Experiments:}\quad \log J_{ev}(H_2O)[\mathrm{molec \cdot cm^{-2} \cdot s^{-1}}] = (36.0 \pm 1.3) - \frac{(77.0 \pm 4.9)\times 10^3}{2.303\ \mathrm{RT}} \quad (15)$$

HCl kinetic measurements on α-NAT and β-NAT indicate that HCl does not displace a significant number of HNO_3 molecules from the ice surface upon deposition, but rather that HCl and HNO_3 do not strongly interact with each other in the condensed phase and that HCl evaporates faster. This observation is also supported by the slower rates of evaporation and the correspondingly higher values of the HNO_3 evaporation activation energy on α-NAT and β-NAT, $E_{ev}(HNO_3)$ = (178.0 ± 27.4) and ~~kJ mol^{-1} and $E_{ev}(HNO_3)$ =~~ (102.0 ± 8.6) kJ mol^{-1} (see Table 4), respectively, compared to the activation energy for HCl evaporation on $HCl \bullet 6H_2O$, $E_{ev}(HCl)$ = (87.0 ± 17) kJ mol^{-1}. This also is consistent with a larger calculated interaction energy of HNO_3 with H_2O ("affinity") in α-NAT compared to β-NAT (Weiss et al., 2016) despite the fact that ΔH_f^0(α-NAT) is less stable by 6.0 ± 20 kJ/mol compared to β-NAT.

Formatiert: Schriftart: Symbol

Formatiert: Schriftart: Symbol

A look at Table 5 reveals evaporative lifetimes of various ice particles with respect to H_2O evaporation. Equation (26) and (27) present the rudiments of a very simple layer-by-layer molecular model used to estimate evaporation lifetimes (θ_{tot}) at atmospheric conditions (Alcala et al., 2002; Chiesa and Rossi, 2013):

$$\theta_{tot} = (r/a)N_{ML}/J_{ev}^{rh} \quad (26)$$

$$J_{ev}^{rh} = J_{ev}^{max}(1-rh/100) \quad (27)$$

with r, a, rh and N_{ML} being the radius of the ice particle, shell thickness, relative humidity in % and the number of molecules cm^{-2} corresponding to one monolayer. J_{ev}^{rh} and J_{ev}^{max} are the evaporation fluxes of H_2O at rh and rh = 0, the latter corresponding to the maximum value of J_{ev} which we calculate following Equation (2) or (8). The salient feature of this simple evaporation model is the linear rate of change of the radius or diameter of the particle, a well- and widely known fact in aerosol physics in which the shrinking or growing size (diameter) of an aerosol particle is linear with time if the rate of evaporation is zero order, that is independent of a concentration term. Table 5 lists the evaporation life times which are not defined in terms of an e-folding time when dealing with first-order processes. In this example the lifetime is the time span between the cradle and death of the particle, this means from a given diameter 2r and "death" at 2r = 0. The chosen atmospheric conditions correspond to 190 K, rh = 80%, a = 2.5 Å for H_2O and 3.35 Å for all other systems, r = 10 µm and estimated values 6 x 10^{14}, 3 x 10^{14} and 1 x 10^{15} molec cm^{-2} for N_{ML} of HNO_3, HCl and H_2O. It is immediately apparent that there is a large variation of θ_{tot} values for atmospherically relevant conditions which goes into the direction of increasing opportunities for heterogeneous interaction with atmospheric trace gases, even for pure ice (PSC type II). Table 5 is concerned with the most volatile component, namely H_2O. If we now turn our attention to the least volatile component such as HNO_3 in β-NAT we obtain θ_{tot} = 5.1 d and 33.9 d for 0 and 85% HNO_3 atmospheric saturation, the former being the maximum possible evaporation rate for 0% HNO_3 saturation. The other boundary conditions are 190 K, polar upper tropospheric conditions at 11 km altitude (226.3 mb at 210 K), 1 ppb HNO_3, 10 ppm H_2O corresponding to 85% HNO_3 saturation. This goes to show that laboratory experiments on gas-condensed phase exchange of lower volatility components in atmospheric hydrates are fraught with complications. It follows as a corollary that both HCl, but especially HNO_3 contamination of H_2O ice is bound to persist for all practical atmospheric conditions.

Formatiert: Tiefgestellt
Formatiert: Tiefgestellt
Formatiert: Tiefgestellt
Formatiert: Tiefgestellt
Formatiert: Hochgestellt
Formatiert: Tiefgestellt
Formatiert: Hochgestellt
Formatiert: Tiefgestellt
Formatiert: Hochgestellt
Formatiert: Tiefgestellt
Formatiert: Hochgestellt
Formatiert: Tiefgestellt
Formatiert: Tiefgestellt
Formatiert: Tiefgestellt
Formatiert: Schriftart: Symbol
Formatiert: Hochgestellt
Formatiert: Hochgestellt
Formatiert: Hochgestellt
Formatiert: Hochgestellt
Formatiert: Tiefgestellt
Formatiert: Tiefgestellt
Formatiert: Tiefgestellt
Formatiert: Tiefgestellt
Formatiert: Schriftart: Symbol
Formatiert: Schriftart: Times New Roman
Formatiert: Tiefgestellt
Formatiert: Tiefgestellt
Formatiert: Tiefgestellt
Formatiert: Tiefgestellt
Formatiert: Tiefgestellt
Formatiert: Tiefgestellt
Formatiert: Tiefgestellt

~~The reliable and reproducible measurement of the vapor pressure of H_2O (P_{H2O}) in the UT/LS still represents a thorny problem on airborne (aircraft and balloon) platforms owing to small absolute values as well as to possible rapid variations as a function of altitude. Fahey and coworkers have found an elegant way to solve this problem using a suitably adapted chilled mirror hygrometer (CMH) where a cryogenic ice deposit on a temperature controlled mirror is monitored during atmospheric sampling using a backreflected IR LED element that controls a mirror heater in a feed back loop (Thornberry et al., 2011). When $\mathbf{P_{H_2O}}$ increases the mirror reflectivity decreases owing to a concomitant, but presumed increase in scattering because of the formation of a polycrystalline ice deposit on the mirror. In this case the mirror heating power is increased in a feedback loop in order to restore the original reflectivity of the former operating conditions. For concentrations of 1-10 ppm H_2O and 1-10 ppb HNO_3 typically encountered in this region of the atmosphere we expect a weak perturbation of the cryogenic ice deposit through co-deposition of HNO_3 on the mirror. In fact, Thornberry et al. (2011) measure a HNO_3 deposit from their laboratory experiment corresponding to roughly a molecular monolayer on the 0.37 cm^2 mirror (geometric) surface at typically 4 ppb P_{HNO3} and a total deposition time of 3 h. This is a negligible quantity of HNO_3 compared to the 2000 or so ice molecular bilayers per µm of ice deposited. Fahey and coworkers have recently introduced an advanced version of a hygrometer that monitors gas phase H_2O using a high resolution diode laser near 2694 nm at a specific H_2O absorption line (Thornberry et al., 2015). This methodology replaces the unspecific monitoring of the broad-band reflectivity by an identifiable spectroscopic molecular IR transition of gas phase H_2O and thus removes the doubt about the identity of the absorber compared to the prior use of the (broad band) IR LED. It is our understanding that this advanced CMH is in the process of actually being tested in the field.~~

~~However, when the CMH was used in a laboratory flow reactor experiment at a higher concentrations of H_2O and HNO_3 (both at typically 80 ppb) the mirror reflectivity increased and led to an approximately 3 K lower mirror temperature at 194 K after approximately 4 hours into the experiment compared to a reference CMH not exposed to HNO_3. At first, the authors identified the first HNO_3/H_2O condensate as an α-NAT coating on a H_2O thin film after approximately 1.8 hours into the codeposition experiment of admitting six ppm H_2O and 80 ppb HNO_3 into the flow reactor. At 2.3 hours after start the HNO_3 flow was halted while maintaining a H_2O flow of 80 ppm which led to the appearance of a "second condensate" after approximately 4 hours of elapsed time. The authors attributed this "second condensate"~~

~~to an unknown HNO_3/H_2O phase that led to a 63% supersaturation with respect to pure ice corresponding to the above-mentioned 3 K depression of the mirror temperature.~~

~~It is perhaps useful to remind the reader at this point that the CMH detector of $\mathbf{P_{H_2O}}$ compensates the change in reflectivity detected as a signal on a photodiode with a change in mirror temperature, but the true molecular identity of the condensate goes unnoticed. Based on the present results we claim that the selective evaporation of the heavier components HNO_3 compared to H_2O evaporation in the binary, and HCl in the ternary condensed phase system is not possible, at least at atmospherically relevant HNO_3 and HCl concentrations because $J_{ev}(HNO_3)$ and $J_{ev}(HCl)$ are always smaller than $J_{ev}(H_2O)$ for the investigated nitric acid hydrates in the range 170-205 K. As far as positive proof for the existence of an as yet unidentified HNO_3/H_2O hydrate ("second condensate") is concerned that results from the CMH equipped flow experiment discussed above, we would like to withhold judgement until possible changes in optical properties of the HNO_3/H_2O condensate as well as its temporal changes under the prevailing experimental conditions will have been considered.~~

~~Using the real part of the index of refraction n at approximately 200 K of 1.333, 1.513 and 1.460 for pure H_2O ice, α- and β-NAT, respectively [Berland et al., 1994; Toon et al., 1994], we calculate a specular reflectivity R of 2.0, 4.2 and 3.5% for pure H_2O ice, α- and β-NAT following the Fresnel expression ($R = (n_0-n_1)^2/(n_0+n_1)^2$) with n_0 related to pure H_2O ice) for normal incidence. This shows that a potentially significant change of the optical properties of a HNO_3-containing ice film relative to pure ice may be expected at these high doses of HNO_3, which, however, will depend on the structure and concentration gradients of the film itself.~~

~~The implementation of a detailed (geometrical) optical model of the cryogenic film interaction with the IR-emission is clearly out of scope of the present work, but it seems to be mandatory in the future to take these optical changes into account for the quantitative interpretation of the experimental results of Gao et al. (2016). In addition, it will be necessary to gauge the importance of film volume absorption as the emitted IR radiation will pass twice across the film thickness on its way to the detector. We have recently measured the optical cross sections of the nitric acid hydrates in the range 4000-750 cm^{-1} (Iannarelli and Rossi, 2015) which completes the set of optical constants of the nitric acid hydrates in the IR spectral region. In the end the decision on the existence of an unknown/unidentified HNO_3/H_2O phase present in the UT/LS and significantly exceeding the saturation vapor pressure of pure ice will probably hinge on experiments performed using the advanced version of the hygrometer that~~

~~is based on the absorption of high resolution radiation near 2.7 µm by gas phase water vapor mentioned above and that seems free of perturbations by other atmospheric gases as long as the dose is kept small (Thornberry et al., 2015) (see above).~~

At last it is useful to view the outcome of a recent laboratory experiment dealing with the binary HNO_3/H_2O system monitored using a cryogenic mirror hygrometer (CMH) (Gao et al., 2016) in light of the present kinetic results. In the basic experimental set-up the behavior of the sample CMH exposed to a combined low pressure H_2O/HNO_3 flow is compared to the response of a reference CMH that is located upstream of the HNO_3 source and exposed to the H_2O flow alone, and has been described in detail by Thornberry et al. (2011). Any increase in scattering of the incident monitoring laser beam owing to growth of the polycrystalline ice deposit will be counterbalanced by heating of the mirror to bring back the optical detector signal to a predetermined set point. The typical experimental sequence in Gao et al. (2016) starts by establishing pure ice frost layers on both CMH mirrors at a stable mixing ratio of < 10 ppm after which a continuous flow of HNO_3 was added such that the flow past the sample CMH contained 80-100 ppb HNO_3.

After typically one hour the gradual build-up of a NAT layer on the CMH was accompanied by a temperature increase of the sample CMH to settle around the saturation temperature T_{sat} of NAT at the chosen H_2O and HNO_3 flow rate. An increase of the H_2O flow from 6 to 80 ppm led to ice growth on both mirrors accompanied by an increase of T_{sat} of NAT adjusting to the new H_2O flow rate. Suddenly, the HNO_3 flow was shut off which first led to a rapidly decreasing MS signal for HNO_3 but ending up in an above background signal corresponding to 0.5 to 1.0 ppb HNO_3. The temperature of the sample CMH continued to decrease below T_{sat} of pure ice monitored by the reference CMH suggesting that $P_{eq}(H_2O)$ of the condensate had become larger than that of pure ice. This solid state on the sample CMH was called "second condensate". The low level of HNO_3 continued to react to repetitive increases (CMH heating) and decreases (CMH cooling) of the H_2O flow in a reproducible manner all the while staying below the level corresponding to T_{sat} of pure ice on the reference CMH. These repetitive H_2O on-off sequences provided additional evidence of the continued evaporation of HNO_3 from the condensate. The response of HNO_3 leaving the condensate undersaturated with respect to NAT is at first sight certainly unexpected based on the results displayed in Figures 2b and 4b. However, if one considers the relatively high mirror temperatures ranging between 207 and 213 K between which the "second condensate" was cycled by way of changing the H_2O flows it suddenly becomes conceivable that $R_{ev}(HNO_3)$ becomes equal to $R_{ev}(H_2O)$ in that

Formatiert: Tiefgestellt

temperature range. Linear extrapolation of the absolute rates of evaporation hints at similar magnitude for temperatures exceeding 210 K β - NAT (Figure 4). For α-NAT the temperature at which the evaporation rates of H_2O and HNO_3 become equal is even below 200 K owing to a steeper T-dependence of $R_{ev}(HNO_3)$ in α-NAT (Figure 2 and Table 4). We conclude, that the observed dynamics of the experiment performed by Gao et al. (2016) is entirely consistent with the kinetic results of the present study. However, the results of the Gao et al. (2016) laboratory experiment would certainly be different at lower temperatures more representative of the UT/LS.

Acknowledgements

The authors would like to acknowledge the generous support of this work over the years by the Swiss National Science Foundation (SNSF) in the framework of projects 200020_125204 and 200020_144431/1. We also sincerely thank Mr. Alwin Frei of PSI for graciously granting the permission to perform the experiments in his laboratory and professors Urs Baltensperger and Alexander Wokaun, both of PSI, for unfailing support over the years.

Formatiert: Schriftart: Symbol
Formatiert: Schriftart: Symbol
Formatiert: Tiefgestellt
Formatiert: Tiefgestellt
Formatiert: Tiefgestellt
Formatiert: Tiefgestellt
Formatiert: Schriftart: Symbol

References

Alcala-Jornod, A., van den Bergh, H., and Rossi, M.J.: Can soot particles emitted by airplane exhaust contribute to the formation of aviation contrails and cirrus clouds? Geophys. Res. Lett. 29, 1820, doi:10.1029/2001GL014115, 2002.

Benson, S.W., "Thermochemical Kinetics", Methods for the Estimation of Thermochemical Data and Rate Parameters", Second Edition, John Wiley and Sons, 1976.

Berland, B.S., Haynes, D.R., Foster, K.L., Tolbert, M.A., George S.M. and Toon, O.B.: Refractive Indices of Amorphous and Crystalline HNO_3/H_2O Films Representative of Polar Stratospheric Clouds, J. Phys. Chem. 98, 4358-4364, 1994.

Biermann, U. M., Crowley J.N., Huthwelker T., Moortgat G. K., Crutzen P. J., and Peter T.: FTIR studies on lifetime prolongation of stratospheric ice particles due to NAT coating, Geophys. Res. Lett., 25(21), 3939–3942, 1998.

Chaix, L., van den Bergh, H., and Rossi, M. J.: Real-Time kinetic measurements of the condensation and evaporation of D_2O molecules on ice at 140 K < T < 220 K, J. Phys. Chem. A, 102(50), 10300–10309, 1998.

Crowley, J.N., Ammann, M., Cox, R.A., Hynes, R.G., Jenkin, M.E., Mellouki, A., Rossi, M.J., Troe, J., and Wallington, T.J.: Evaluated kinetic and photochemical data for atmospheric chemistry: Volume V – heterogeneous reactions on solid substrates, Atmos. Chem. Phys. 10, 9059-9223, 2010.

Chiesa, S., and Rossi, M. J.: The metastable $HCl{\bullet}6H_2O$ phase – IR spectroscopy, phase transitions and kinetic/thermodynamic properties in the range 170-205 K, Atmos. Chem. Phys., 13(23), 11905–11923, 2013; doi:10.5194/acp-13-11905-2013.

Delval, C., Flückiger, B., and Rossi, M. J.: The rate of water vapor evaporation from ice substrates in the presence of HCl and HBr: implications for the lifetime of atmospheric ice particles, Atmos. Chem. Phys. 3, 1131–1145, 2003.

Delval, C., and Rossi, M. J.: The kinetics of condensation and evaporation of H_2O from pure ice in the range 173-223 K: a quartz crystal microbalance study, Phys. Chem. Chem. Phys., 6: 4665–4676, 2004.

Formatiert: Englisch (USA)

Formatiert: Standard, Abstand Nach: 12 Pt., Leerraum zwischen asiatischem und westlichem Text nicht anpassen, Leerraum zwischen asiatischem Text und Zahlen nicht anpassen

Formatiert: Schriftart: (Standard) Times New Roman, 12 Pt., Englisch (USA)

Formatiert: Schriftart: (Standard) Times New Roman, 12 Pt., Englisch (USA)

Formatiert: Schriftart: (Standard) Times New Roman, 12 Pt., Englisch (USA)

Formatiert: Abstand Nach: 12 Pt.

Delval, C., and Rossi, M. J.: Influence of monolayer amounts of HNO_3 on the evaporation rate of H_2O over ice in the range 179 to 208 K: A quartz crystal microbalance study, J. Phys. Chem. A, 109(32), 7151–7165, 2005.

Escribano, R. M., Fernandez-Torre, D., Herrero, V. J., Martin-Llorente, B., Maté, B., Ortega, I. K., and Grothe, H.: The low-frequency Raman and IR spectra of nitric acid hydrates, Vib. Spectrosc., 43, 254–259, 2007.

Fahey, D.W., Gao, R.S., Carslaw, K.S., Kettleborough, J., Popp, P.J., Northway, M.J., Holecek, J.C., Ciciora, S.C., McLaughlin, R.J., Thompson, T.L., Winkler, R.H., Baumgardner, D.G., Gandrud, B., Wennberg, P.O., Dhaniyala, S., McKinney, K., Peter, Th., Salawitch, R.J., Bui, T.P., Elkins, J.W., Webster, C.R., Atlas, E.L., Jost, H., Wilson, J.C., Herman, R.L., Kleinböhl, A., von König, M.: The Detection of Large HNO_3-Containing Particles in the Winter Arctic Stratosphere, Science 291, 1026-1031, 2001.

Friedel, R. A., Shultz, J. L., and Sharkey, A. G.: Mass spectrum of nitric acid, Anal. Chem., 31(6), 1128–1128, 1959.

Gao, R.S., Popp, P.J., Fahey, D.W., Marcy, T.P., Herman, R.L., Weinstock, E.M., Baumgardner, D.G., Garrett, T.J., Rosenlof, K.H., Thompson, T.L., Bui, P.T., Ridley, B.A., Wofsy, S.C., Toon, O.B., Tolbert, M.A., Kärcher, B., Peter, Th., Hudson, P.K., Weinheimer, A.J., Heymsfield, A.J.: Evidence That Nitric Acid Increases Relative Humidity in Low-Temperature Cirrus Clouds, Science 303, 516-520, 2004.

Gao, R.S., Gierczak, T., Thornberry, T.D., Rollins, A.W., Burkholder, J.B., Telg, H., Voigt, C., Peter, T. and Fahey, D.W.: Persistent Water-Nitric Acid Condensate with Saturation Water Vapor Pressure Greater than That of Hexagonal Ice, J. Phys. Chem. A 120, 1431-1440, 2016.~~, DOI: 10.1021/acs.jpca.5b06357.~~

Hamill, P., Turco, R. P., and Toon, O. B.: On the growth of nitric and sulfuric acid aerosol particles under stratospheric conditions. J. Atmos. Chem., 7(3), 287–315, 1988.

Hanson, D. R., and Mauersberger, K.: Laboratory studies of the nitric acid trihydrate: Implications for the south polar stratosphere, Geophys. Res. Lett., 15(8), 855–858, 1988.

Hanson, D. R.: The uptake of HNO_3 onto Ice, NAT and frozen sulfuric acid, Geophys. Res. Lett., 19(20), 2063–2066, 1992.

Herrero, V. J., Ortega, I. K., Maté, B., Martin-Llorente, B., Escribano, R., and H. Grothe: Comment on “Theoretical investigation of the coexistence of α- and β-nitric acid trihydrates

(NAT) molecular conformation" [Chem. Phys. 324 (2006) 210], Chem. Phys., 331, 186–188, 2006.

Höpfner, M., Luo, B.P., Massoli, P., Cairo, F., Spang, R., Snels, M., Di Donfrancesco, G., Stiller, G., von Clarmann, T., Fischer, H., Biermann, U.: Spectroscopic evidence for NAT, STS, and ice in the MIPAS infrared limb emission measurements of poolar stratospheric clouds, Atmos. Chem. Phys., 6, 1201-1219, 2006.

Hynes, R. G., Fernandez, M. A., and Cox, R. A.: Uptake of HNO_3 on water-ice and coadsorption of HNO_3 and HCl in the temperature range 210–235 K, J. Geophys. Res. Atmos., 107(D24), AAC 19–1–AAC 19–11, 2002.

Iannarelli, R., and Rossi, M. J.: H_2O and HCl trace gas kinetics on crystalline HCl hydrates and amorphous HCl/H_2O in the range 170 to 205 K: the HCl/H_2O phase diagram revisited, Atmos. Chem. Phys., 14(10), 5183-5204, 2014.

Iannarelli, R., and Rossi, M. J.: The mid-IR Absorption Cross Sections of α- and β-NAT (HNO_3•$3H_2O$) in the range 170 to 185 K and of metastable NAD (HNO_3•$2H_2O$) in the range 172 to 182 K, J. Geophys. Res. Atmos., 120, 11707-11727, 2015.

Ji, K. and Petit, J.-C., Calorimetric Identification of a new Nitric Acid Hydrate able to play a Role in the heterogeneous Chemistry of the Stratosphere, Compt.~~es~~ Rend. Acad~~em~~. Sciences Ser II, 316(12), 1743-1748, 1993.

Koehler, B. G., Middlebrook, A. M., and Tolbert, M. A.: Characterization of model polar stratospheric cloud films using Fourier transform infrared spectroscopy and temperature programmed desorption, J. Geophys. Res., 97(D8), 8065–8074, 1992.

Kuhs, W. F., Sippel, C., Falenty, A., and Hansen, T. C.: Extent and relevance of stacking disorder in "ice I_c", PNAS, 109(52), 21259– 21264, 2012.

Marti, J., and Mauersberger, K.: A survey and new measurements of ice vapor pressure at temperatures between 170 and 250 K, Geophys. Res. Lett., 20, 363–366, 1993.

Martin-Llorente, B., Fernandez-Torre, D., Herrero, V. J., Ortega, I. K., Escribano, R., and Maté, B.: Vibrational spectra of crystalline hydrates of atmospheric relevance: Bands of hydrated protons, Chem. Phys. Lett., 427, 300–304, 2006.

Mauersberger, K., and Krankowsky, D.: Vapor pressure above ice at temperatures below 170 K, Geophys. Res. Lett., 30(3), 1121, 2003.

Formatiert: Abstand Vor: 0 Pt.

McElroy, M. B., Salawitch, R. J., and Wofsy, S. C.: Antarctic O_3: Chemical mechanisms for the spring decrease. Geophys. Res. Lett., 13(12), 1296–1299, 1986.

McNeill, V. F., Loerting, T., Geiger, F. M., Trout, B. L., and Molina, M. J.: Hydrogen chloride-induced surface disordering on ice. PNAS, 103(25), 9422–9427, 2006.

McNeill, V. F., Geiger, F. M., Loerting, T., Trout, B. L., Molina, L. T., and Molina, M. J.: Interaction of hydrogen chloride with ice surfaces: the effects of grain size, surface roughness, and surface disorder. J. Phys. Chem. A, 111(28), 6274–6284, 2007.

Middlebrook, A. M., Koehler, B. G., McNeill, L. S., and Tolbert, M. A.: Formation of model polar stratospheric cloud films, Geophys. Res. Lett., 19(24), 2417–2420, 1992.

Middlebrook, A.M., Tolbert, M.A., and Drdla, K.: Evaporation studies of model polar stratospheric cloud films, Geophys. Res. Lett. 23, 2145-2148, 1996.

Molina, L. T., Molina M. J., Stachnik, R. A., and Tom, R. D.: An upper limit to the rate of the HCl + $ClONO_2$ reaction, J. Phys. Chem. 89, 3779-3781, 1985.

Molina, M. J., Tso, T. L., Molina, L. T., and Wang, F. C. Y.: Antarctic stratospheric chemistry of chlorine nitrate, hydrogen chloride and ice: release of active chlorine, Science 238, 1253-1257, 1987.

Molina, M. J.: The Probable Role of Stratospheric 'Ice' Clouds: Heterogeneous Chemistry of the Ozone Hole, in "The Chemistry of the Atmosphere: Its Impact on Global Change", Blackwell Scientific Publications, London, ch. 3, pp 27- 38, 1994.

Moussa, S. G., Kuo, M. H., and McNeill, V. F.: Nitric acid-induced surface disordering on ice, Phys. Chem. Chem. Phys., 15, 10989–10995, 2013.

Ortega, I. K., Escribano, R., Fernandez, D., Herrero, V. J., Maté, B., Medialdea, A., and Moreno, M. A.: The structure and vibrational frequencies of crystalline nitric acid, Chem. Phys. Lett., 378, 218–223, 2003.

Ortega, I. K., Maté, B., Moreno, M. A., Herrero, V. J., and Escribano, R.: Infrared spectra of nitric acid trihydrate (β-NAT): A comparison of available optical constants and implication for the detection of polar stratospheric clouds (PSC's), Geophys. Res. Lett., 33 L19816, 2006.

Peter, Th.: Microphysics and heterogeneous chemistry of Polar Stratospheric Clouds, Annu. Rev. Phys. Chem. 48, 785-822, 1997.

Pratte P., van den Bergh H., and Rossi, M. J.: The kinetics of H_2O vapor condensation and evaporation on different types of ice in the range 130-210 K, J. Phys. Chem A, 110(9), 3042–3058, 2006.

Reinhardt, H., Fida, M., and Zellner, R.: DRIFTS-studies of the interactions of HNO_3 with ice and HCl (HNO_3)-hydrate surfaces at temperatures around 165 K, J. Mol. Struct., 661–662, 567–577, 2003.

Ritzhaupt, G., and Devlin, J. P.: Infrared spectra of nitric and hydrochloric acid hydrate thin films, J. Phys. Chem. 95, 90-95, 1991.

Schreiner, J., Voigt, C., Kohlmann, A., Arnold F., Mauersberger, K. and Larsen, Niels, Chemical Analysis of Polöar Stratospheric Cloud Particles, Science, 283, 968-970, 1999.

Schreiner, J., Voigt, C., Weisser, C., Kohlmann, A., Mauersberger, K., Deshler, T., Kröger, C., Rosen, J., Kjome, N., Larsen, N., Adriani, A., Cairo, F., Di Donfrancesco, G., Ovarlez, J., Ovarlez, H., and Dörnbrack, A.: Chemical, microphysical, and optical properties of polar stratospheric clouds, J. Geophys. Res., 108(D5), 8313, 2003.

Solomon, S., Garcia, R.R., Rowland, F.S., and Wuebbles, D.J.: On the depletion of Antarctic ozone, Nature 321, 755-758, 1986.

Solomon, S.: Progress towards a quantitative understanding of Antarctic ozone depletion, Nature 347, 347-354, 1990.

Thornberry, T.D., Gierczak, T., Gao, R.S., Vömel, H., Watts, L.A., Burkholder, J.B., Fahey, D.W.: Laboratory evaluation of the effect of nitric acid uptake on frost point hygrometer performance, Atmos. Meas. Tech. 4, 289-296, 2011.

~~Thornberry, T.D., Rollins, A.W., Gao, R.S., Watts, L.A., Ciciora, S.J., McLaughlin, R.J., Fahey, D.W.: A two-channel, tunable diode laser-based hygrometer for measurement of water vapor and cirrus cloud ice water content in the upper troposphere and lower stratosphere, Atmos. Meas. Tech. 8, 211-224, 2015~~

Tolbert, M. A., and Middlebrook, A. M.: Fourier transform infrared studies of model polar stratospheric cloud surfaces: Growth and evaporation of ice and nitric acid/ice, J. Geophys. Res., 95(D13), 22423–22431, 1990.

Tolbert, M. A., Koehler, B. G., and Middlebrook, A. M.: Spectroscopic studies of model polar stratospheric cloud films, Spectrochim. Acta Part A: Mol. Spectrosc., 48(9), 1303–1313, 1992.

Toon, O.B., Tolbert, M.A., Koehler, B.G., Middlebrook, A.M. and J. Jordan, J.: Infrared optical constants of H_2O ice, amorphous nitric acid solutions, and nitric acid hydrates, Geophys. Res. 99(D12), 25631-25654 (1994).

Tso, T.-L., and Leu, M.-T.: Quantitative analysis of the infrared absorptivities of nitric acid ices existing in polar stratospheric clouds, Anal. Sci., 12, 615–622, 1996.

Voigt, C., Schreiner, J., Kohlmann, A., Zink, P., Mauersberger, K., Larsen, N., Deshler, T., Kröger, C., Rosen, J., Adriani, A., Cairo, F., Di Donfrancesco, G., Viterbini, M., Ovarlez, J., Ovarlez, H., David, C., and Dörnbrack A.: Nitric Acid Trihydrate (NAT) in Polar Stratospheric Clouds, Science, 290, 1756-1758, 2000.

Voigt, C., Schreiner, J., Kohlmann, A., Zink, P., Mauersberger, K., Larsen, N., Deshler, T., Kröger, C., Rosen, J., Adriani, A., Cairo, F., Di Donfrancesco, G., Viterbini, M., Ovarlez, J., Ovarlez, H., David, C. and Dörnbrack, A., Science 290, 1756-1758, 2000.

Voigt, C., Schlager, H., Luo, B.P., Dörnbrack, A., Roiger, A., Stock, P., Curtius, J., Vössing, H., Borrmann, S., Davies, S., Konopka, P., Schiller, C., Shur, G.~~,~~ and Peter, T.: Nitric Acid Trihydrate (NAT) formation at low NAT supersaturation in Polar Stratospheric Clouds (PSC's), Atmos. Chem. Phys., ~~-~~5, 1371-1380, 2005.

Warshawsky, M.S., Zondlo, M.A., and Tolbert, M.A.: Impact of nitric acid on ice evaporation rates, Geophys. Res. Lett. 26, 823-826, 1999.

Weiss, F., Kubel, F., Gálvez, O., Hoelzel, M., Parker, S. F., Baloh, P., Iannarelli, R., Rossi, M. J., and Grothe, H.: Metastable Nitric Acid Trihydrate in Ice Clouds, Angew.~~andte~~ Chemie I.E. 55, 3276-3280, 2016, doi: 10.1002/anie.201510841.~~, 2016 (on.line version)~~.

Wooldridge, P. J., Zhang, R., and Molina, M. J.: Phase equilibria of H_2SO_4, HNO_3, and HCl hydrates and the composition of polar stratospheric clouds, J. Geophys. Res. Atmos., 100(D1), 1389–1396, 1995.

Zondlo, M. A., Barone, S. B., and Tolbert, M. A.: Condensed-phase products in heterogeneous reactions: N_2O_5, $ClONO_2$, and HNO_3 reacting on ice films at 185 K, J. Phys. Chem. A, 102, 5735–5748, 1998.

Zondlo, M.A., Hudson, P.K., Prenni, A.J., and Tolbert, M.A.: Chemistry and microphysics of polar stratospheric clouds and cirrus clouds, Ann. Rev. Phys. Chem. 51, 473-499, 2000.

Table 1: Characteristic parameters of the used~~present~~ Stirred F~~f~~low R~~r~~eactor (SFR).

Reactor volume (upper chamber)	$\mathbf{V_R}$ = 2036 cm^3		
MS (lower) chamber	$\mathbf{V_{MS}}$ = 1750 cm^3		
Reactor internal surface	$\mathbf{S_W}$ = 1885 cm^2		
H_2O calibrated volume – inlet line	$\mathbf{V_{water}}$ = 62 cm^3		
HNO_3 calibrated volume – inlet line	$\mathbf{V_{acid}}$ = 20 cm^3		
Si support area (one side)	$\mathbf{A_{Si}}$ = 0.99 cm^2		
Surface to Volume ratio	$\mathbf{2\ A_{Si}/V_R}$ = 0.9725×10^{-4} cm^{-1}		
Reactor wall temperature	$\mathbf{T_w}$ = 315 K		
Conversion of evaporation rate and flux	$\mathbf{R_{ev} \cdot V_R = 2 \cdot A_{Si} \cdot J_{ev}}$		
	HNO_3	**H_2O**	**HCl**
Base Peak Signal MS [m/z]	46	18	36
MS Calibration Factor $\mathbf{C^X}$ [molec^{-1} s A]	4.53×10^{-25}	6.65×10^{-25}	1.30×10^{-25}
Escape rate constant $k^S_{esc} = C^S\sqrt{\frac{T}{M}}$ (small orifice) [s^{-1}] $k^M_{esc} = C^M\sqrt{\frac{T}{M}}$ (both orifices) [s^{-1}]	 0.0913 0.4331	 0.1710 0.8102	 0.1213 0.5729
Gas-surface collision frequency at 315 K, one side [s^{-1}] [(a)] $\boldsymbol{\omega} = \frac{\bar{c}}{4V} \cdot A_{Si} = \sqrt{\frac{8\,R\,T}{\pi\,M}} \cdot \frac{A_{Si}}{4V}$	3.95	7.39	5.22

[(a)] M in kg; A_{Si} in m^2; V in m^3; R = 8.314 J K^{-1} mol^{-1}. "One side" corresponds to front or rear side of Si-window.

In order to calculate the accommodation coefficient α using equation (3) we have used 2ω as the total collision frequency for both sides of the Si-window.

Formatiert: Schriftart: 10 Pt.

Formatiert: Zeilenabstand: Mehrere 1.15 ze

Table 2: Fit parameters of the Langmuir adsorption isotherms for H_2O, HNO_3 and HCl interaction with the internal stainless steel (SS304) surfaces of the SFR~~reactor~~.

Adsorbed Gas (Additional Gas) [(a)]	**K_L** [$\times10^{-14}$] [(b)]	**N_{TOT}** [$\times10^{17}$] [(c)]	**N_{MAX}** [$\times10^{14}$] [(d)]	**α_w** [$\times10^{-6}$] [(e)]
H_2O	3.18 ± 0.38	7.03 ± 0.42	3.73 ± 0.22	6.19 ± 0.08
H_2O (HCl, $F_{in} = 8\times10^{14}$)	4.67 ± 0.39	8.38 ± 0.29	4.45 ± 0.15	–
HNO_3	1.10 ± 0.16	93 ± 11	49 ± 6	2.92 ± 0.10
HNO_3 (H_2O, $F_{in} = 2\text{-}3\times10^{15}$)	1.61 ± 0.40	76 ± 15	40 ± 8	–
HNO_3 (average values)	1.28 ± 0.17	84 ± 8	45 ± 4	–
HCl	437 ± 21	5.06 ±0.06	2.68 ± 0.03	16.9 ± 0.3
HCl (H_2O, $F_{in} = 6\times10^{15}$)	63.1 ± 4.9	4.85 ± 0.07	2.57 ± 0.04	–
HCl (H_2O, $F_{in} = 3\times10^{15}$)	64.6 ± 6.3	3.79 ± 0.09	2.01 ± 0.04	–

[(a)] F_{in} is the flow rate of the additional gas in molec s^{-1}.
[(b)] K_L is the Langmuir adsorption equilibrium constant in cm^3 $molec^{-1}$.
[(c)] N_{TOT} is the total number of adsorbed molecules onto the internal surfaces, reported is the saturation value for total internal surface (1885 cm^2) of SFR.
[(d)] N_{MAX} is the adsorption site density in molec cm^{-2}.
[(e)] α_w is the reactor wall accommodation coefficient.

Formatiert: Schriftart: 10 Pt.

Formatiert: Abstand Vor: 0 Pt., Zeilenabstand: Mehrere 1.15 ze

Table 3. Peak Positions in cm^{-1} in the mid-IR of HNO_3 and HNO_3/HCl Hydrates[a].

α-NAT/HCl this work	**β-NAT/HCl this work**	**α-NAT/ice Iannarelli et al., 2015**	**β-NAT/ice Iannarelli et al., 2015**	**HCl/H_2O am Iannarelli et al., 2014**
3430 (sh) *3354* (sh) 3233[b]	 *3360* 3227[b]	3430 3233[b]	 3377 3233[b]	 3360 3236[b]
1767[c,d] *1828*[c,d], *1625-1560*[c,d]	1850[c]	1760[c]	1850[c]	1730[c] 1639[c]
1375 *1328*	1378 1339	1385	1378 1339	
1196	*1198*			

[a] Values in italics indicate significant changes in the spectrum upon addition of HCl to α- or β-NAT.
[b] The vibration on the third entry invariably corresponds to ν_3 (antisymmetric stretch) H-O-H in H_2O ice.
[c] Broad band. The estimated uncertainty in the peak position is ± 7.5 compared to the usual ± 2 cm^{-1}.
[d] With increasing HCl content broad band at 1767 cm^{-1} splits into two bands at 1828 and 1525-1650 cm^{-1}.

Formatiert: Schriftart: Fett
Formatiert: Hochgestellt
Formatiert: Hochgestellt
Formatiert: Hochgestellt
Formatiert: Hochgestellt
Formatiert: Hochgestellt
Formatiert: Schriftart: Kursiv
Formatiert: Schriftart: Kursiv
Formatiert: Schriftart: Kursiv
Formatiert: Schriftart: 10 Pt.
Formatiert: Abstand Vor: 0 Pt., Zeilenabstand: Mehrere 1.15 ze
Formatiert: Schriftart: Symbol
Formatiert: Schriftart: 10 Pt.
Formatiert: Schriftart: Symbol
Formatiert: Schriftart: 10 Pt.
Formatiert: Hochgestellt
Formatiert: Schriftart: Symbol
Formatiert: Tiefgestellt
Formatiert: Tiefgestellt
Formatiert: Schriftart: 10 Pt.
Formatiert: Schriftart: 10 Pt.
Formatiert: Schriftart: 10 Pt.
Formatiert: Zeilenabstand: 1.5 Zeilen

Table ~~3~~4: Synopsis of thermodynamic (P_{eq}) and kinetic (J_{ev}) parameters of the Arrhenius and van 't Hoff representation of data from Figure 2, Figure 4, ~~Figure 6~~Figure 8 and ~~Figure 7~~ Figure 9.

			J_{ev} [(a)]		P_{eq} [(b)]	
			E_{ev}	A	ΔH^0_{ev}	$\Delta S/R$
Sample	**Gas**	**Exp.**				
α-NAT	H_2O	TO	75.3 ± 9.9	35.9 ± 2.8	70.3 ± 14.1	15.2 ± 4.0
		PV	3.5 ± 4.2	15.1 ± 1.2	56.5 ± 5.1	11.8 ± 1.5
	HNO_3	TO	178.0 ± 27.4	62.3 ± 7.8	128.6 ± 42.4	29.3 ± 12.0
	HCl	PV	78.3 ± 19.2	34.8 ± 5.3	78.4 ± 11.4	15.7 ± 3.2
β-NAT	H_2O	TO	77.0 ± 4.9	36.0 ± 1.3	76.7 ± 17.7	16.7 ± 4.9
		PV	52.1 ± 2.4	28.7 ± 0.7	75.5 ± 11.1	16.7 ± 3.0
	HNO_3	TO	102.0 ± 8.6	40.6 ± 2.4	96.5 ± 12.0	19.8 ± 3.3
	HCl	PV	56.7 ± 4.6	28.6 ± 1.3	69.6 ± 5.8	13.3 ± 1.6

[(a)] for gas X, R = 8.314 J K^{-1} mol^{-1}: $\log J_{ev}(X)[\text{molec} \cdot \text{cm}^{-2} \cdot \text{s}^{-1}] = A - \frac{E_{ev} \times 10^3}{2.303\,RT}$

[(b)] for gas X, R = 8.314 J K^{-1} mol^{-1}: $\log P_{eq}(X)[\text{Torr}] = \frac{\Delta S}{R} - \frac{\Delta H^0_{ev} \times 10^3}{2.303\,RT}$

Formatiert: Schriftart: 10 Pt.
Formatiert: Schriftart: 10 Pt.
Formatiert: Abstand Vor: 0 Pt., Nach: 12 Pt., Zeilenabstand: Mehrere 1.15 ze
Formatiert: Schriftart: 10 Pt.
Formatiert: Schriftart: 10 Pt.
Formatiert: Schriftart: 10 Pt.
Formatiert: Schriftart: 10 Pt.
Formatiert: Schriftart: 10 Pt.
Formatiert: Schriftart: 10 Pt.
Formatiert: Schriftart: 10 Pt.
Formatiert: Schriftart: 10 Pt.
Formatiert: Schriftart: 10 Pt.
Formatiert: Schriftart: 10 Pt.
Formatiert: Schriftart: 10 Pt.
Formatiert: Schriftart: 10 Pt.
Formatiert: Schriftart: 10 Pt.
Formatiert: Schriftart: 10 Pt.
Formatiert: Schriftart: 10 Pt.
Formatiert: Schriftart: 10 Pt.
Formatiert: Schriftart: 10 Pt.
Formatiert: Schriftart: 10 Pt.
Formatiert: Schriftart: 10 Pt.
Formatiert: Schriftart: 10 Pt.
Formatiert: Schriftart: 10 Pt.
Formatiert: Schriftart: 10 Pt.
Formatiert: Schriftart: 10 Pt.
Formatiert: Schriftart: 10 Pt.
Formatiert: Schriftart: 10 Pt.
Formatiert: Schriftart: 10 Pt.
Formatiert: Schriftart: 10 Pt.
Formatiert: Schriftart: 10 Pt.
Formatiert: Schriftart: 10 Pt.
Formatiert: Schriftart: 10 Pt.
Formatiert: Schriftart: 10 Pt.
Formatiert: Schriftart: 10 Pt.
Formatiert: Schriftart: 10 Pt.
Formatiert: Schriftart: 10 Pt.
Formatiert: Schriftart: 10 Pt.

Table 5: Atmospheric Lifetimes of various 20 µm diameter Ice Particles at 190 K calculated using the measured absolute rate of H_2O evaporation of corresponding ice particle[a]

Molecular System	**Evaporation Flux $J_{ev}(M)$ (molecule cm^{-2} s^{-1})**	**Lifetime θ/h**	**Dopant Dose/ML (molecular monolayer)**
H_2O	$2.1\ 10^{16}$	2.6	pure
HCl/H_2O	$5.1\ 10^{15}$ $1.4\ 10^{15}$	10.9 39.7	< 3 ML 23 ML
HBr/H_2O	$2.1\ 10^{15}$	26.5	<3 ML
α-NAT/H_2O	$1.8\ 10^{15}$	23.1	pure
β-NAT/H_2O	$6.0\ 10^{14}$	69.4	pure

[a] Conditions: T= 190 K, rh = 80%, a corresponds to experimentally measured interlayer distance (XRD), a=2.5 and 3.35 Å for H_2O, HCl-, HBr-H_2O and NAT, resp., r=10 µm ice particle, ML for HNO_3, HCl, H_2O is 6 x 10^{14}, 3 x 10^{14}, 1 x 10^{15}, respectively.

Formatiert: Schriftart: 12 Pt., Nicht Fett

Formatiert: Tiefgestellt

Formatiert: Schriftart: 12 Pt., Nicht Fett

Formatiert: Hochgestellt

Formatiert: Hochgestellt

Formatiert: Schriftart: 10 Pt.

Formatiert: Abstand Vor: 0 Pt., Nach: 12 Pt., Zeilenabstand: Mehrere 1.15 ze

Formatiert: Schriftart: 10 Pt.

Formatiert: Schriftart: 10 Pt.

Formatiert: Schriftart: 10 Pt.

Formatiert: Schriftart: 10 Pt.

Formatiert: Englisch (USA)

Formatiert: Abstand Nach: 12 Pt., Zeilenabstand: Mehrere 1.15 ze

Formatiert: Links, Abstand Vor: 0 Pt., Nach: 12 Pt., Zeilenabstand: Mehrere 1.15 ze

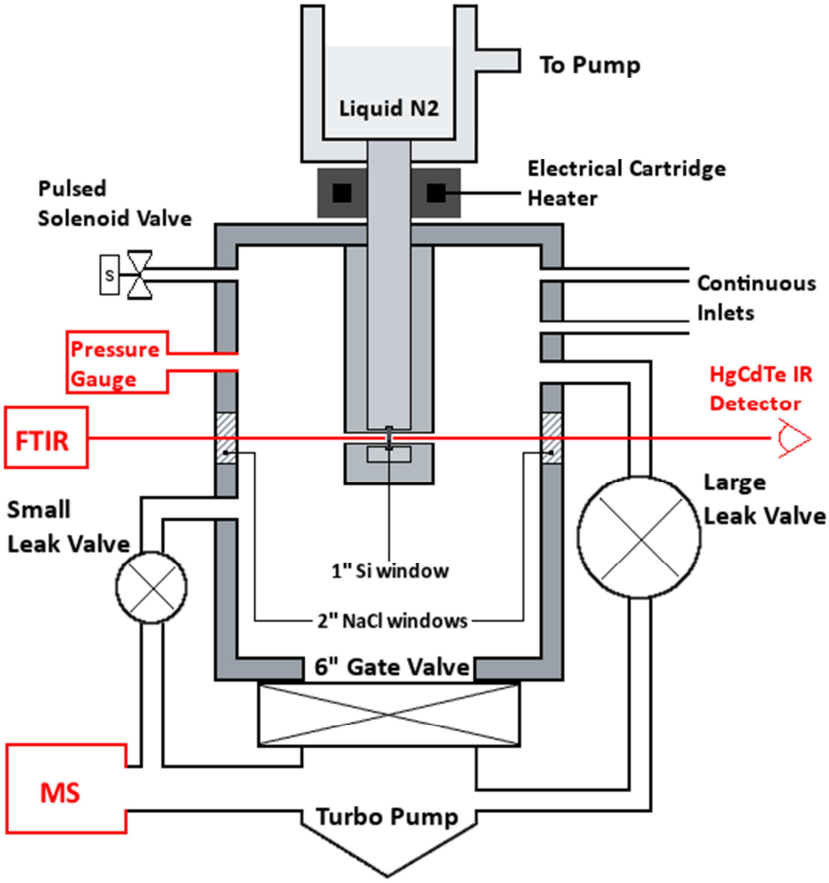

Figure 1: Schematic drawing of the reactor used in this work. The diagnostic tools are highlighted in red and important parameters are listed in Table 1 and Table 2. The ice film is deposited on both sides of the 1” diameter Si window (black vertical symbol hanging from cryostat inside reaction vessel).

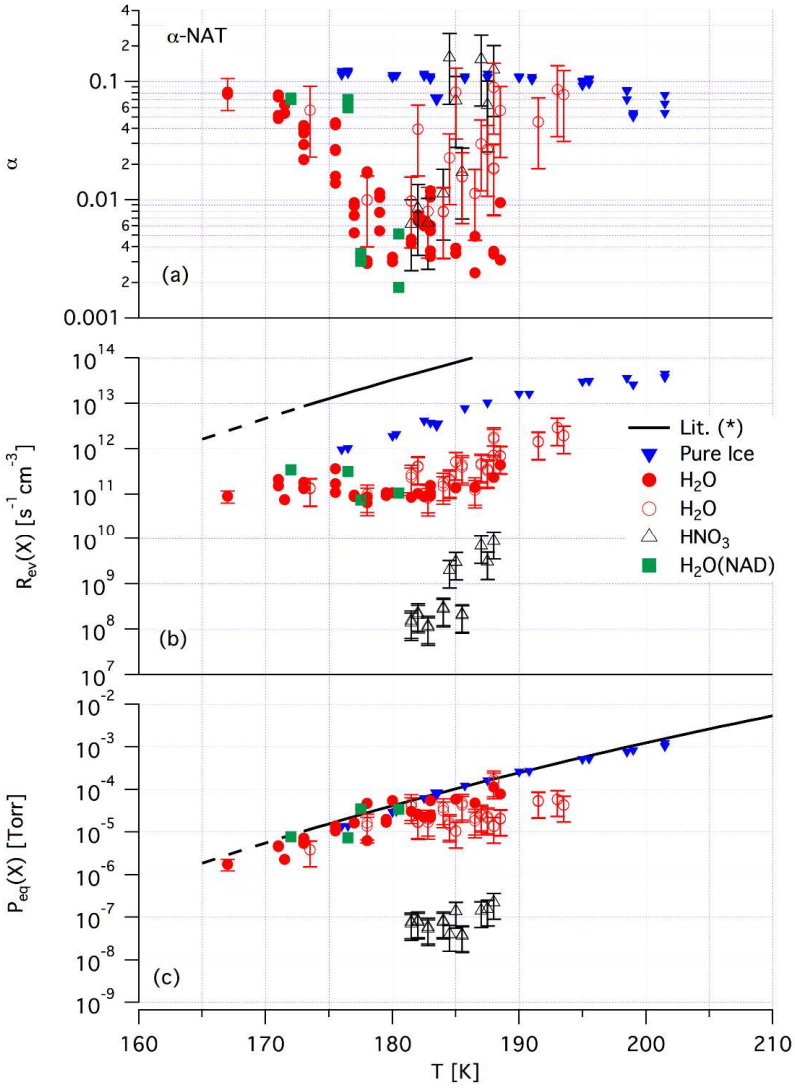

Figure 2: Synopsis of kinetic results for α-NAT and NAD using H_2O as a probe gas in PV experiments and H_2O and HNO_3 in two-orifice (TO) experiments. Full symbols represent PV experiments and empty symbols represent TO experiments. The different symbols are coded in panel b. ~~Further explanations of the used symbols may be found in the text.~~ The calculated relative error for PV experiments is 30% whereas for TO experiments we estimate a relative error of 60%. Examples of the amplitude of the errors are reported for selected points. The black line shows results from Marti and Mauersberger (1993) with $R_{ev}(H_2O)$ of pure ice calculated for the system in use using $\alpha = 1$.

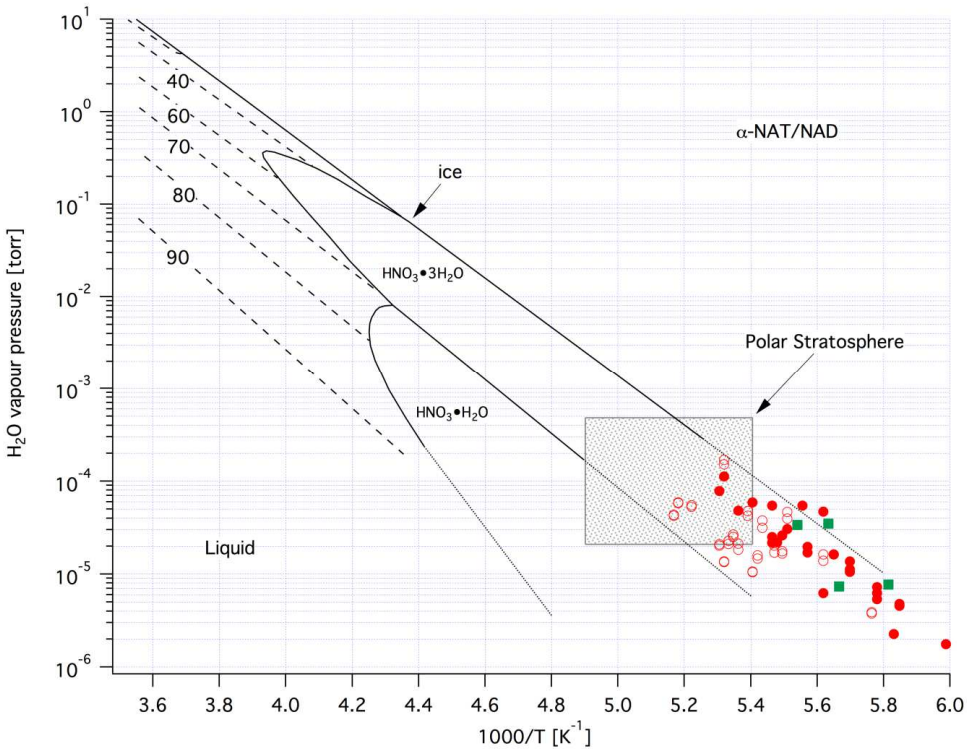

Figure 3: Binary phase diagram of the HNO_3/H_2O system reconstructed from McElroy et al. (1986); Hamill et al. (1988); Molina (1994). The full symbols represent calculated values of $P_{eq}(H_2O)$ for α-NAT and NAD using the kinetic data of PV experiments. Empty circles represent calculated values of $P_{eq}(H_2O)$ for α-NAT using the kinetic data of two-orifice (TO) experiments. The solid lines represent the coexistence conditions for two phases and the dashed lines represent vapor pressures of liquids with composition given as % (w/w) of HNO_3. The shaded gray represents polar stratospheric conditions.

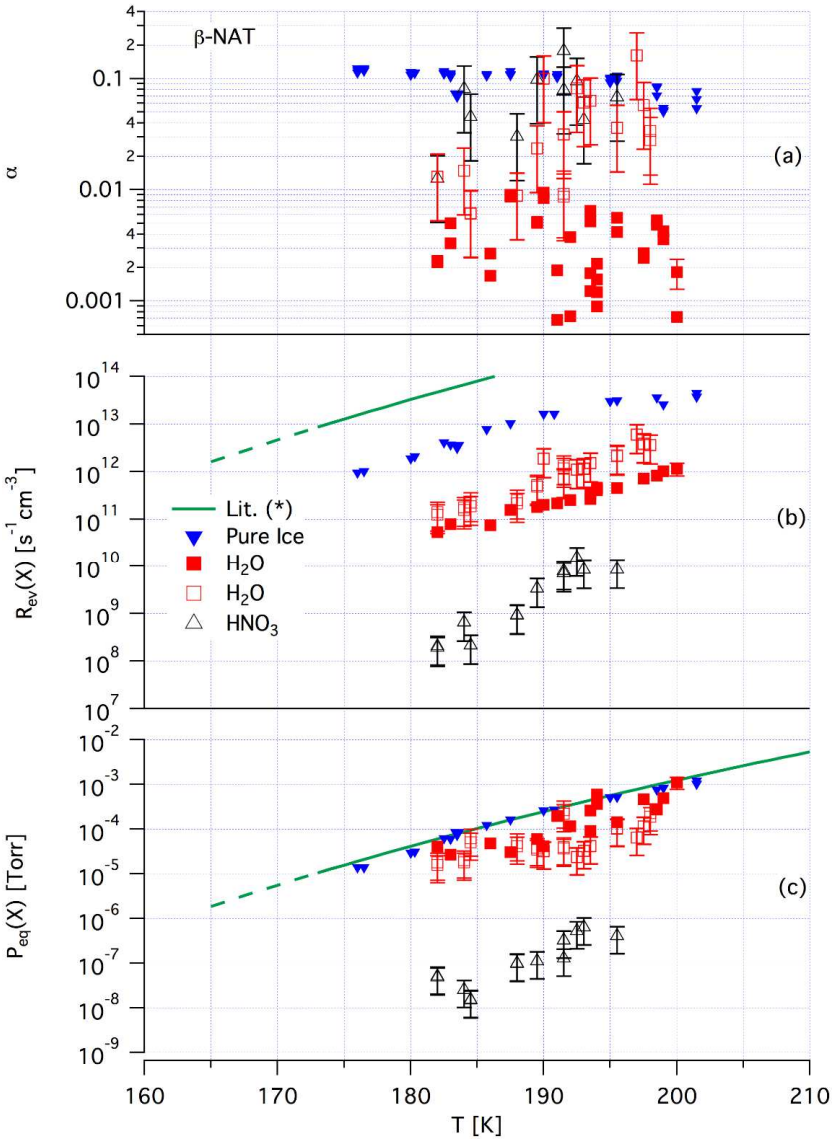

Figure 4: Synopsis of kinetic results for β-NAT using H_2O as a probe gas in PV experiments and H_2O and HNO_3 in two-orifice experiments. Full symbols represent PV experiments and empty symbols represent TO experiments. The different symbols are coded in panel b. ~~Further explanation of the used symbols may be found in the text~~. The calculated relative error for PV experiments is 30% whereas for TO experiments we estimate a relative error of 60%. Examples of the amplitude of the errors are reported for selected points. The green line shows results from Marti and Mauersberger (1993).

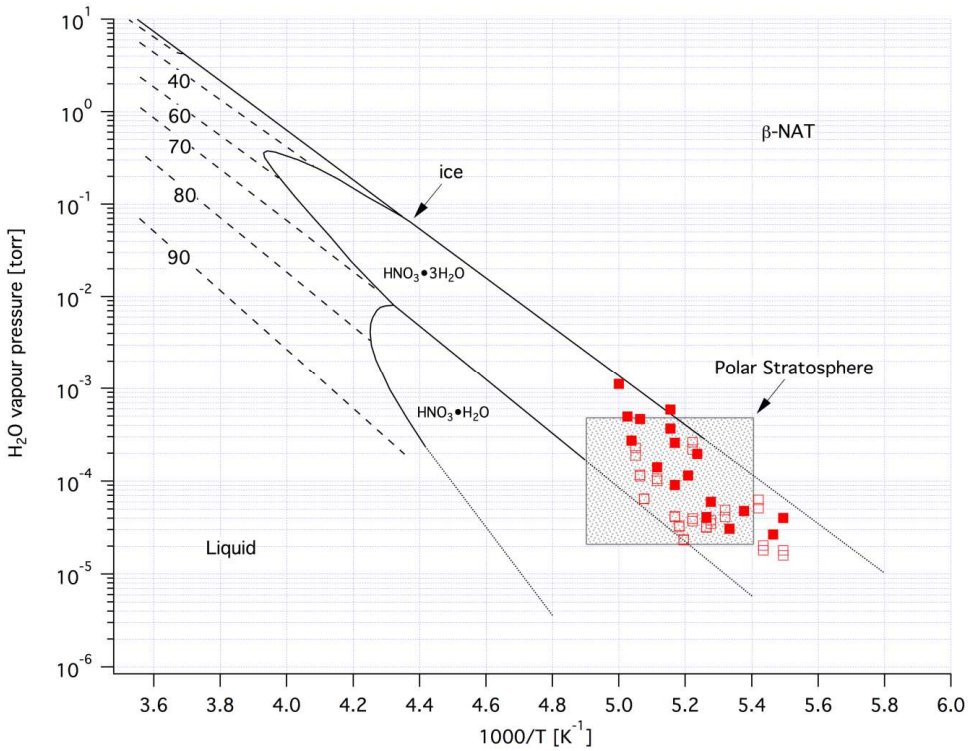

Figure 5: Binary phase diagram of the HNO_3/H_2O system reconstructed from McElroy et al. (1986); Hamill et al. (1988); Molina (1994). The full symbols represent calculated values of $P_{eq}(H_2O)$ for β-NAT using the kinetic data of PV experiments. Empty circles represent calculated values of $P_{eq}(H_2O)$ using the kinetic data of TO (T~~t~~wo-O~~o~~rifice) experiments. The solid lines represent the coexistence conditions for two phases and the dashed lines represent vapor pressures of liquids with composition given as % (w/w) of HNO_3. The shaded gray represents polar stratospheric conditions.

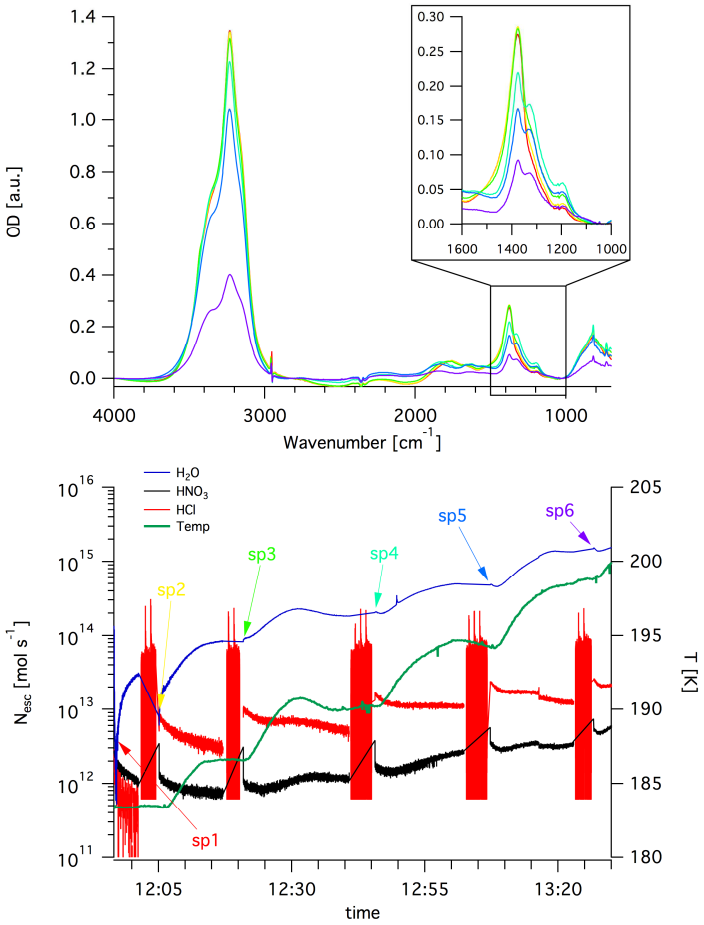

Figure 6: Repetitive PV (Pulsed Valve) deposition experiment of HCl on an α-NAT/ice substrate under SFR conditions followed by MS (lower panel) and FTIR transmission across the thin film (upper panel) as a function of time. In the lower panel the temperature is displayed as the green trace, the red MS signal represents HCl at m/e 36 amu with the pulsed forcing recognizable as single peaks (12) on top of the red columns. The individual HCl doses correspond to approximately (4-5)x10^{16} molecule per pulse resulting in a total dose of 3x10^{17} molecules. The blue and black traces represent the response of H_2O (m/e 18 amu) and HNO_3 (m/e 46 amu) as a function of time (temperature) and HCl forcing. The upper trace displays FTIR transmission spectra at selected times indicated in the lower panel through color coding. The principal peak positions are listed in Table 3 and the changes are discussed in the text.

Formatiert: Standard

Formatiert: Schriftart: Symbol

Formatiert: Hochgestellt

Formatiert: Hochgestellt

Formatiert: Tiefgestellt

Formatiert: Tiefgestellt

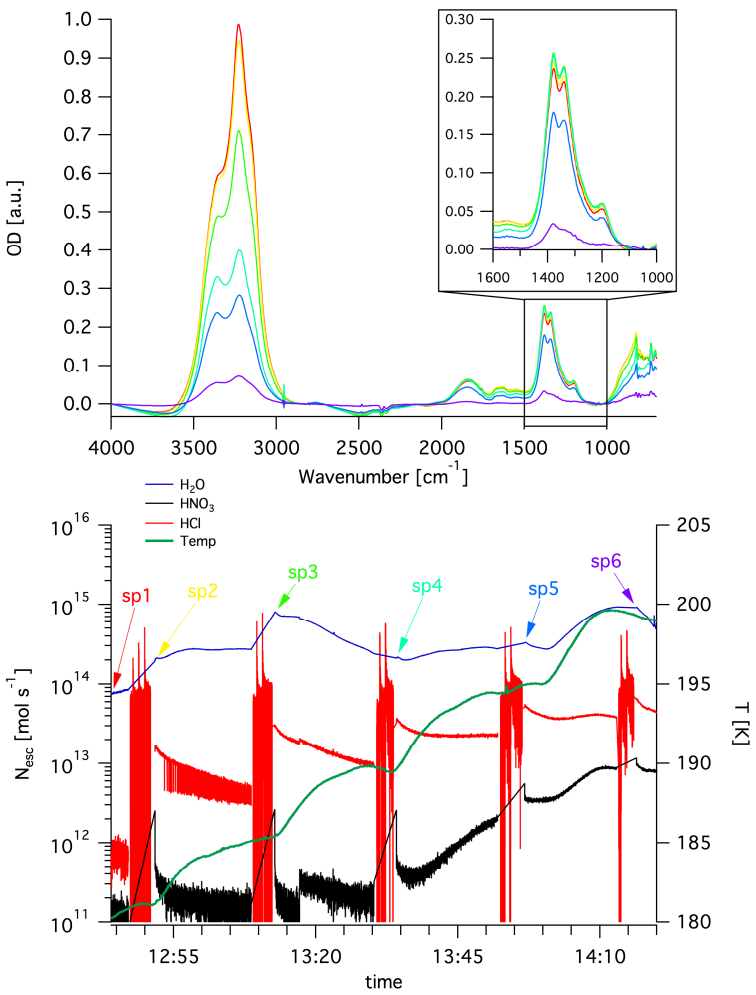

Figure 7: Repetitive PV (Pulsed Valve) deposition experiment of HCl on an β-NAT/ice substrate under SFR conditions followed by MS (lower panel) and FTIR transmission across the thin film (upper panel) as a function of time. In the lower panel the temperature is displayed as the green trace, the red MS signal represents HCl at m/e 36 amu with the pulsed forcing recognizable as single peaks (11) on top of the red columns. The individual HCl doses correspond to approximately (6-7)x10^{16} molecule per pulse resulting in a total dose of 4x10^{17} molecules. The blue and black traces represent the response of H_2O (m/e 18 amu) and HNO_3 (m/e 46 amu) as a function of time (temperature) and HCl forcing. The upper trace displays FTIR transmission spectra at selected times indicated in the lower panel through color coding. The principal peak positions are listed in Table 3 and the changes are discussed in the text.

Formatiert: Standard

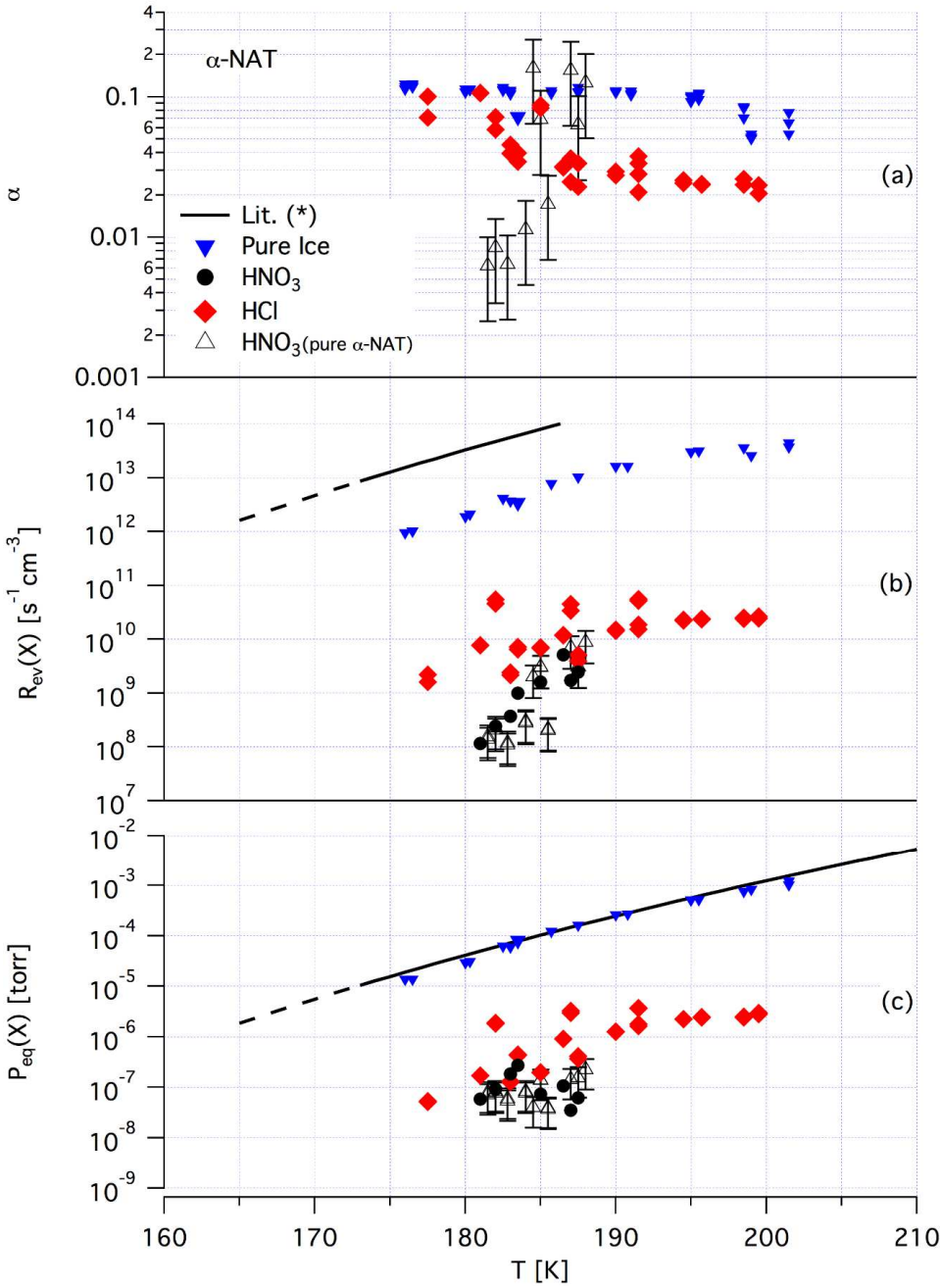

Figure ~~6~~8: Synopsis of kinetic results for α-NAT using HCl as a probe gas in PV experiments. The used symbols are coded in the upper panel~~explained in the text~~. The calculated relative error for PV experiments is 30%. The black line shows results from Marti and Mauersberger (1993).

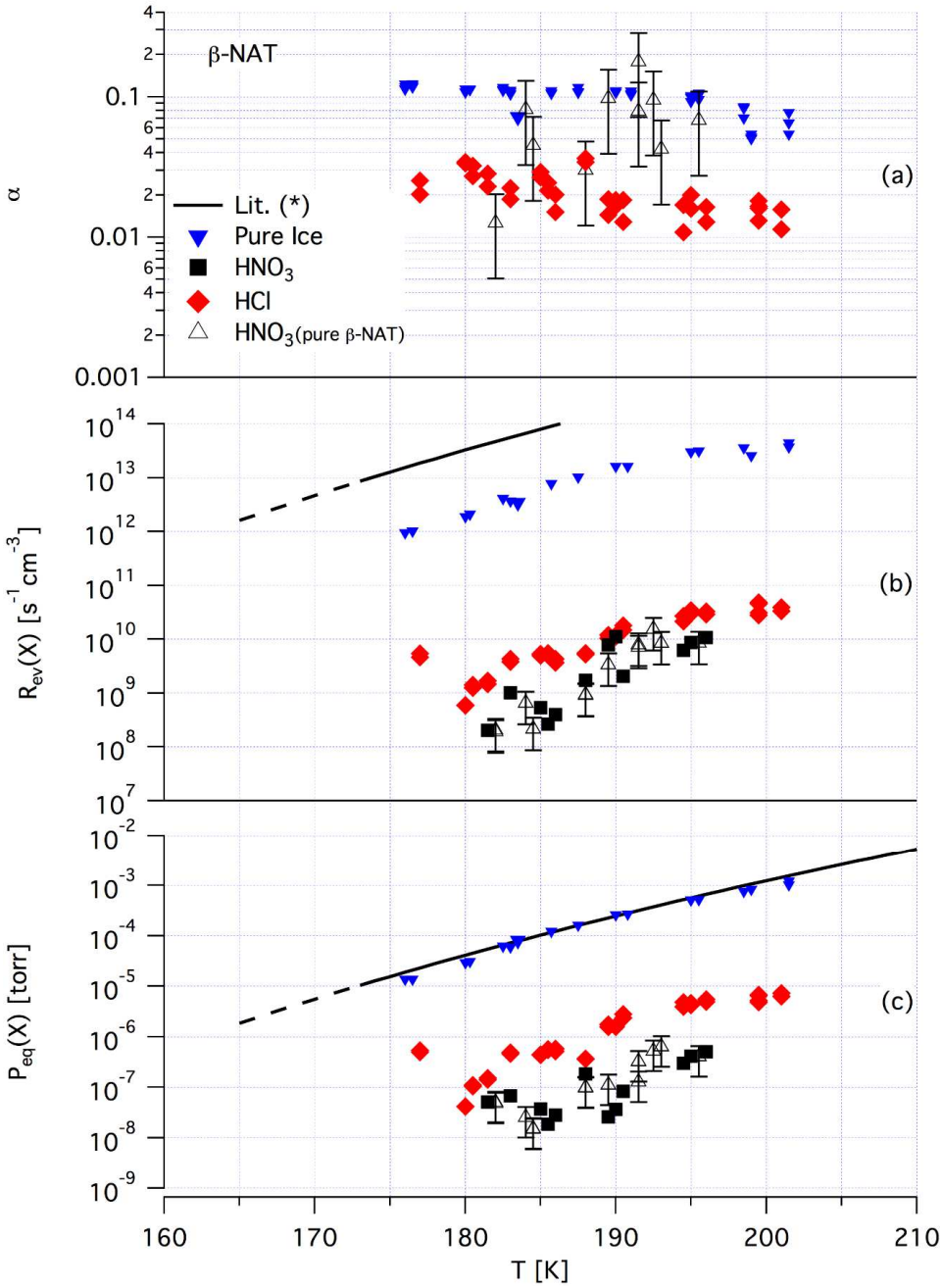

Figure ~~7~~9: Synopsis of kinetic results for β-NAT using HCl as a probe gas in PV experiments. The used symbols are~~-~~ coded in the upper panel~~explained in the text~~. The calculated relative error for PV experiments is 30%. The black line shows results from Marti and Mauersberger (1993).

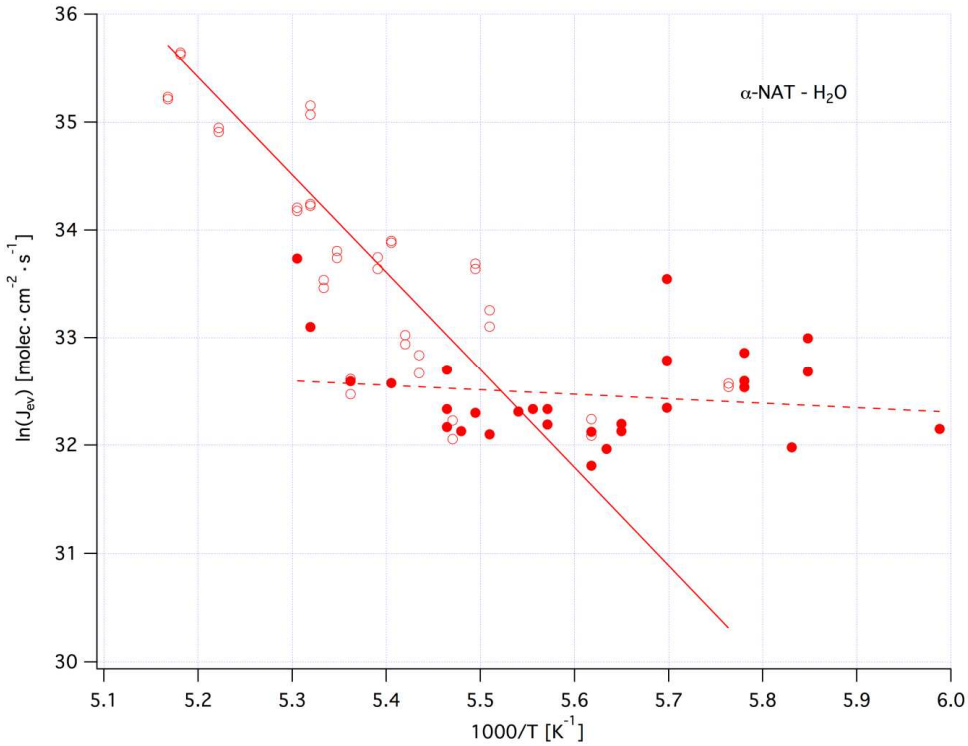

Figure ~~8~~10: Arrhenius plot of $J_{ev}(H_2O)$ for α-NAT. Full and empty red circles represent results of PV and TO experiments, respectively. Data are taken from Figure 2b and the equations for the linear fits may be found in the text.

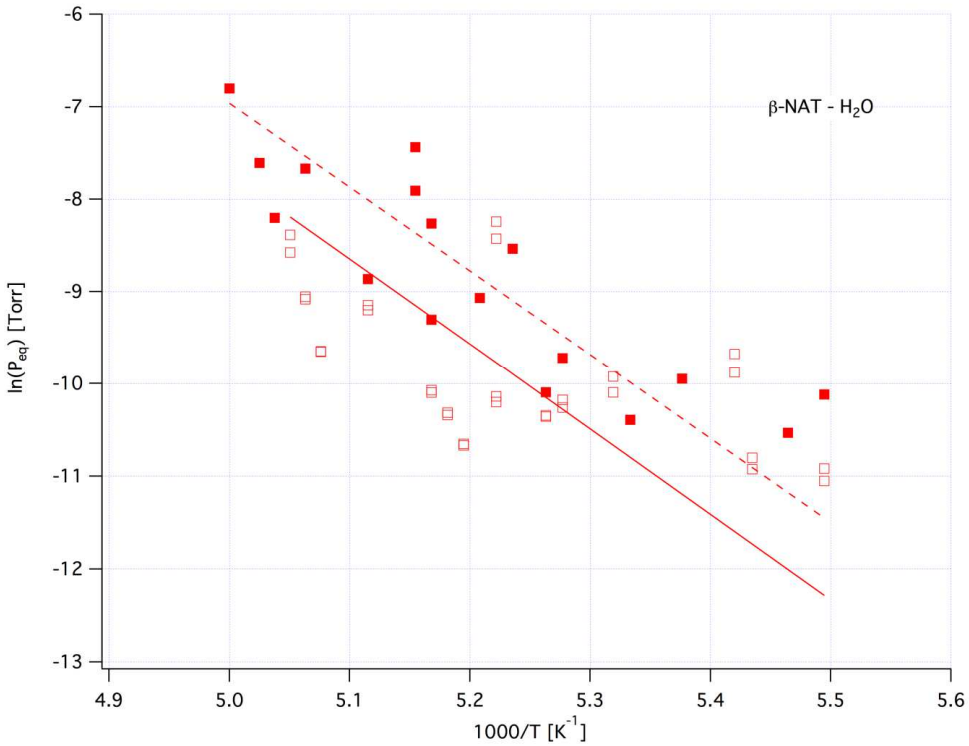

Figure ~~9~~11: van 't Hoff plot of $P_{eq}(H_2O)$ for β-NAT data displayed in Figure 4c. Full and empty red squares represent results of PV and TO experiments, respectively. The equations for the linear fits may be found in the text.

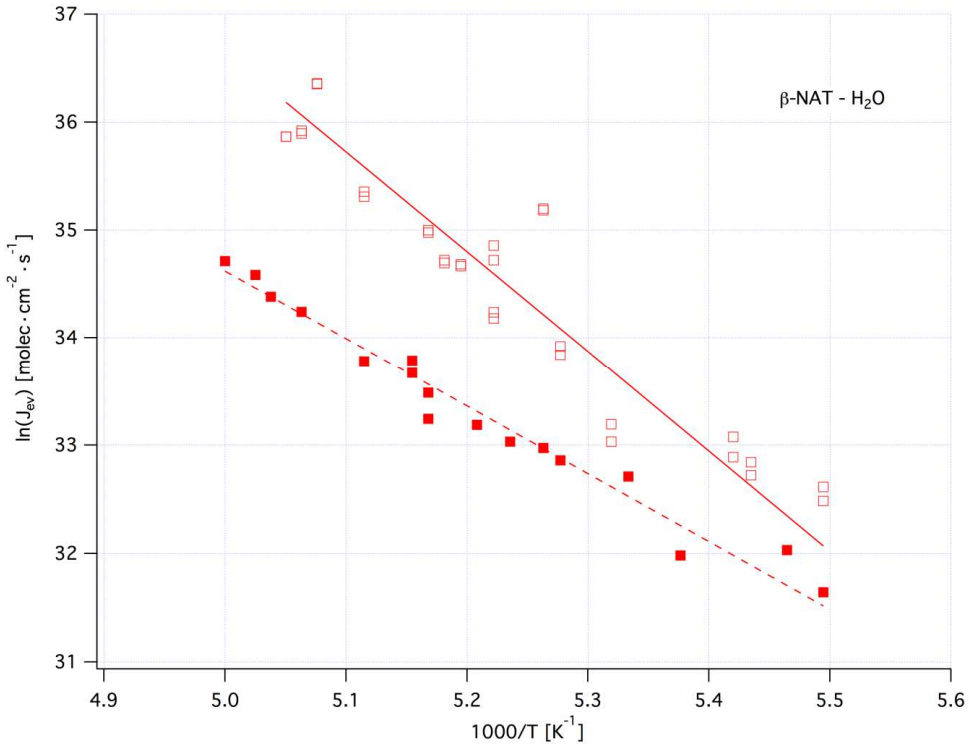

Figure ~~10~~12: Arrhenius plot of $J_{ev}(H_2O)$ for β-NAT data displayed in Figure 4b. Full and empty red squares represent results of PV and TO experiments, respectively. The equations for the linear fits may be found in the text.

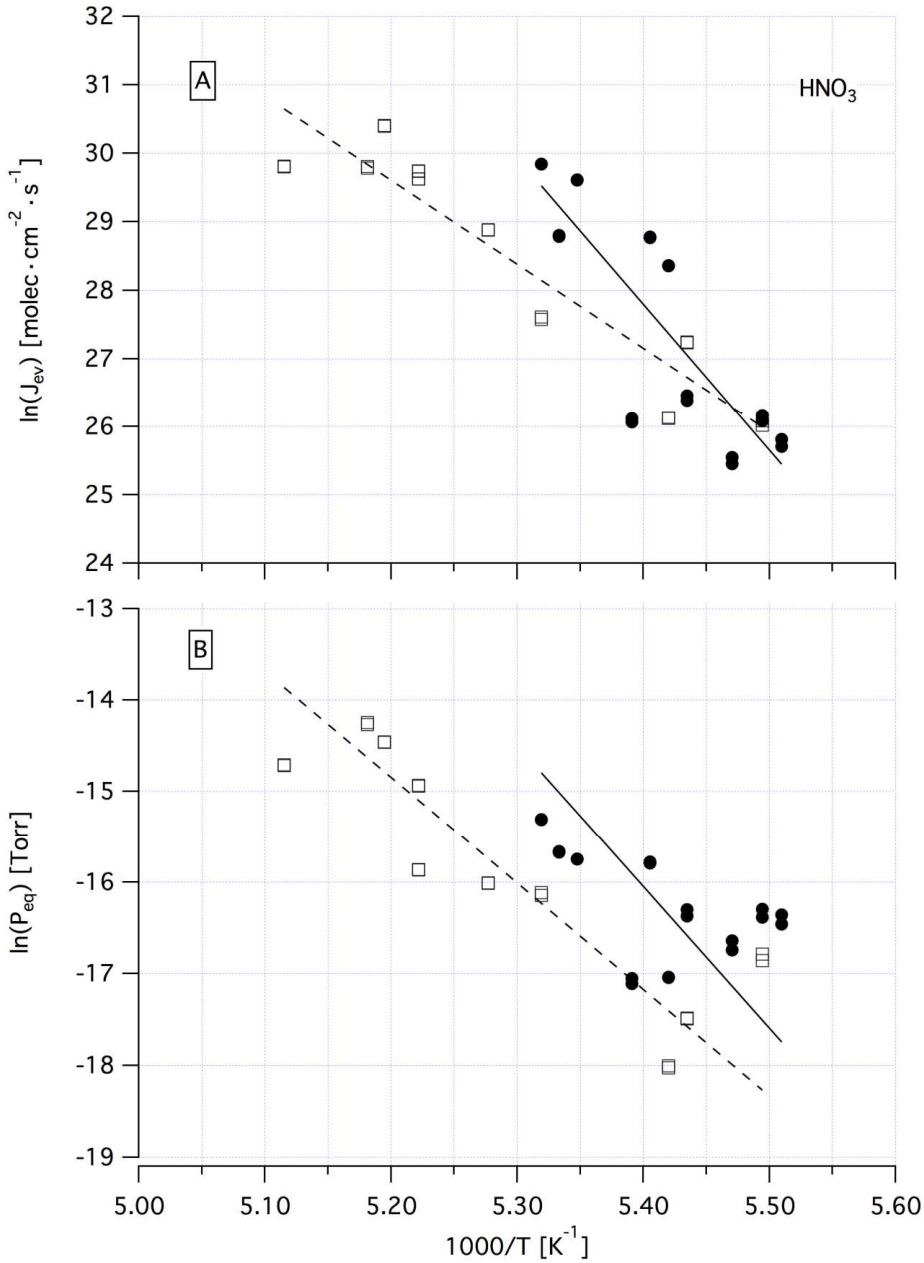

Figure ~~11~~13: Arrhenius plot of $J_{ev}(HNO_3)$ (A) and van 't Hoff plot of $P_{eq}(HNO_3)$ (B) for α-NAT (Figure 2b and Figure 2c) and β-NAT (Figure 4b and Figure 4c) resulting from TO experiments. Full black circles and empty black squares represent the interaction of HNO_3 with α- and β-NAT films, respectively. The equations for the fitting lines may be found in the text.

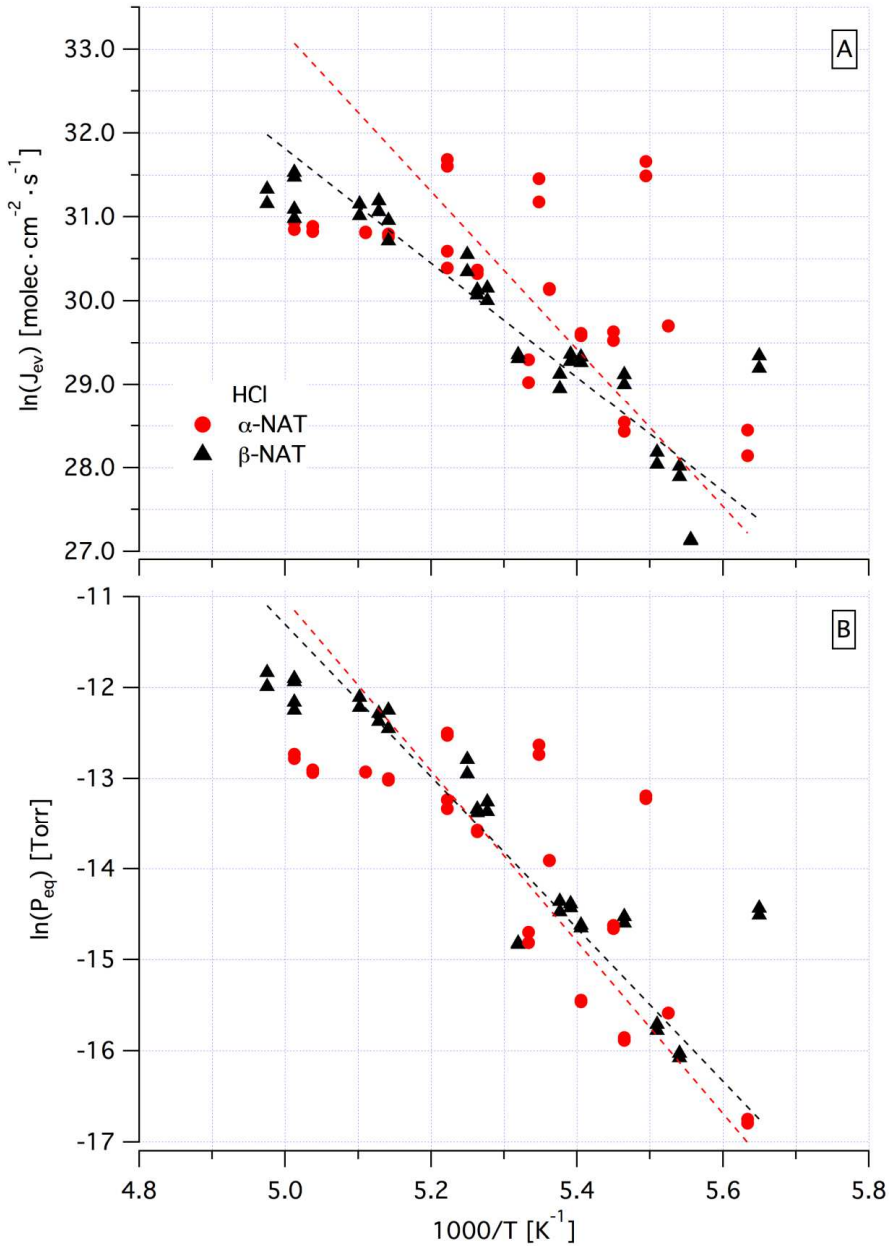

Figure ~~14~~12: Arrhenius plot of J_{ev}(HCl) (A) and van 't Hoff plot of P_{eq}(HCl) (B) for α-NAT (Figure 8b and Figure 8c) and β-NAT (Figure 9b and Figure 9c) resulting from PV experiments. Full red circles and black triangles represent the interaction of HCl with α- and β-NAT films, respectively. The equations for the fitting lines may be found in the text.